

universität ulm

Doctoral Thesis

Exploring mechanisms of gene expression regulation in the developing murine adipose tissue

Monography submitted in partial fulfillment of the requirement for the degree of

"Doctor rerum naturalium" (Dr. rer. nat.)

of the Faculty of Natural Sciences,

Ulm University

Supervisor:

Priv. Doz., Dr. habil. Tamás Röszer

Institute of Neurobiology

Ulm University

Thesis submitted by

M.Sc. Anh Cuong Hoang

Born in Lauingen, Germany

Ulm, 2021

Title	Exploring mechanisms of gene expression regulation in the developing murine adipose tissue
Dean of faculty	Prof. Dr. Thorsten Bernhardt
Department	Institute of Neurobiology University Ulm Albert-Einstein-Allee 11 M25 - Niveau 5 89081 Ulm, Germany
Surname, First Name	Hoang, Anh Cuong
Supervisor	Priv. Doz., Dr. habil. Tamás Röszer
Reviewers **(2. und 3. Gutachter)**	Associate Prof. Dr. Rudolf Gesztelyi Institute of Pharmacology and Pharmacotherapy, Faculty of Medicine, and Doctoral School of Nutrition and Food Sciences Debrecen University, Hungary Ph. D. Vissarion Efthymiou Joslin Diabetes Center Harvard University, Boston MA 02215
Date of defense	24. March 2022

Table of contents

Acknowledgements and dedication 1
Abstract 2
List of abbreviations 3
1. Introduction 5
1.1. Obesity: a rising disease with many co-morbidities 5
1.2. The traditional two types of adipose tissue 7
1.3. Beige adipocytes: cells with white & brown adipocyte features 8
1.4. The mitochondrial network in beige adipocytes: indispensable for fat catabolism 9
1.5. The possible role of thermogenic versus fat storing adipocytes in childhood obesity 10
1.6. Hypothesis and aims of the thesis 11
2. Materials and methods 13
2.1. Materials 13
2.1.1. List of Equipment 13
2.1.2. List of Softwares 14
2.1.3. List of chemicals 15
2.1.4. List of Kits 17
2.1.5. Antibodies 17
2.1.6. Primers 18
2.2. Methods 20
2.2.1. Animal and cell samples 20
2.2.2. Cell culture treatments 20
2.2.3. Histology and image analysis of adipose tissues 21
2.2.4. Flow cytometry analysis 21
2.2.5. Analysis of RNA and next generation sequencing 21
2.2.6. Mitochondrial RNA and DNA isolation and their transfection *in vitro* 22
2.2.7. Extracellular vesicle isolation of culture media, breast, and formula milk 23
2.2.8. ELISA assays 23
2.2.9. High fat diet feeding and *in vivo* mtRNA transfection 24
2.2.10. Statistics and Data representation 24

3. Results 25
3.1. The P6 adipose tissue is rich in beige adipocytes in mouse 25
3.2. Differentially-expressed genes of adipose tissues in P6 and P56 mice 27
3.3. Beige marker gene transcription in P56 brown- and P6 adipose tissue. 29
3.4. Neuropeptide and GABA signaling in P56 brown- and P6 inguinal adipose tissue 32
3.5. Immune gene networks in P6 adipose tissue 36
3.6. Suppressed IFN response in P6 adipose tissue 39
3.7. Beige adipocyte development through the mtRNA signaling 43
3.8. Vitamin D receptor mediated IRF7 suppression in infant adipose tissue 47
3.9. Obesity-driven loss of mitochondria immune tolerance in P6 adipocytes 51
4. Discussion 53
5. Conclusion 64
7. References 67
8. Appendix 81
8.1. Publication and preprint presented in the thesis 81
8.2. List of figures 133
8.3. List of tables 133
9. Statutory declaration 134

Acknowledgements and dedication

At the beginning, I would like to thank my mentor, teacher, and supervisor Priv. Doz. Dr. habil. Tamás Röszer for the chance to perform my doctoral program in his working group. I am grateful for his guidance, patience, and trust during my studies. His guidance refines my laboratory and personal skills. Overall, due to his supervision, I could improve myself to become a better scientist.

Next, I would like to thank my laboratory colleagues mainly Dr. Haidong Yu who helped me a lot during my study time. I also want to thank all the former lab members, especially Vincent Pflüger and Yun Chen, for their contributions to my work. Therefore, I could learn to see obstacles from another perspective to solve them more efficiently.

Hereby, I would like to thank Associate Prof. Dr. Rudolf Gesztelyi to spend time and interest reviewing my thesis. In addition, I would like to thank my colleagues and superiors from the Institute of Neurobiology, such as Prof. Dr. Harald Wolf for his life improving tips. Special thanks to Prof. Dr. Annika Herwig and Dr. Viktoria Diedrich for the productive collaborations. I also want to highlight my gratitude towards Ms. Ursula Seifert who helped me with all the administrative work.

Lastly, I would like to thank my lovely family for their support and faith in me. I am deeply grateful for the help and love of my girlfriend Angelika who gave me strength and confidence to accomplish my studies. Without all of them and my mentor, I would not be the scientist I am today.

Abstract

Background and objectives: Obesity is an epidemic, noncommunicable, metabolic disease which can develop early in life, leading to a rapid and dramatic increase in the global prevalence of obesity-associated diseases. To avoid obesity, we have to understand the developing adipose tissue at the level of its molecular mechanisms and genomics.

Hypothesis and aims: Gene expression changes and immune-metabolic mechanisms of the obese adipose tissue in adulthood are well studied, however we know much less about these in the developing adipose tissue. In this thesis we aimed to identify unique and defining transcriptional landscape and morphology of the adipose tissue in the early postnatal life. Furthermore, since fat catabolism is greater in early life than in adulthood, we hypothesize that adipocytes in the developing fat household a high amount of mitochondria to fulfil the demand of fat metabolism. It is plausible to assume that the extensive mitochondrial network may require a suppression of the immune response elicited by mitochondrial contents. Therefore, we searched for immune regulators, signals and mechanisms which favour mitochondrial network expansion.

Results: We found that during postnatal development, infant fat depots contained beige adipocytes. We show that these adipocytes perform thermogenesis and develop independently from the brown adipose tissue (BAT). Thermogenic adipocytes in the early postnatal life expand their mitochondrial network by suppressing the innate immune recognition of mitochondrial DNA and RNA (mtDNA and mtRNA). This was achieved through a suppressed interferon (IFN) regulatory factor 7 (IRF7) expression. A unique mtRNA-driven signal mechanism triggers the mitobiogenesis and beige adipogenesis. The role of mtRNA is restricted to infant adipocytes, since adult adipocytes respond with an IFN burst after mtRNA exposure. Obesity increased IRF7 expression, leading to IFN response towards mitochondria, eventually impairing the mitochondrial network. Vit-D3 allows IFN-free, mtRNA-mediated mitobiogenesis in diet-induced obese adult mice which ultimately reduce obesity development.

Summary and impact: This thesis showed that (i) beige adipocytes could be identified in the developing fat, and that (ii) maintaining these adipocytes´ mitochondria is key for the lipid catabolism and beige adipogenesis. These finding have impact on the adipose tissue field because it may add a 3rd adipocyte type which is present during infancy and has to be re-establishing in adulthood to potentially reduce obesity.

Key words: developmental genomics – obesity – adipogenesis – nucleic acid immunity

List of abbreviations

ATMs	adipose tissue macrophages
ATP	adenosine triphosphate
BAT	brown adipose tissue
BMI	body mass index
CCCP	carbonyl cyanide m-chlorophenyl hydrazone
CIMs	clustered image maps
DEGs	differentially-expressed genes
dsRNA	double stranded RNA
EVs	extracellular vesicles
FACS	fluorescence-activated cell sorting
FCS	fetal calf serum
FFA	free fatty acid
GO	gene ontology
H&E	hematoxylin and eosin
HFD	high fat diet
iAT	inguinal adipose tissue
IFN	interferon
IL	interleukin
IRF7	interferon regulatory factor 7
MDA5	RIG-I-like melanoma differentiation-associated gene 5
mtDNA	mitochondrial DNA
MTR	MitoTracker Red
mtRNA	mitochondrial RNA
MTY	MitoThermo Yellow
MVB	multivesicular body
NCD	normal chow diet
NIH	National Institutes of Health
p(dA:dT)	poly(deoxyadenylic-deoxythymidylic) acid sodium salt
p(I:C)	polyinosinic-polycytidylic acid
PAF	platelet activated factor

PAS	periodic acid–Schiff
P6	postnatal day 6
P56	postnatal day 56
pCMV6	plasmid cytomegalovirus 6
RIG-I	retinoic acid-inducible gene 1
RT-qPCR	reverse transcription PCR
s.e.m.	standard error of mean
SDH-A	succinate dehydrogenase complex, subunit A
STAT3	signal transducer and activator of transcription 3
STING	stimulator of interferon genes
SVF	stromal vascular fraction
T1DM	type 1 diabetes mellitus
T2DM	type 2 diabetes mellitus
Th1	T helper 1
Th2	T helper 2
TLR	Toll-like receptor
VDR	vitamin D receptor
Vit-D3	vitamin D3
WAT	white adipose tissue
WT	wild-type

1. Introduction

1.1. Obesity: a rising disease with many co-morbidities

Adipose tissue biology gains intensive attention today, due to the worldwide incidence of obesity and its related co-morbidities, such as insulin resistance, diabetes, and other immune-metabolic diseases (1). Incidence of these diseases increases rapidly - affecting not only industrial countries but also developing countries (2) - and are predicted to affect approximately 60 % of the adult population by 2030 worldwide (3). Highlighted by a recent report of the World Health Organization, obesity develops into a serious pandemic health problem which is well illustrated by the fact that 650 million adults worldwide were obese in 2016 (4). Furthermore, 39 million children, below the age of 5, were overweight or obese in 2020 (4). Obesity is classified according to the body mass index (BMI) (3, 5) which is calculated by the individual´s body weight in kilogram divided by its height in meters squared (kg/m^2) (3). Overweight is associated with a BMI of ≥ 25 kg/m^2, obesity is defined with BMI ≥ 30 kg/m^2 and morbid or extreme obesity is associated with a BMI ≥ 40 kg/m^2 (2, 3, 6).

Causes of obesity are diverse and include high calorie intake and poor exercising (7). In addition to that, genetics and diseases affect obesity development as well; while the genetic inheritance is poorly understood due to the interaction of multiple genes with environmental factors (8–10), diseases such as Cushing syndrome, polycystic ovary syndrome or an underactive thyroid are known to induce overweight and obesity (11–13). All these factors can lead to obesity which is considered to be an excess adipose tissue development.

The adipose tissue is known as a lipid storage site, although it has many other roles, such as body temperature control through thermal insulation and the regulation of systemic metabolism through endocrine factors and immune mediators (14, 15). For instance, leptin, a 16-kDA large adipokine secreted mainly by white adipocytes, activates immune cells and regulates the proliferation, phagocytosis and chemotaxis of neutrophils (16). The production of leptin is dependent on adipose tissue mass (16–18) which along with adipocyte size affects the blood level of leptin, and the immune effects of obesity (19, 20). The positive correlation of that adipokine and adipose tissue mass indicates leptin as a potential marker for obesity-related complications (21, 22).

Besides adipokines, adipose tissues are also able to produce and secrete immune mediators, such as interleukin-6 (IL-6) or interleukin-10 (IL-10) (23). IL-10 is a known anti-inflammatory cytokine which has the potential to increase insulin sensitivity by impeding obesity-associated immune cell infiltration in the skeletal muscle (24). Hence, it might play a role in the treatment of type 2 diabetes mellitus (T2DM). Furthermore, low blood level of IL-10 in obese women is associated with metabolic syndrome, abnormal obesity, hypertriglyceridemia or high blood pressure (25).

As indicated by these examples, subcutaneous fat depots can adjust endocrine and immune functions through hormones, adipokines and cytokines to affect distant organs including liver, muscle, endocrine pancreas, as well as the cardiovascular and the skeletal system (1). Fat pads can also be found on muscles to reduce mechanical stress, or around deep nerves serving as a protecting layer (26).

Obesity develops as a result of uncontrolled and excess adipose tissue development leading to co-morbidities which are partly incurable and negatively affect the lifespan (3, 27, 28). To expand the adipose tissue depot, the organ can either induce hypertrophy which is an enlargement of the adipocytes or hyperplasia which increases the number of adipocytes within the depot (29). Since adipocytes have a limited lipid storage capacity, excess caloric intake leads to the accumulation of fat in the distant organs, such as liver, skeletal muscle or heart. Excess amount of lipids in these organs causes “lipotoxicity” which results in development of insulin resistance (29). Insulin signaling requires many signal transducers, such as insulin receptor substrate-1 (IRS-1), 1-phosphatidylinositol 3-kinase (PI-3K), TBC1 domain family member 4 (AS160) and glucose transporter type 4 (GLUT4) (30). In the skeletal muscle, insulin evokes, upon binding to its receptor, IRS-1 activation. Through a signal cascade via PI-3K, AS160 is activated to impair GLUT4 interaction with Rab protein which ultimately leads to the GLUT4 presence in the plasma membrane (31). Circulating free fatty acids (FFA) in obese individuals impair IRS-1-mediated PI-3K activation in muscle, pancreas and heart (32, 33). Hence, decreased PI-3K activity reduces insulin-driven glucose uptake leading to insulin resistance.

Lipotoxicity in the adipose tissue enhances immune cell infiltration (29). Therefore, T- and B-cells, macrophages, neutrophils and mast cells invade the lipid storing organ and generate a low-grade and chronic inflammation, a hallmark of obesity development (34). Hence, obesity research aims to understand excess adipose tissue development to find treatment strategies reverting or preventing this process.

1.2. The traditional two types of adipose tissue

Adipose tissue is classified into two types according to their cell morphology and function: white adipose tissue (WAT) and brown adipose tissue (BAT) (35, 36). However, WAT and BAT have distinct ontogeny making it plausible that BAT is not a “true” adipose tissue. Adipocytes are lipid-storing cells which are involved endocrine, nervous and immune functions (37).

WAT adipocytes are able to accumulate and store neutral lipids in a large fat droplet for a long period of time; however, this droplet can be dismantled in demand of energy, such as during starvation (15). In contrast, BAT adipocytes actively disintegrate fat droplets to oxidize fatty acids which results in the production of ATP or heat (38, 39). Adipocytes of the BAT are rich in mitochondria and organize their lipids in multiple small droplets which are located around the mitochondria (36, 40–42).

Apart from neutral lipids, BAT contains glycogen abundantly, which is also used as a metabolic fuel after cold stress (36, 40–42). Maintaining multiple small lipid droplets in BAT allows an increased accessibility of the stored cargo to perform mitochondrial β-oxidation (35, 43). The different morphology of WAT and BAT is a distinguishing hallmark. Due to their multiple fat droplet organization, BAT adipocytes are termed multilocular, while WAT adipocyte rearranged their lipids to one large lipid droplet (unilocular) (35, 36, 44). WAT can be found in all vertebrates while BAT, in many species located in the interscapular region, is restricted to mammals (45). In addition to that, among the mammalian fat depots, WAT is more prevalent than BAT.

BAT consists abundantly mitochondria which express uncoupling protein 1 (UCP1) (46). UCP1 needs to be activated for instance through long-chain fatty acids (47). Located in the inner mitochondrial membrane (IMM), it can manipulate the H^+ gradient as a transport protein (48). Thereby, IMM changes its conductance which leads to uncoupling of the mitochondrial respiration. Thus, a heat production rather than ATP is mediated by UCP1, due to which effect BAT is also known as the thermogenic fat performing non-shivering thermogenesis (47, 49–51). This shows that brown adipocytes are able to increase energy expenditure and thermogenesis through the uncoupling process (46). Obesity is the consequence of excess adipose tissue development which means in specific the expansion of WAT at the expense of BAT prevalence (52–54). Therefore, generating heat through the uncoupling process in adipocyte by using stored lipids, is a desired strategy to combat obesity (49, 55–58).

1.3. Beige adipocytes: cells with white & brown adipocyte features

Besides the two traditional types of adipose tissue, there is a third type of adipose tissue which is called brown-in-white adipose tissue (“brite”) or “diffuse BAT” (38). Accordingly, this adipose tissue accommodates uni- and multilocular fat cells. Furthermore, it has a higher potential in fat oxidation compared to WAT and it can generate heat through uncoupling which is a key feature of BAT (59). Multilocular adipocytes located in the brown-in-white adipose tissue are able to oxidize fat and to perform thermogenesis; and they often termed as beige adipocytes (i.e., a transitional cell type between “white” and “brown” fat cells) (60, 61).

Beige adipocytes appear in WAT depots in response to cold stress, allowing adaptive thermogenesis. Since beige fat cells burn off energy stored in fat in the form of heat, the induction of beige adipocyte development in WAT depot is a desired approach to reduce obesity. Many studies show that adipocytes exposed to cold, T helper type 2 (Th2) cytokines, β-adrenergic stimuli, thiazolidinediones, and some lipid species respond to these stimuli with beige differentiation or “browning” (60, 62–64). In addition to the induced beige adipocytes, there are permanent thermogenic fat depots in the supraclavicular region, around the large arteries, and in the kidney capsule. These fat depots are considered as beige adipocytes. Of note, previously these fat depots were identified in the literature as BAT (65–67).

Furthermore, there is a debate about beige adipocyte lineage whether it develops from BAT preadipocytes located within WAT (68) or as the term “brite” indicates through special differentiation programs in the adipocyte precursors (69). These programs define the adipocyte to be involved in the fat storing or fat oxidation and thermogenesis (69). Thermogenic fat, like beige and brown adipocytes have a heterogenous ontogeny in mice (70). BAT and the skeletal muscle have the same progeny which can be seen in in the development of brown adipocytes from myogenic factor 5 (Myf5)-positive progenitors (70). Cells deriving from $Myf5^{+}$ progenitors are hardly visible in WAT depots (71). In addition to that, a development of thermogenic fat in WAT was proceed independently from the $Myf5^{+}$ lineage (71). Furthermore, there are studies highlighting that thermogenic fat cells can also derived from ectodermal progenitors, in detail from stem cells of the neural crest (72, 73). Indicated by the previous evidence, beige adipocyte lineage is still a fact to debate. Nevertheless, WAT

accommodates inducible, fat-oxidizing beige adipocytes as well as fat-storing white adipocytes (74).

1.4. The mitochondrial network in beige adipocytes: indispensable for fat catabolism

For over 50 years the endosymbiotic theory shapes the way of thinking of scientists to discriminate prokaryotic and eukaryotic cells (75). Interestingly, there are more than 20 different versions of the theory available in the literature to explain the origin of mitochondria-consisting eukaryotes (76). The most updated version explains that the host cell was not a eukaryote, but an archaeon, also known as an archaebacterium (76–78). Whereas the symbiont used to be a prokaryote, since prokaryotic DNA and mitochondrial DNA are very similar (79).

The main function of a mitochondrion is to generate ATP through oxidative phosphorylation (79). However, it is also able to use fat as a substrate to generate energy supply (β-oxidation) or to generate heat which process is called mitochondrial uncoupling (80). Cell metabolism of fat to perform mitochondrial uncoupling and β-oxidation demands an extensive mitochondrial network (59). Householding a large number of mitochondria increases the unintended leaking of mitochondria-associated danger signals into the cytosol, such as prokaryotic-like mitochondrial DNA (mtDNA) and virus-resembling double stranded RNA (dsRNA). These signals are also known as mitochondrial damage-associated molecular patterns (DAMPs) (81). They evoke inflammasome activation and interferon (IFN) response through the promotion of mitochondrial reactive oxygen species (mROS), NOD-, LRR- and pyrin domain-containing 3 (NLRP3) inflammasome signaling, or caspase 1 activation (81, 82). Inflammatory products from these signal mechanisms impair the mitochondrial network expansion and the fat-oxidizing potential of adipocytes (83–85). Furthermore, they trigger metabolic inflammation leading to a hyper-inflammatory disorder which is associated with obesity (86). Nevertheless, beige adipocytes maintain a high amount of mitochondria regardless of a potential inflammatory burst.

1.5. The possible role of thermogenic versus fat storing adipocytes in childhood obesity

Obesity does not affect only adults and can develop already in the early life which is termed as childhood obesity. Childhood obesity is considered to be a public health challenge, exclusive formula milk feeding or the extinction of BAT supports obesity development in children and adolescents, respectively (63, 87, 88). Overweight or obese children are prone to take the obese-status until adulthood causing a life-long obesity (89).

Growing up in the intrauterine environment generated by the mother, the fetus receives carbohydrate-rich nutrients provided by the maternal metabolism. The human adipose tissue primordia start to expand in the last trimester of gestation which requires lipogenic substrates, such as maternal ketone bodies and glucose (90). In addition, around 70 % of the glucose in the fetus is metabolized into fat before birth (70, 91). Furthermore, primordial fat cells accommodate glycogen and neutral lipids (41, 44, 92, 93). Adipocytes perform lipolysis after birth which is accompanied by *de novo* fatty acid synthesis, lipogenesis, and catabolism of glycogen (glycophagy) (44). According to that, glycophagy enhances the formation of lipid droplets in the developing adipocytes (92). In infancy, building up the lipid storage requires constant lipid supply which is achieved by the consumption of breast-, or formula milk (90).

Hence, glycophagy and breast milk support thermogenic fat development (63, 92). In contrast to that and indicated by previous studies, the loss of fat-oxidizing and thermogenic adipocytes favour the expansion of fat-storing adipocytes in the infant adipose tissue (88, 94, 95). Like adults, infant adipose tissue may start to increase adipocyte size (hypertrophy) and number (hyperplasia) (29) which ultimately leads to the WAT expansion and childhood obesity. Reverting this process may require thermogenic fat cells, first to deal with the number of fat-storing cells (weight reduction) and second to exclude FFA which affect distant organs (lipotoxicity reduction). Due to their ability to oxidize fat, mitochondria-rich fat cells may be key players to prevent obesity.

However, householding a vast amount of mitochondria is potentially dangerous and metabolically demanding process. Mitochondria dysfunction or damage leads to hyper-inflammation response which supports obesity development. This observation

prompted us to question whether thermogenic fat cells developed an immune-modulated mechanism to avoid the loss of their mitochondrial network.

1.6. Hypothesis and aims of the thesis

Since beige adipocyte induction is a potential strategy to treat obesity and the majority of experiments were done in adult fat cells (60, 61, 96), studies about beige adipocytes during infancy are underrepresented. Located within the subcutaneous fat depot, thermogenic fat is involved in the postnatal intense fat oxidation (40, 97, 98). Hereby, we propose beige adipocytes located within the infant adipose tissue able to perform thermogenesis and energy expenditure like BAT. Therefore, this thesis aims to identify weather infant adipose tissue consists beige adipocytes and do they have differences or similarities towards other fat depots.

Aim 1.

First, we explored the morphology of adipose tissues, for that, fat tissues were compared from the inguinal and interscapular regions at different age of mice. Furthermore, we checked their ability to perform thermogenesis by the immunohistochemical staining of UCP1.

Aim 2.

Second, we investigated the transcriptional landscape of infant and adult adipose tissue to reveal specific hallmark gene networks and hub genes. These investigations should identify beige adipocyte existence in the developing fat and highlight its unique gene expressions pattern of the developing fat depots.

Beige adipocytes household a high amount of mitochondria to perform fat-oxidation and thermogenesis. Mitochondrial danger signals can leak into the cytosol evoking inflammation and as a result triggering the loss of mitochondrial network. To keep the abundant mitochondrial content, we hypothesize that beige adipocytes suppress their innate immune mechanisms in favour to expand the mitochondrial network. Furthermore, we propose that re-establishing this mechanism in adults allows white adipocytes to be converted to infant-like beige adipocytes which may reduce obesity development.

Aim 3.

To test our hypothesis, we explored the transcriptional landscape of immune response related genes to find underrepresented immune-related hub genes in the infant adipose tissue. We further challenged infant and adult fat cells to detect possible differences in their innate immune response. Next, we aimed to reveal anti-inflammatory immune regulators differently expressed in adults and infants. We manipulated these regulators *in vivo* and *in vitro* to treat diet-induced obesity.

Aim 4.

Lastly, we revealed the signals which allow mitochondrial network expansion. Therefore, this work aimed to highlight the importance of that signal regarding early adipose tissue development and obesity protection.

2. Materials and methods

2.1. Materials

2.1.1. List of Equipment

Equipment	Supplier
BGISEQ-500 platform	BGI Genomics Inc.
Bürker cell counting chamber	Marienfeld GmbH
camera MC190 HD	Leica
cell culture flask (T-25, T-75)	Thermo Fisher Scientific
centrifuge 5423R and 5810R	Eppendorf
coverslips 24 x 60 mm	Herenz
culture plates (6, 24 wells)	Thermo Fisher Scientific
Eppendorf tubes (1.5, 2ml)	Thermo Fisher Scientific
FACS analysis	BD LSR II cytometer
Falcon™ tubes (15, 50 ml)	Thermo Fisher Scientific
Falcon™ cell strainer (40 µm)	Thermo Fisher Scientific
freezer (8, -20 °C)	Liebherr
homogenizer MagNA Lyzer	Roche
humidity chamber	Sigma-Aldrich
incubator HeraTherm	Thermo Fisher Scientific
incubator Incubat (for ELISA)	Melag
Isotemp® freezer (-80 °C)	Thermo Fisher Scientific
laminar flow hood BioAir	EuroClone
light microscope 61717192	Motic
light microscope Olympus CKX53	Olympus
MicroAmp® optical 96-wells reaction plate	Thermo Fisher Scientific
MicroAmp® optical adhesive film	Thermo Fisher Scientific
microscope glass slides	Herenz
microscope slides Polysine® slides	Thermo Fisher Scientific
microtome	Pfm Medical

Equipment	Supplier
Nanodrop 2000	Thermo Fisher Scientific
PHOmo photometer	Anthos
Pipette Boy (Easypet 3)	Eppendorf
pipettes (10, 200, 1000 µl)	Thermo Fisher Scientific
plastic chambers for staining	DiaPath
QuantStudio 3 Real-Time PCR systems	Thermo Fisher Scientific
serological pipette (5, 10 ml)	Thermo Fisher Scientific
tubes with 1.4 ceramic beads	Thermo Fisher Scientific
Vilber Fusion FX6 Edge	Vilber
water bath Isotemp™ GPD02	Thermo Fisher Scientific

2.1.2. List of Softwares

Software	Supplier
AUTOsoft	Autobio Co. LTD
clustered image maps	CIM-Miner, Heatmapper
DEseq2 algorithm	Love et. al. 2014 (99)
EnrichR	Kuleshov et. al. 2016 (100)
Fusion FX6 Edge	Vilber
GraphPad Prism 5	GraphPad Software Inc.
ImageJ	NIH (101)
Interferome-2.0	Rusinova et. al. 2013 (102)
Leica Application Suite X	Leica
Leica Application Suite Z	Leica
Microsoft Office 365	Microsoft
NanoDrop 2000/2000c	Thermo Fisher Scientific
NGS Analysis Software	BGI Genomics Inc.
Olympus cellSense Entry	OLYMPUS
Panther	Mi et. al. 2013 (103)
QuantStudio™ Design & Analysis Software	Thermo Fisher Scientific
SMART Servier Medical Art	Servier (104)
STRING	ELIXIR's

2.1.3. List of chemicals

Chemical	Supplier
10x PBS	Sigma-Aldrich
absolute ethanol (100%)	Thermo Fisher Scientific
acidified alcohol (30x)	Roth
agarose	Sigma-Aldrich
bovine serum albumin (BSA)	Sigma-Aldrich
calcitriol	Sigma-Aldrich
carbonyl cyanide m-chlorophenyl hydrazone (CCCP)	Sigma-Aldrich
cGAMP	Invivogen
chloroform	VWR
collagenase P	Sigma-Aldrich
CpG	Invivogen
DEPC treated water	Roth
dexamethasone	Sigma-Aldrich
Entellan®	Merck-Schuchardt
eosin	Sigma-Aldrich
ethanol (analytical graded)	Sigma-Aldrich
ethanol (molecular biology graded)	Thermo Fisher Scientific
FCS - extracellular vesicle-free (EV-free)	Gibco
fetal bovine serum (FBS)	Gibco
fetal calf serum (FCS)	Gibco
formula milk	Commercial brand
glacial acetic acid	Roth
glycogen (RNAse-free)	Thermo Fisher Scientific
Hanks´ balanced salt solution	Sigma-Aldrich
hematoxylin (Harris)	Sigma-Aldrich
HEPES buffer solution	Gibco
high fat diet	SSNIFF
High-Capacity cDNA Reverse Transcription Kit	Thermo Fisher Scientific
hydrogen peroxide	Thermo Fisher Scientific
IBMX	Sigma-Aldrich

Chemical	Supplier
insulin solution human	Sigma-Aldrich
isopropanol	VWR
L-15 medium (Leibovitz) with L-glutamine	Sigma-Aldrich
Lipofectamine 3000	Invivogen
Magnetofection™ (DogtorMag)	OZBIOSCIENCE
methyl green	Sigma-Aldrich
my Budget 5x EvaGreen® qPCR Mix II	Bio Budget Tech. GmbH
p(dA:dT)/LV	Invivogen
pCMV6	Sigma-Aldrich
penicillin/streptomycin	Sigma-Aldrich
periodic acid solution	Roth
pIpC/LV	Invivogen
rosiglitazone	Sigma-Aldrich
Schiffs reagent	Roth
sodium pyruvate solution	Sigma-Aldrich
TRI Reagent® (tissue, cultured cells)	Sigma-Aldrich
TRI Reagent® LS (fluid samples)	Sigma-Aldrich
Triton™ X-100	Sigma-Aldrich
trypsin EDTA solution 10x	Sigma-Aldrich
TurboFect™	Sigma-Aldrich
Tween-20	Merck-Schuchardt
VACV/LV	Invivogen
antigen unmasking solution (Citrate-based)	Vector Laboratories
ImmPACT DAB Substrate (Peroxidase, HRP)	Vector Laboratories
vitamin D3	Sigma-Aldrich
xylene	VWR

2.1.4. List of Kits

Kit	Supplier
Cell Meter Autophagy Fluorescence Imaging kit	AAT Bioquest
Caspase-Glo® 1 Inflammasome Assay	Promega
Exosome Precipitation Solution Kit	Immunostep
MitoTracker Dyes	Thermo Fisher Scientific
MitoBiogenesis™ Flow Cytometry Kit	Abcam
Mitochondria Isolation Kit For Tissue	Thermo Fisher Scientific
MitoThermo Yellow	Chrétien et. al. 2018
Mouse TNFa ELISA Kit	BD Biosciences
Mouse VDR ELISA Kit	MybioSource
Mouse Vitamin D3 ELISA Kit	MybioSource

2.1.5. Antibodies

Table 1: Antibodies used in the thesis for protein detection

Target	Class, Host, Company
anti-rabbit IgG (H+L)	polyclonal, HRP-conjugated, goat, Invitrogen, Carlsbad, CA
anti-rabbit IgG (H+L)	polyclonal, Alexa Fluor® 488, goat, Invitrogen, Carlsbad, CA
CD11b	Monoclonal, rat, ThermoFisher Scientific, Rockford, IL
F4/80	Polyclonal, rabbit, Santa Cruz Biotechnology Inc., Dallas, TX
GABA-A receptor	Polyclonal, rabbit, Alomone Labs, Jerusalem, Israel
h/m AIM2	Polyclonal, rabbit, Sino Biological, Eschborn, Germany
h/m DDX41	Polyclonal, rabbit, Sino Biological, Eschborn, Germany
h/m p204 (IFI16)	Polyclonal, rabbit, Novus Biologicals, Denver, CO
h/m UCP1	Polyclonal, rabbit, ThermoFisher Scientific, Rockford, IL
h/m ZBP1	Polyclonal, rabbit, Sino Biological, Eschborn, Germany
J2 (dsRNA)	Monoclonal, rabbit, Absolute Antibody, Wilton, UK

2.1.6. Primers

Table 2: Mouse primer pairs for RT-qPCR

Target gene	Forward (fw) and Reverse (rev)	Primer sequence (5´-3´)
Bactin	FW	GCACCAGGGTGTGATGGTG
	REV	CCAGATCTTCTCCATGTCGTCC
Ppia	FW	ATTTCTTTTGACTTGCGGGC
	REV	AGACTTGAAGGGGAATG
Gapdh	FW	TGACGTGCCGCCTGGAGAAA
	REV	AGTGTAGCCCAAGATGCCCTTCAG
Aim2	FW	GATTCAAAGTGCAGGTGCGG
	REV	TCTGAGGGTTAGCTTGAGGAC
Ddx41	FW	ACAGGAGAAGCGGTTGCCTTTC
	REV	GACGGCAGTAATACTCCAGGATG
Ifi204	FW	CAGGGAAAATGGAAGTGGTG
	REV	CAGAGAGGTTCTCCCGACTG
Ifi205	FW	CAAGCAGGCCACTTCTGTTG
	REV	TCAAACGGGTCTGTTGCAGT
Zbp1	FW	AACCCTCAATCAAGTCCTTTACCGC
	REV	TCTTCCACGTCTGTCCGTCATAGCT
Tmem173	FW	GGGCCCTGTCACTTTTGGTC
	REV	GAGTATGGCATCAGCAGCCAC
Irf7	FW	CGACTTCAGCACTTTCTTCCGAGA
	REV	AGATGGTGTAGTGTGGTGACCCTT
Il6	FW	GCTACCAAACTGGATATAATCAGGA
	REV	CCAGGTAGCTATGGTACTCCAGAA
Ifnb	FW	CCAGCTCCAAGAAAGGACGA
	REV	CGCCCTGTAGGTGAGGTTGAT
Tnfa	FW	TGCCTATGTCTCAGCCTCTTC
	REV	GAGGCCATTTGGGAACTTCT
Ifna	FW	TGAAGGACAGGAAGGACTTTG
	REV	GAATGAGTCTAGGAGGGTTGT
Ucp1	FW	CCTGCCTCTCTCGGAAACAA
	REV	CTGTAGGCTGCCCAATGAAC
Ppargc1a	FW	GACTCAGTGTCACCACCGAAA
	REV	TGAACGAGAGCGCATCCTT
Cox7a1	FW	ATGAGGGCCCTACGGGTCTC
	REV	CATTGTCGGCCTGGAAGAG
Cidea	FW	TACTACCCGGTGTCCATTTCT
	REV	ATCACAACTGGCCTGGTTACG
Dio2	FW	GTCCGCAAATGACCCCTTT
	REV	CCCACCCACTCTCTGACTTTC

Target gene	FW and REV	Primer sequence (5´-3´)
Cyp27b1	FW	AGCTCCTGCGACAAGAAAGT
	REV	ATTCTTCACCATCCGCCGTTA
Vdr	FW	ACTTTGACCGGAATGTGCCT
	REV	CATGCTCCGCCTGAAGAAAC

Table 3: Mouse primers for the detection of mitochondrial DNA

Target gene	FW and REV	Primer sequence (5´-3´)
Nd1	FW	GCTTTACGAGCCGTAGCCCA
	REV	GGGTCAGGCTGGCAGAAGTAA
16S	FW	ACACCGGAATGCCTAAAGGA
	REV	ATACCGCGGCCGTTAAACTT
12S	FW	ACACCTTGCCTAGCCACACC
	REV	GTGGCTGGCACGAAATTTACCA
D-loop	FW	AATCTACCATCCTCCGTGAAACC
	REV	TCAGTTTAGCTACCCCCAAGTTTAA
Cytb	FW	TCCTTCATGTCGGACGAGGC
	REV	AATGCTGTGGCTATGACTGCG
Atp6	FW	AGCTCACTTGCCCACTTCCT
	REV	AAGCCGGACTGCTAATGCCA
Nd5	FW	GGCCCTACACCAGTTTCAGC
	REV	AGGGCTCCGAGGCAAAGTAT
Co1	FW	TCAACATGAAACCCCCAGCCA
	REV	GCGGCTAGCACTGGTAGTGA

Table 4: Mouse primers for the detection of mitochondrial RNA

Target gene	FW and REV	Primer sequence (5´-3´)
28S (Rn28s)	FW	CAGGGGAATCCGACTGTTTA
	REV	ATGACGAGGCATTTGGCTAC
18S (Rn18s)	FW	CGCGGTTCTATTTTGTTGGT
	REV	AGTCGGCATCGTTTATGGTC
16S	FW	GACTTCACCAGTCAAAGCGA
	REV	ACATCGAGGTCGTAAACCCT
12S	FW	ACTGCTCGCCAGAACACTAC
	REV	GGTGAGGTTGATCGGGGTTT
ND1	FW	GCAGCCGCTATTAAAGGTTCG
	REV	TATCATTTACGGGGGAAGGCG
ND5	FW	TATGTGCTCCGGGTCCATCA
	REV	CTGCTAATGCTAGGCTGCCA
CO1	FW	TCAGGCTACACCCTAGACCA
	REV	CCGGATAGGCCGAGAAAGTG
CYTB	FW	AACTTCGGCTCACTCCTTGG
	REV	CTCGAGTGATGTGGGCGATT

2.2. Methods

2.2.1. Animal and cell samples

C57BL/6 (Charles River Laboratories, Wilmington, MA, USA) mice were used as wild-type (WT) animals and accommodated under pathogen free conditions. Additionally, we used and kept *Irf7*$^{-/-}$ (RIKEN, Wako, Japan) animals under the same conditions. Under the approval of the local ethic commission, animal experiments were performed and registered. The isolation and culture of adipocytes from infant and adult inguinal adipose tissue through collagenase digestion and cell fraction separation was performed as described in previous studies (63, 105, 106). Magnetic bead cell purification with an anti-F4/80 antibody was performed to isolate adipose tissue macrophages (ATMs) from the stromal vascular fraction (SVF) (107). Isolated preadipocytes were maintained in 20 µg/ml insulin-supplemented L-15 Leibovitz cell culture medium (10 % fetal calf serum (FCS), 1 % penicillin/streptomycin, 1% pyruvate and 1 % L-glutamine). White adipogenic differentiation of preadipocytes were induced through 50 µm IBMX, 1 µM dexamethasone, 1 µM rosiglitazone and 20 µg/ml insulin, according to a previous study (63). Obtained from the ATCC (Sigma-Aldrich), 3T3-L1 preadipocytes were maintained, as described (108).

2.2.2. Cell culture treatments

In vitro treatments were performed on the immortalized 3T3-L1 cell line and isolated adipocytes from infants and adults. Cells were seeded in 6- or 24-well plates until the confluency of 80-90% was achieved. Cells were treated with pCMV6, poly(deoxyadenylic-deoxythymidylic) acid sodium salt (p(dA:dT)), polyinosinic-polycytidylic acid (p(I:C)), mitochondrial RNA (mtRNA), mitochondrial DNA (mtDNA) or carbonyl cyanide m-chlorophenyl hydrazone (CCCP). Treatment time and dose are indicated in the respective figure legends.

2.2.3. Histology and image analysis of adipose tissues

Adipose tissue samples taken from the inguinal (iAT) and interscapular brown (BAT) region were fixed in 4 % paraformaldehyde. After fixation of tissues, samples were embedded in paraffin and processed as described (3). Adipose tissue-containing paraffin sections were stained with haematoxylin-eosin (H&E) or periodic acid Schiffs (PAS)-reagent. In addition, UCP1 and GABA-A receptor immunohistochemistry staining were performed on adipose tissue paraffin sections. J2 (dsRNA), AIM2, DDX41, p204 and ZBP1 immunohistochemistry were detected through antibodies against the respective target in isolated infant and adult adipocytes. The list of antibodies is illustrated in Table 1. Autophagosomes were labelled using Cell Meter Autophagy Fluorescence Imaging Kit and further visualized under the fluorescence microscope.

2.2.4. Flow cytometry analysis

Isolated ATMs were marked through incubation with antibodies against CD11b and F4/80 antigen. $CD11b^+$ and $F4/80^+$ immune cells were analysed through fluorescence associated cell sorting (FACS) performed on a BD LSR II cytometer (107). FACS analysis of mitochondrial biogenesis, content and uncoupling were performed by the use of MitoTracker dyes (mitochondrial content), Mitobiogenesis™ Flow Cytometry Kit (mitobiogenesis) and MitoThermo Yellow (mitochondrial uncoupling, thermogenesis), as described (93, 109, 110). Therefore, succinate dehydrogenase complex flavoprotein subunit A (SDH-A) was labelled after mtRNA transfection to measure by FACS the mitobiogenesis. In addition, Flow Repository identifiers of raw FACS data are highlighted in the publication or manuscript, respectively (43, 93).

2.2.5. Analysis of RNA and next generation sequencing

Total RNA extraction was performed as indicated in previous studies (63, 105). The quality of the RNA isolated from the whole cell was determined by the integrity of ribosomal RNAs which were labelled in a denaturing gel electrophoresis. Reverse transcription quantitative PCR (RT-qPCR) assays were done on the Quantabio platform and *Bactin*, *Gapdh* and *Ppia* (*CycloA*) were used as reference genes (63). Samples used for the RT-qPCR assays are homogenized fat tissues, cell culture from the immortalized cell line and isolated preadipocytes. Primer sequences of the

respective target genes are highlighted in Table 2. Furthermore, primer pairs to identify mtDNA species are shown in Table 3 and primer pairs to discriminate mtRNA are presented in Table 4. PCR analysis of DNA-isolated samples or mtDNA detection in the respective matrices were performed as described in the preprint (93).

For the next generation sequencing (NGS) analysis the BGISEQ-500 platform was used which generated approximately 26.2 million reads per sample (43, 93). Sequencing reads were performed to exclude low-quality, adaptor-polluted and unknown base reads. Thereby, filtered clean reads could be mapped to the reference genome which was performed by the use of HISAT (43, 111) to show the comparability of the respective samples. Clean reads were further process through the mapping on Bowtie2, a reference transcript. In the following, a gene expression could be calculated for each sample by REM (112, 113). Additionally, sequencing data saturation analysis was applied to ensure that the depth of the data is enough for bioinformatic analysis. Due to the respective gene expression levels and the application of the DEseq2 algorithm, we could determine differentially-expressed genes (DEGs) among sample groups (99).

Gene Ontology (GO) classification and functional enrichment were used to identify biological functions, pathways, and biological processes. EnrichR, Panther and Interferome-2.0 generated annotations of transcripts which revealed enrichment of predicted transcription factor sites and additional pathway analysis (43, 100, 102, 103). CIM-Miner and Heatmapper were used to create clustered image maps (CIMs, heat-maps). STRING Functional Protein Associations Network was used to develop interactome maps of the DEGs (114). Raw NGS data are saved and accessible as indicated by in the publication (43) or preprint (93).

2.2.6. Mitochondrial RNA and DNA isolation and their transfection *in vitro*

Mitochondria were isolated from adipocytes through a commercial mitochondria isolation kit which uses a reagent-based method. Therefore, a mitochondria pellet could be achieved. An aliquot of that pellet was checked according to functionality and integrity of the isolated mitochondria by MitoTracker Red labelling and FACS analysis. Afterwards, TRI Reagent was applied to the mitochondria pellet to isolate mtRNA and mtDNA. TRI Reagent-based phase separation allows the isolation of mtRNA and mtDNA from the same mitochondria pellet. The procedure of RNA isolation was identical as previously described (63, 105). DNA pellet from the mitochondria needed

to be reconstituted in TE buffer (10 mM TRIS-HCL, 1 mM EDTA, pH 8.0). The transfection of 2 µg/ml mtRNA or mtDNA was performed on 3T3-L1 cells and P6 or P56 adipocytes. The confluency of cells was 80-90%. Cells were seeded in 6- or 24-well cell culture plates. Lipofectamine 3000 was used as a mtRNA transfection reagent with a 1:3 ratio. TurboFect™ was used to introduce mtDNA into the cells. Control cells were treated with the respective cargo-free transfection reagent. Cells were harvested after 18 hours of treatment for further analysis.

2.2.7. Extracellular vesicle isolation of culture media, breast, and formula milk

EVs were isolated from commercially available cattle milk-based formula. Throughout the study, EV-depleted FCS was used to avoid bovine EV contamination. EVs were collected through precipitation by the use of EPStep exosome precipitation solution. Concentrated EV pellets were checked for diameter and area by ImageJ (NIH), and EV classification were performed according to their morphology and electron density as described by others (115, 116). EVs were used to as a treatment *in vitro* or analysed to detect mtRNA and mtDNA species as described in the preprint (93).

2.2.8. ELISA assays

After recording the weight, tissue samples were homogenized in RIPA buffer using ceramic beads and the MagNA Lyzer at 4000 rpm for 1 min. Cell culture supernatants were centrifuged at 0.8 g for 10 min and cell debris-free supernatants were further analysed to measure the protein level of vitamin D3 (Vit-D3) and vitamin D receptor (VDR). In addition, infant adipocyte EVs were tested for Vit-D3. Upon the analysis, all samples were stored at -80°C to avoid protein degradation.

2.2.9. High fat diet feeding and *in vivo* mtRNA transfection

Rodent high fat diet (HFD) was used in the HFD feeding of mice including dams with litters P6 to P9 and mice at P28 for 12 weeks. Vit-D3 was supplemented in the diet and mtRNA was transfected with Magnetofection™ for 14 days *in vivo*. Therefore, mtRNA was packed mixed with *Dogtor* and combined with *CombiMag* to generate mtRNA-containing magnetizable nanoparticle complexes. Upon injection to the inguinal adipose tissue, a magnet is placed closely to the injection point to concentrate and enrich the mtRNA transfection on the desired location as described (117).

2.2.10. Statistics and Data representation

Data of gene expressions are illustrated as mean ± s.e.m. in bar graphs or with each individual data point. Gene transcription differences between samples were visualized, through transcript levels relative to the reference gene or to the relative abundance of the respective transcripts. Uniquely expressed genes of the respective sample groups were highlighted by Venn diagrams. Venn diagrams also allows to visualize number of genes which are restricted to a given sample or expressed in various sample groups. In addition to the Venn diagram, volcano and scatter plots were applied as well to illustrate the number of DEGs in the multiple sample groups. Regarding the volcano plots, the X-axis shows the $\log_2$ transformed fold change of DEGs, while the Y-axis illustrates the $-\log_{10}$ transformed significance. Scatter plots were generated with an X-axis showing the value A ($\log_2$ transformed mean expression level) and a Y-axis highlighting the vale M ($\log_2$ transformed fold change). Within the scatter plots, blue dots represent the downregulated DEGs, red dots indicate upregulated DEGs and gray dots show non-DEGs. Data illustrated as CIMs show gene transcription differences and they include either Z-scores of the relative abundance or fold change. Applied statistical tests were highlighted and described in the legends of the respective figures.

3. Results

3.1. The P6 adipose tissue is rich in beige adipocytes in mouse

Due to the paucity of information of beige adipocytes development in early life, we first aimed to define whether beige adipocytes naturally exist in the early postnatal life. Fat depots develop before birth in human, however in mouse the subcutaneous fat depot expands from birth to weaning age. In contrast, BAT depots are already established at birth in both human and mouse. We studied inguinal adipose tissue (iAT) of mice in the early postnatal life (postnatal day 6) and in adulthood (postnatal day 56). At postnatal day 6 (P6), iAT is already well-developed in mice, allowing us to collect sufficient sample size for analysis. Furthermore, at P6 the milk spot starts to disappear which is an indicator for proper breastfeeding and a healthy development of the young animal (118), and there is proper nutritional supply from breastfeeding allowing adipocyte development (63). P56 animals were mature adults, which are often used in age-dependent studies (119).

First, we tried to identify if P6 animals had beige adipocytes, we checked the morphology of P6 and P56 iAT and compares them to their respective BAT counterparts by hematoxylin and eosin (H&E) staining (Figure 1A). It is known that thermogenic fat is built up from multilocular adipocytes, which store neutral lipids in multiple lipid droplets (38, 39). In contrast to that WAT adipocytes, which store neutral lipids in a large lipid droplet (unilocular) for later demands such as starvation (15). As a next step, we detected uncoupling protein 1 (UCP1) in the fat depots, using immunohistochemistry. UCP1 expression is a hallmark of thermogenic (beige and brown) fat cells.

We found numerous multilocular fat cells in P6 iAT, which were also strongly positive for UCP1. In turn, multilocular, UCP1^{+} adipocytes were lacking in P56 iAT (Figure 1B). A strong UCP1 expression was observed in BAT adipocytes in both age groups (Figure 1B). Thermogenic adipocytes store glycogen and use it as a lipogenic substrate. Accordingly, we found that P6 iAT, P6 and P56 BAT adipocytes were stained positively for cytoplasmic glycogen granules by periodic acid Schiff (PAS) staining. Especially the multilocular adipocytes had an intense PAS staining, which is in agreement with previous findings (92, 120).

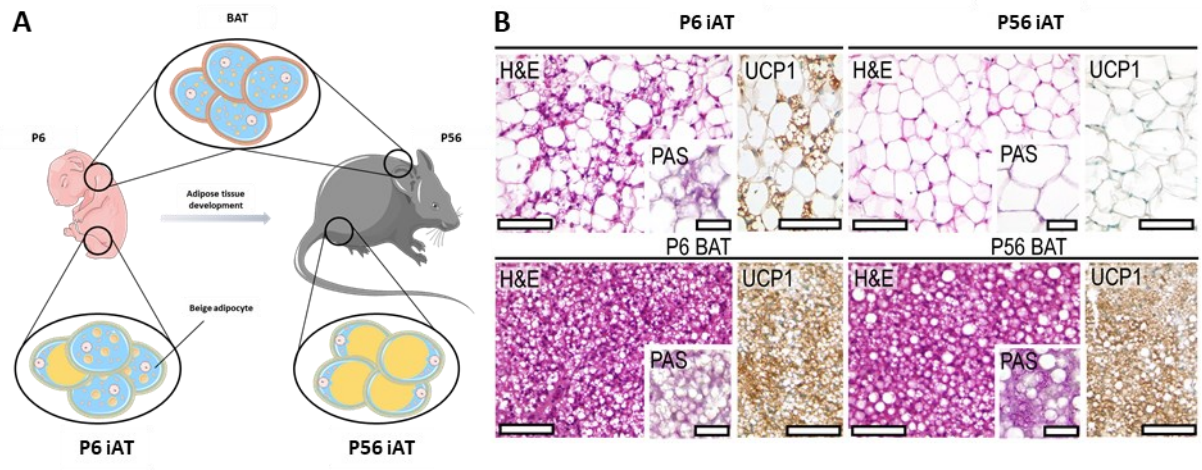

Figure 1: Anatomy and histology of iAT in young and adult mice.

(A) Scheme of the anatomical location of iAT and BAT in P6 and P56 animals. (B) Hematoxylin-eosin (H&E) staining and UCP1 immunostaining of BAT and iAT at P6 and P56. Inlets show periodic acid Schiff staining (PAS). Scale bars: 50 µm. Source: Figure from (43), reused under license CC BY 4.0 (https://creativecommons.org/licenses/by/4.0/).

Based on these histological observations, we could conclude that P6 iAT had both uni- and multilocular adipocytes. Therefore, it could not be defined as WAT or BAT. Although P6 iAT was located in the same body region as P56 iAT (Figure 1A), it shared features with the interscapular BAT, such as glycogen storage and UCP1 expression.

Besides these morphological differences, we also highlighted similarities and unique expression patterns among P6 iAT, P6 BAT, P56 iAT and P56 BAT. We used NGS analysis on the BGISEQ-500 platform to generate “raw” sequencing reads. After, filtering the sequencing reads to create clean reads, the quality of clean reads were checked through HISAT (111). Clean reads were normalized to the reference sequence by Bowtie2 and the level of gene expression for each sample was generated through REM (112, 113). After another quality check, differently-expressed genes (DEGs) were identified by the use of the DEseq2 algorithm for each sample group (99).

Furthermore, through the expression level of all samples we could perform a hierarchical clustering analysis. The analysis reveals that the transcriptional landscape of P6 iAT and P56 BAT were the most distinct from each other (43). This was surprising due to the fact that both tissues expressed UCP1 and consisted of multilocular adipocytes (Figure 1B). Beige adipocytes visibly occurred in early life and their transcription pattern did not resemble neither P6 BAT, P56 iAT or P56 BAT. Hence, it was highly interesting to further define gene networks and pathways unique to P6 iAT.

3.2. Differentially-expressed genes of adipose tissues in P6 and P56 mice

First, we sought to identify unique genes which are expressed differently in P6 and P56 iAT, allowing us to define genes and gene networks that are necessary for adipose tissue functioning after birth. Moreover, this analysis also allowed us to define genes involved in adipose tissue maturation.

Pairwise comparison of P6 iAT with P56 iAT and P6 BAT with P56 BAT was performed to identify DEGs (Figure 2A,B). DEGs were illustrated as a volcano plot and the most over- and underrepresented genes were shown. A comparison between P6 and P56 iAT revealed that 3398 DEGs were overrepresented, while 1782 DEGs were underrepresented in P6, when it was compared to P56 iAT (Figure 2A). Thereby, the most overrepresented gene at P6 was keratin 5, which was encoded by *Krt5*. Interactome analysis shows *Krt5* as a core gene for three gene networks (cadherin, caveolin-3 and keratin networks). Genes from these networks are involved in the vinculin binding and cell-cell-adhesion according to their gene onthology (GO) analysis (43). The most underrepresented gene in P6 iAT was major urinary protein 2 encoded by *Mup2* (Figure 2A). *Mup2* is a core gene involved in the gene network of steroidogenesis (43).

Seeing these gene expression differences appearing during iAT development, we asked whether BAT development was associated with similar chenges. We next analyzed the transcriptome of BAT at P6 and P56 (Figure 2B). Therefore, we identified 2437 overrepresented DEGs and 1230 underrepresented DEGs in the developing BAT compared to P56 BAT. Regarding the overrepresented DEGs, angiotensin II receptor type 2 (*Agtr2*) had the highest abundance. Among the underrepresented DEGs in P6 BAT, *H2-Q9* had the lowest abundance (Figure 2B). This gene encodes a a member of the H-2 and class I histocompatibility antigen network, whereas *Agtr2* is associated with multiple networks including the network of chemokine ligands (CCLs), the network of CXC chemokine receptors (CXCRs) and certain components of the angiotensin- and kininogen-signaling (43).

Next, we aimed to define the extenct of similarity beween iAT and BAT, the “bona fide” thermogenic fat depot. We compared DEGs of BAT and iAT. Therefore, we initiated a third assay by comparing BAT and iAT at P6 (Figure 2C). P6 BAT had 1183 DEGs overrepresented and 1827 DEGs underrepresented, when it was compared to

P6 iAT. The strongest expression was *Ucp1*, the major thermogenic gene transcript. *Ucp1* encodes UCP1 which was also detetcted in P6 iAT and BAT by immunostaining (Figure 1A). The most underrepresented DEG in this comparision was keratin 71 encoded by the gene *Krt71* (Figure 2C). *Krt71* belongs to the network of keratins which members are associated with keratin filament binding and bioactive lipid receptor activity according to the GO analysis (43).

In the final assay, we compared BAT and iAT of P56 and could reveal 1641 overrepresented, and 2321 underrepresented DEGs in P56 BAT (Figure 2D). Fatty acid-binding protein 3 (*Fabp3*) was the most overrepresented DEG. *Fabp3* belongs to the *Fabp3* network which has functions in fatty acid transport and lipid catabolism (43). Among the underrepresented DEGs, glycosylation-dependent cell adhesion molecule 1 (*Glycam1*) had the lowest abundance (Figure 2D). *Glycam1* is a pseudogene of the innate immune system and belongs to the network of genes associated with leukocyte tethering and adhesion (43).

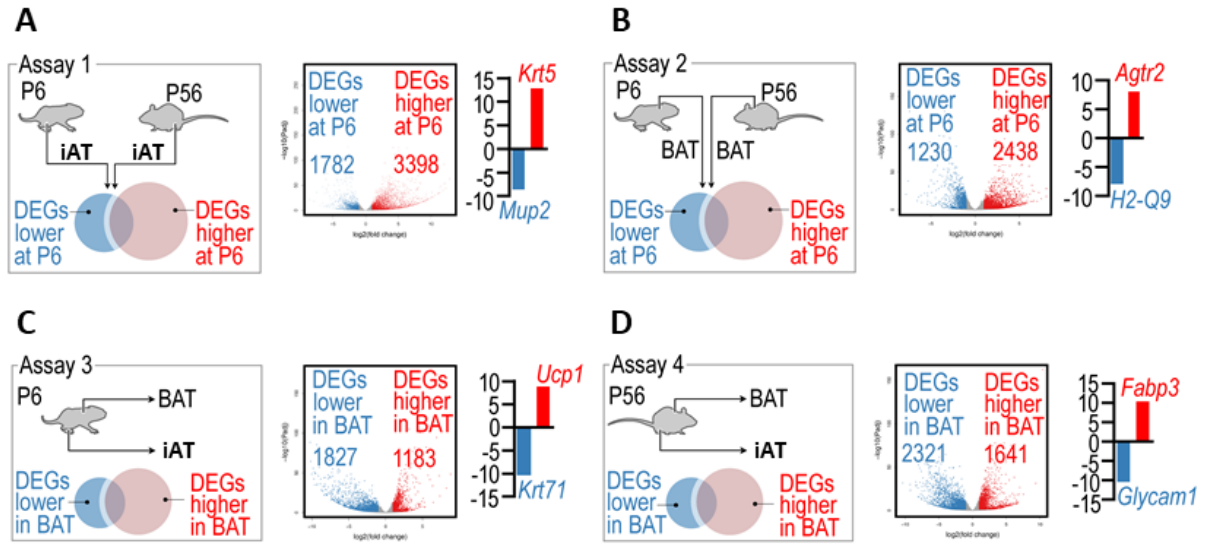

Figure 2: Assays to compare DEGs in different adipose tissues of both age groups

(A) Assay 1: P6 and P56 iAT expression profile comparison with corresponding volcano plot. (B) Assay 2: P6 and P56 BAT expression profile comparison with corresponding volcano plot. (C) Assay 3: P6 BAT and iAT expression profile comparison with corresponding volcano plot. (D) Assay 4: P56 BAT and iAT expression profile comparison with corresponding volcano plot. Source: Figure from (43), reused under license CC BY 4.0 (https://creativecommons.org/licenses/by/4.0/).

These results suggested the existence of thermogenic (UCP1$^+$) fat cells in the iAT of young mice. UCP1$^+$ adipocytes develop from at least two cell lineages, which are often described as “classical brown” and “beige” adidpoyte lineages. The former builds BAT in mouse, while the latter gives rise to induced BAT or beige/brite fat cells within WAT depots during adaptive thermogenesis. These two forms of thermogenic fat have their distinct transcriptional landscapes (43), hence as a next step, we asked whether iAT at P6 expressed BAT-like or beige-like gene networks. Therefore, we analyzed further classical brown, and beige marker genes in all fat depots.

3.3. Beige marker gene transcription in P56 brown- and P6 adipose tissue.

Adipose tissue challenged with cold led to the discovery of brown and beige marker genes which was achieved by transcriptional profiling (43, 60, 62). In mammals, *Ucp1* is one of the most important thermogenic genes which was expressed abundantly in BAT of both age groups. Compared to BAT, iAT expressed less *Ucp1*, but a reasonable amount of the transcript could be detected in P6 iAT (Figure 3A).

Another strongly expressed gene in both BATs is peroxisome proliferator-activated receptor gamma coactivator 1α (*Ppargc1a* or *Pgc1a*), a crucial mitobiogenesis gene, which was moderately and similarly expressed in iAT of P6 and P56 mice (Figure 3A). After chemical or cold exposure, brown-like adipocytes appear within the WAT, genes which support this process are termed “browning” genes. (121, 122). These genes, such as cell death inducing DFFA like effector A (*Cidea)*, cytochrome c oxidase subunit 7A1 (*Cox7a1*) and iodothyronine deiodinase 2 (*Dio2*) (121), were plentifully expressed in P56 BAT and less prevalently in the infant BAT. In relation to BAT, iAT in both age groups hardly expressed these genes. Interestingly, a higher level of *Dio2* could be measured in P6 iAT compared to P56 iAT (Figure 3A).

Besides *Ucp1* and brown marker genes, we also investigated beige marker genes, such as transmembrane protein 26 (*Tmem26*) and T-box transcription factor 1 (*Tbx1*) (66). As we wanted to test the possibility that P6 iAT accommodated beige adipocytes, we measured *Tmem26* and *Tbx1* which were abundantly expressed in the young iAT (Figure 3A). Adult iAT could also express these genes, however, not as strongly as in P6 iAT. Interestingly, P6 BAT had a low expression of both beige genes,

whereas P56 BAT failed to express *Tmem26* and *Tbx1*. Therefore, we could see *Tmem26* and *Tbx1* as unique hallmark genes for P6 iAT (Figure 3A).

Next, we were investigating BAT and WAT markers in the given adipose tissues. Eva-1 homolog A (*Eva1a*) was described in previous studies as a BAT marker gene (66, 123). As expected, it was present in P6 BAT and P56 BAT (Figure 3B). P6 iAT was able to express *Eva1a* at the same level as both BAT tissues, whereas *Eva1a* level was significantly lower in P56 iAT compared to the other adipose tissues. According to that, this gene can be seen as a BAT and P6 iAT marker.

In the following, we checked mRNA level of myogenic factor 5 (*Myf5*) in adipose tissues of P6 and P56. *Myf5*$^{+}$ cells are progenitors of BAT adipocytes (71). *Myf5* was highly expressed in P6 BAT and less expressed in both adipose tissues at P56 (Figure 3B). In addition to that, P6 iAT expressed a significantly higher level of *Myf5* level compared to P56 iAT. We investigated further other BAT marker genes, such as LIM homeobox 8 (*Lhx8*) which was expressed abundantly in P6 BAT, similarly to *Myf5*. *Lhx8* could be also expressed in P56 BAT but not as strong as in P6 BAT. Inguinal AT of both age groups repressed *Lhx8* compared to BATs. As mentioned before, many BAT and beige markers were discovered after cold induction of mice, one of them is encoding zinc finger protein 1 (*Zic1*) (66, 124). *Zic1* was highly expressed in P6 and P56 BAT and minimally expressed in iAT of young and old animals (Figure 3B). Nevertheless, P6 iAT was able to express more *Zic1* than P56 iAT.

Lastly, we examined WAT marker genes from the homeobox family, such as *Hoxc8* and *Hoxc9* which have an increasing expression level during WAT differentiation (66). As expected, both genes were abundantly expressed in iATs, whereas BATs had a minimal *Hoxc8* and *Hoxc9* expression (Figure 3B).

Our previous study highlighted that ether lipids, known as alkylglycerols (AKGs), assist beige adipogenesis in the subcutaneous adipose tissue of young mice (63). AKGs can be degraded by AKG monooxygenase (AGMO) which is encoded by *Agmo*. Hence, *Agmo* expression acts against beige adipogenesis and supports fat maturation. By analysing adipose tissues for *Agmo*, we found that it was highly expressed in the adults regardless of adipose tissue type (Figure 3B). The highest *Agmo* level could be found in P56 iAT.

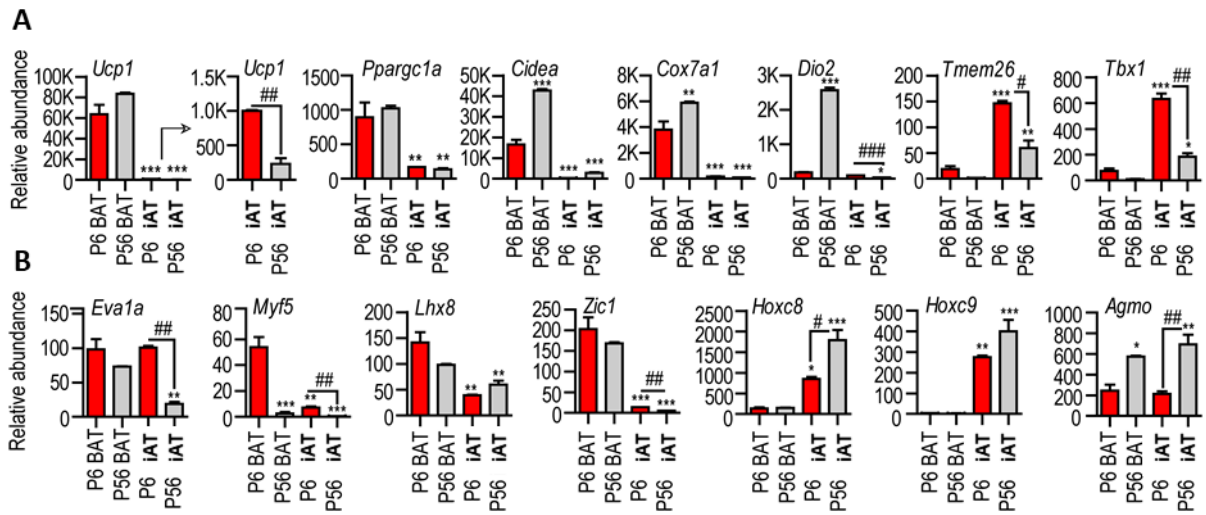

Figure 3: BAT and beige adipocyte defined marker genes in P6 and P56 fat depots

(A) Transcription level of nonshivering thermogenesis, mitobiogenesis and beige marker genes. Nonshivering thermogenesis requires *Ucp1*, mitobiogenesis is regulated by *Ppargc1a*. *Cidea*, *Cox7a1*, *Dio2*, *Tmem26* and *Tbx1* are marker genes for beige adipocyte development. (B) Transcription level of BAT and WAT marker genes. *Eva1a*, *Lhx8* and *Zic1* are BAT marker gene while *Myf5* is expressed by its progenitor adipocytes. *Hoxc8* and *Hoxc9* rise during adipocyte development of WAT. *Agmo* degrades alkylglycerols (AKGs) which is known to induce beige adipocyte lipid species. *Ucp1*: uncoupling protein 1, *Ppargc1a*: peroxisome proliferator-activated receptor gamma coactivator 1-α, *Cidea*: cell death inducing DFFA like effector A, *Cox7a1*: cytochrome c oxidase subunit 7A1, *Dio2*: iodothyronine Deiodinase 2, *Tmem26*: transmembrane protein 26, *Tbx1*: T-box transcription factor 1, *Eva1a*: eva-1 homolog A, *Myf5*: myogenic factor 5, *Lhx8*: LIM homeobox 8, *Zic1*: zinc finger protein 1, *Hoxc8/9*: homeobox C8/9, *Agmo*: AKG monooxygenase. Source: Figure from (43), reused under license CC BY 4.0 (https://creativecommons.org/licenses/by/4.0/).

In summary, P6 iAT was able to express specific white and brown marker genes nearly comparable to adult iAT and BAT. Additionally, beige marker genes were highly express in P6 iAT compared to the others. These results indicated that the subcutaneous fat depot was a BAT-independent thermogenic and fat-oxidizing adipose tissue in young developing mice. The loss of thermogenic fat cells may leads to childhood obesity, which was indicated through studies in a childhood obesity mouse model (63, 95) Hence, understanding differences and changes of beige adipocyte content within the developing adipose tissue was key to prevent childhood obesity. Our study highlighted beige adipocytes in P6 iAT and showed similar and unique transcriptional patterns of young iAT compared to the other adipose tissues. Next, we aimed to find shared gene networks to show similarities between adipose tissues.

3.4. Neuropeptide and GABA signaling in P56 brown- and P6 inguinal adipose tissue

Venn diagram of P6 BAT compared to P56 BAT revealed 203 unique transcripts in adult BAT, 1745 unique transcripts in P6 BAT and 16000 transcripts which were equally present in the two age groups (Figure 4). GO analysis of the unique transcripts of P56 BAT were associated with neuropeptide signaling pathways. The same analysis in P6 BAT highlighted genes related to chemical synaptic transmission.

By comparing P6 iAT and P6 BAT, GO analysis of overrepresented DEGs in P6 iAT were associated with neuropeptide signaling (Figure 5A) which could be also seen in P56 BAT (Figure 4). In detail, P6 iAT had overrepresented DEGs linked to pancreatic polypeptide (PP), neuropeptide Y (NYP) and gamma aminobutyric acid (GABA) receptor signaling.

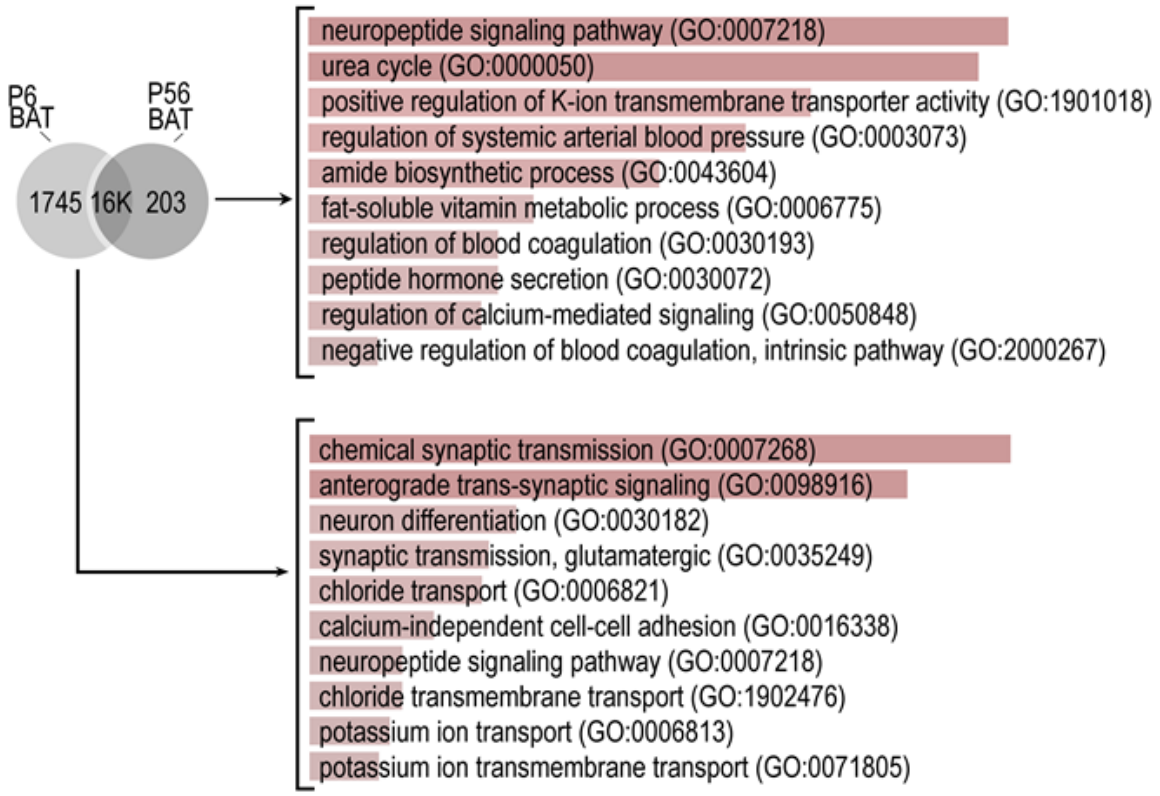

Figure 4: Gene ontology analysis of young and adult BAT

Venn diagram highlighting representative genes in infant and adult BAT. GO terms was performed with P6- and P56-specific transcripts. Source: Figure from (43), reused under license CC BY 4.0 (https://creativecommons.org/licenses/by/4.0/).

The same comparison in the adults revealed overrepresented DEGs from the GABA receptor signaling in P56 BAT. A comparison of P6 iAT with P56 iAT showed overrepresented DEGs from the GABA receptor signaling in P6 iAT. As mentioned before and supported by the following comparison, DEGs from the neuropeptide signaling were also overrepresented in P6 iAT compared to P56 iAT showing that P6 iAT and P56 BAT had the similar expression pattern regarding neuropeptide and GABA signaling.

These DEGs involved NPY (*Npy*) and its receptor, several genes form the GABA-A receptor signaling, PP receptors (*Npy2r*, *Npy4r* and *Npy6r*), neuropeptide B/W receptor (*Npbwr1*) and galanin (*Gal*). Like P56 BAT, P6 iAT overrepresented more DEGs involved in the GABA signaling compared to P56 iAT.

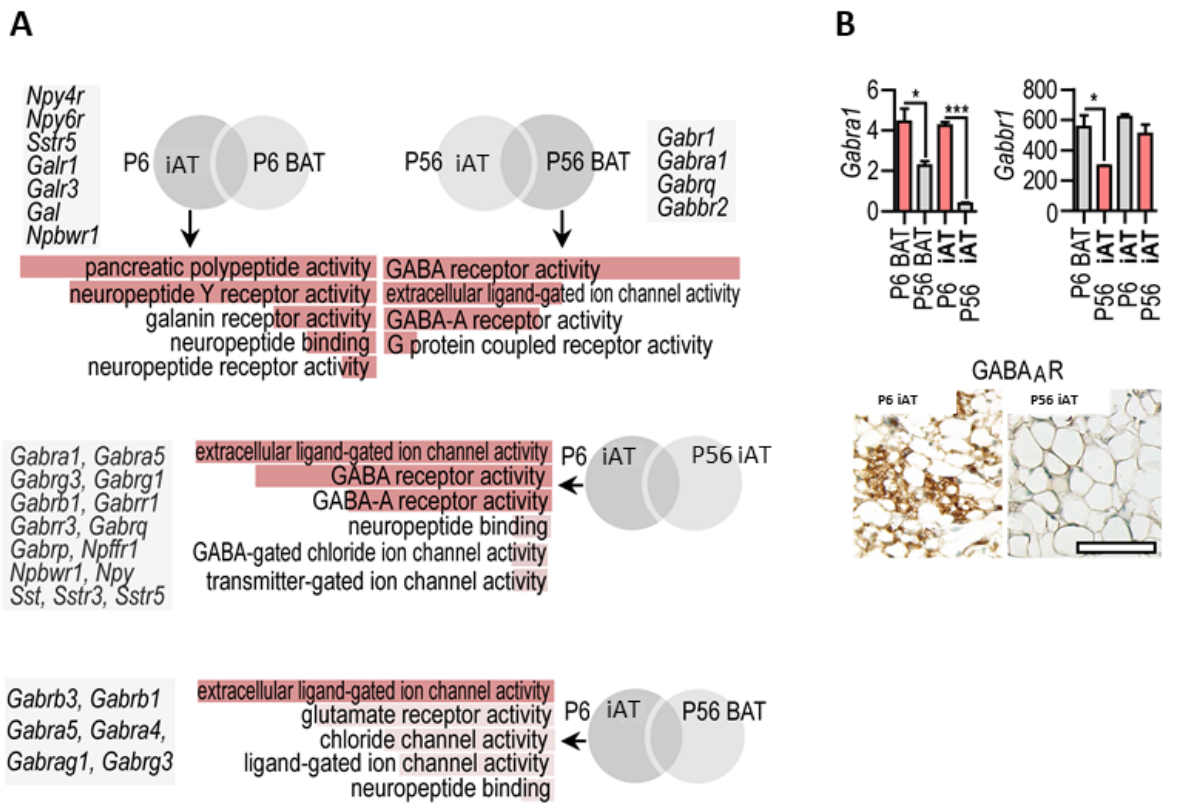

Figure 5: Signaling networks overrepresented in P56 BAT and in P6 iAT

(A) Distinct gene transcripts of P56 BAT and P6 iAT with the respective gene ontology (GO) analysis. (B) Left: GABA-A receptor encoded by the expression of *Gabra1,* and GABA-B-receptor encoded by the expression of *Gabbr1* in P6 and P56 adipose tissues. * $p < 0.05$, *** $p < 0.001$, Student´s two-tailed unpaired t-test. Right: GABA-A receptor immunostaining in iAT of P6 and P56, scale: 50 µm. Source: Figure from (43), reused under license CC BY 4.0 (https://creativecommons.org/licenses/by/4.0/).

Therefore, we sought to check *Gabra1*, encoding $GABA_AR$ (GABA-A receptor), and *Gabbr1*, encoding $GABA_BR$ (GABA-B receptor), expression in the respective tissues (Figure 5B). Irrespective from the adipose tissues, P6 animals expressed more *Gabra1* compared to their adult counterparts. This outcome was supported by $GABA_AR$ immunostaining of P6 and P56 iAT (Figure 5B). *Gabbr1* was equally expressed in infant and adult iAT but a comparison of P6 BAT with P56 iAT revealed more *Gabbr1* in the former mentioned one. The data underlined that GABA signaling was a specific BAT trait and P6 iAT was able to express the very same signaling showing that infant iAT had similarities in DEG overrepresentation to P56 BAT regarding neuropeptide and GABA signaling. To identify more gene networks associated with these signal pathways, we performed an interactome mapping of DEGs.

This analysis revealed that P6 iAT had another signaling pathway related to GABA receptor and G_0 protein-coupled neuropeptide receptor signaling. The related signaling pathway included genes from the NFκB-, signal transducer and activator of transcription 3 (STAT3)- and IRF-signaling. Due to their functions, GABA and neuropeptides might play a role in the anti-inflammatory or in the immune suppressive response towards NFκB-, STAT3- or IRF-induced inflammation in P6 iAT and P56 BAT (43, 125) (Figure 6A). To proof that possibility, we performed several GO analyses on P56 BAT. Therefore, we could show that DEGs related to NFκB signaling were underrepresented in adult BAT (Figure 6B).

Our results showed that P6 iAT shared many overrepresented DEGs with P56 BAT from several signaling pathways. While DEGs from the NFκB signaling, inflammatory genes and IFN-regulated genes were not prevalent in P56 BAT, P6 iAT overrepresented genes of the NFκB signaling (Figure 6A).

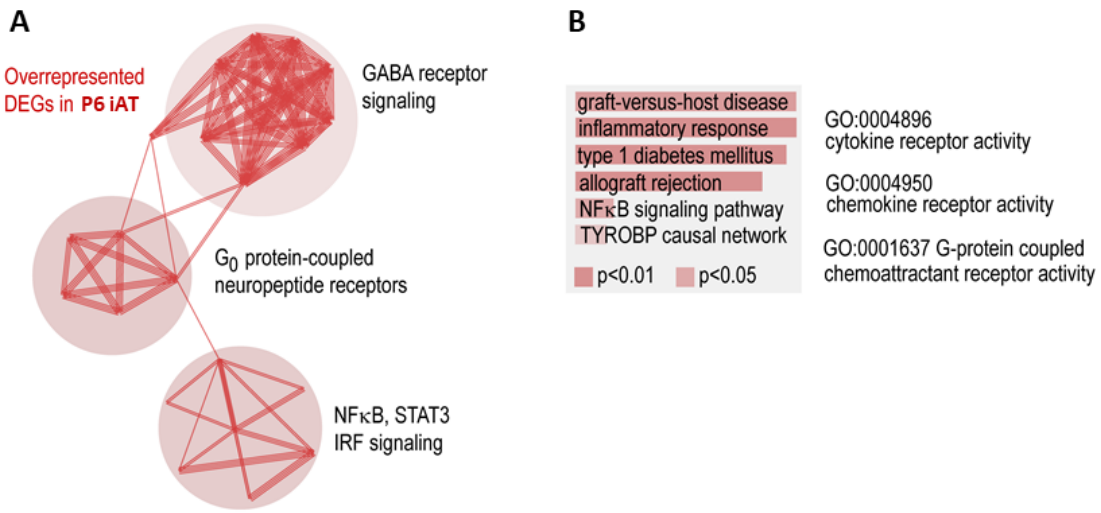

Figure 6: Difference in NFκB signaling-related gene expression in P6 iAT and P56 BAT.

(A) Interactome analysis of DEGs in P6 iAT highlighted three signaling pathways: GABA receptor, G_0 protein-coupled neuropeptide and NFκB signaling. PPI enrichment p-value < 1.0×10^{-16}. (B) Immune-related transcripts in P56 BAT regarding cellular and biological functions. p-values were combined and illustrated by colour code. TYROBP: TYRO protein tyrosine kinase-binding protein (transmembrane immune signaling adaptor). Source: Figure from (43), reused under license CC BY 4.0 (https://creativecommons.org/licenses/by/4.0/).

Due to the functional annotation of DEGs overrepresented in P6 iAT, we could indicate a possible inhibitory signaling of GABA and neuropeptides towards NFκB, STAT3 and IRFs (43). This might give GABA and neuropeptides an immune-suppressive or anti-inflammatory role in P6 iAT.

Since we wanted to identify beige adipocytes in P6 iAT, we tried to identify common and unique gene networks, distinguishing P6 iAT from the other adipose tissues. Inflammatory genes, ISGs and genes involved in the NFκB signaling were underrepresented in P56 BAT (Figure 6B), but overrepresented in P6 iAT (Figure 6A). This shows a marked difference in the immune functioning of the young and the adult adipose tissue. Therefore, we continued our study focusing on immune gene networks in the young adipose tissue.

3.5. Immune gene networks in P6 adipose tissue

To have an overview on the immune gene transcription landscape in BAT and iAT, we compared first both adipose tissues in adult mice. Thereby, we could identify distinct transcriptional profiles regarding IFN-stimulated genes (ISGs) in the respective tissues (Figure 7A). ISGs were target of type-I and -II IFNs. 1179 DEGs were highly present in BAT, from these, 44% were ISGs. Within these ISGs thermogenic (*Ucp1*) and mitobiogenesis (*Cox7a1*, *Cidea*, *Cpt1b* and *Dio2*) related genes were included (Figure 7B). Further ISGs overrepresented in adult BAT were involved in macrophage activation and antiviral response (Figure 7B). In contrast to that, 35% of the 3295 underrepresented DEGs in P56 BAT were ISGs. These ISGs were involved in IFN response, RNA metabolism and they were associated with macrophage genes. Hence, macrophage genes were absent in BAT and further analysis confirmed the shortage of adipose tissue macrophages (ATMs) in BAT (Figure 7C,D) (43).

Since we wanted to investigate P6 iAT immune gene network, and genes related to immune response were underrepresented in BAT, we further compared P6 with P56 iAT. We found the gene network involving *Agtr2* was highly expressed in P6 iAT (Figure 7E). In addition, angiotensin converting enzyme 2 (*Ace2*) and bradykinin receptor 2 (*Bdkrb2*) were overrepresented in P6 iAT as well. Our NGS analysis revealed a solid *Ace2* expression in young iAT compared to its adult counterpart (Figure 7F). *Ace2*, angiotensin (*Ang*), chymase (*Cma1*) and genes expressing kallikreins belonged the *Agtr2* network (Figure 7F). They are required to form angiotensinogen to ANG-2 and ANG(1-7) (126). The two receptors – angiotensin II receptor type 2 (AGTR2) and bradykinin receptor B2 (BDKRB2) – can form a heterodimer which phosphorylates IκBα and dephosphorylates p38-MAPK and STAT3 (127). Hence, P6 iAT might be able to inhibit NFκB and STAT3 signaling through the angiotensin-kallikrein network. Comparing P6 with P56 iAT by GO analysis of biological function, we could see that P56 iAT highly expressed neutrophil chemotaxis and migration, which could be achieved by the expression of inflammatory genes (Figure 7G).

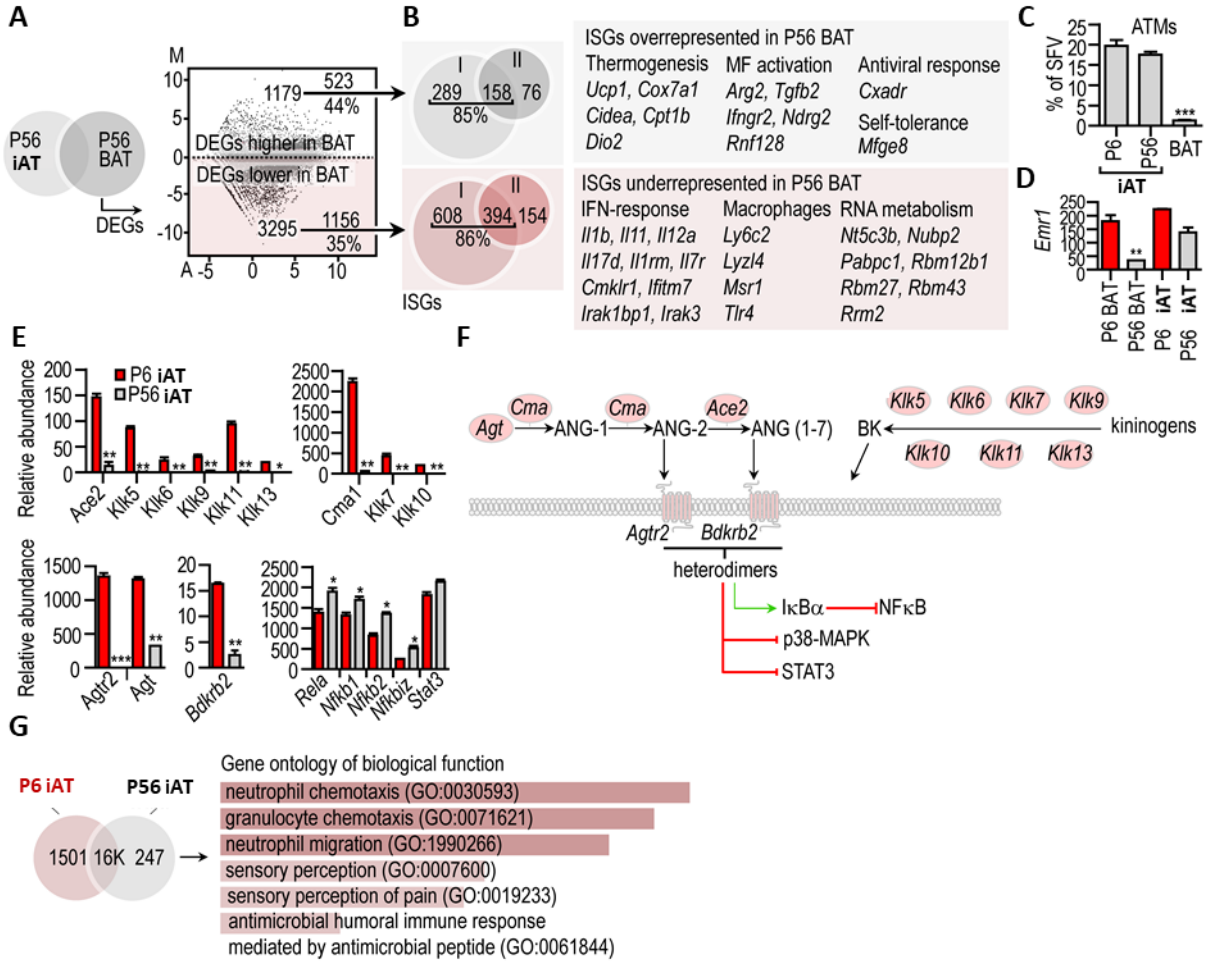

Figure 7: Genes involved in the immune response of iAT and BAT

(A) The comparison of P56 iAT and P56 BAT revealed over- and underrepresented DEGs in adult BAT which are shown in the scatter plot, respectively. DEGs related to the IFN-stimulated genes (ISGs) were given in percentage. (B) Detailed description of the respective ISGs categorized in over- and underrepresented DEGs in P56 BAT. (C) Percentage of adipose tissue macrophages (ATMs) residing in the stromal vascular fraction (SVF) of P6 iAT, P56 iAT and P56 BAT. *** $p < 0.001$, two-way ANOVA with Dunnett´s post hoc test. P6 BAT was used as reference group. (D) Emr1, a macrophage marker encoding the antigen F4/80, expression level. ** $p < 0.01$, two-way ANOVA with Dunnett´s post hoc test. P6 BAT was used as reference group. (E) Gene expression level of local kininogen and angiotensin pathway. * $p < 0.05$, ** $p < 0.01$, *** $p < 0.001$, Student´s two-tailed unpaired t-test. (F) Summary scheme of the angiotensin and kininogen pathway. Highlighted genes were strongly expressed by P6 iAT. (G) GO analysis of highly expressed DEGs in P56 iAT related to biological functions with a combined p-value < 0.01. Source: Figure from (43), reused under license CC BY 4.0 (https://creativecommons.org/licenses/by/4.0/).

Therefore, iAT maturation leads to an inflammatory milieu which agrees with previous studies stating an upregulation in NFκB subunits expression due to adipogenesis (128). To sum up, P6 iAT shared numerous signaling pathways with P56 BAT. Furthermore, P6 iAT had unique traits, such as the expression of the angiotensin-kallikrein network which allowed it to control NFκB signaling. Hence, this feature could be seen as a distinguishing hallmark of P6 iAT.

Adipose tissue inflammation is associated with obesity (129–131). As we showed in P6 iAT, DEGs from the NFκB, STAT3 and IRF signaling were overrepresented and needed to be controlled to avoid inflammation leading to childhood obesity (95). Less is known how P6 iAT controls inflammation and a complete “shut-down” of the inflammation response is undesired, since interleukin-6 (IL-6) for instance, is obligatory for iAT to maintain beige adipocytes (63). Therefore, ATMs take up and convert breast-milk-derived AKGs to platelet activated factor (PAF). Emitted PAF from the ATM are taken up by the infant adipocyte to generate IL-6 over the IL-6/STAT3 pathway (63). IL-6 is known to sustain beige adipocyte development (132). Indicated by our previous study, P6 iAT needed to have a tight regulated inflammation and immune response. Therefore, we aimed to investigate further immune functions-related gene expression patterns of the developing adipose tissue.

3.6. Suppressed IFN response in P6 adipose tissue

Inflammatory signals are harmful for the extended mitochondria network (83–85), but certain inflammatory stimuli, such as interleukin-6 (IL-6), are crucial for beige adipocyte development in infant iAT (63). Therefore, we checked the transcriptional landscape of P6 and P56 iAT regarding underrepresented DEGs involved in the inflammation response. The analysed NGS of P6 iAT revealed that 63% of the 1782 underrepresented DEGs belonged to one large network including the stimulator of interferon genes (STING) and the IFN-inducible protein absent in melanoma 2 (AIM2) signaling (Figure 8A,B). Genes from that network were underrepresented in P6 iAT compared to P56 iAT (Figure 8A). Their role in cellular immune response was the assembly of DNA-inflammasomes and to generate IFNs in response to cytosolic DNA (133). In the cytosol, B-DNA can be sensed by DDX41 (DEAD-box helicase 41) and p204 which is also known as IFNγ-inducible protein 204 (IFI204) in BALB/C mice, IFI205 in C57/BL6 mice and in human under the name IFI16 (133). In an active cell associated with high transcription output, Z-DNA can be prevalent in the cytosol (134) which is detected by another DNA sensor known as ZBP1 (Z-DNA-binding protein 1, also alternatively named as DAI (135)). If these DNA sensors bind one of their targets, the production of type-I IFNs are enrolled by the activation of several proteins such as the stimulator of interferon genes (STING), TANK binding kinase 1 (TBK1) and interferon regulatory factors (IRF3 and IRF7), respectively (133).

To have a better overview of the underrepresented DEGs in P6 iAT involved in this network, we classified the investigated proteins into functional clusters: receptors (AIM2, DDX41, p204 and ZBP1), adaptor (STING) and effector (IRF7) (Figure 8B). NGS analysis of P6 and P56 iAT revealed low transcription of receptors, adaptor and effector in P6 adipocytes (Figure 8A). Indicated by NGS, we tried to verify the findings by two-step RT-qPCR in which we found nearly the same outcome in tissue (iAT) and adipocytes of P6 and P56 animals (Figure 8C,D). Only one gene, encoding STING, was expressed equally in both tissues.

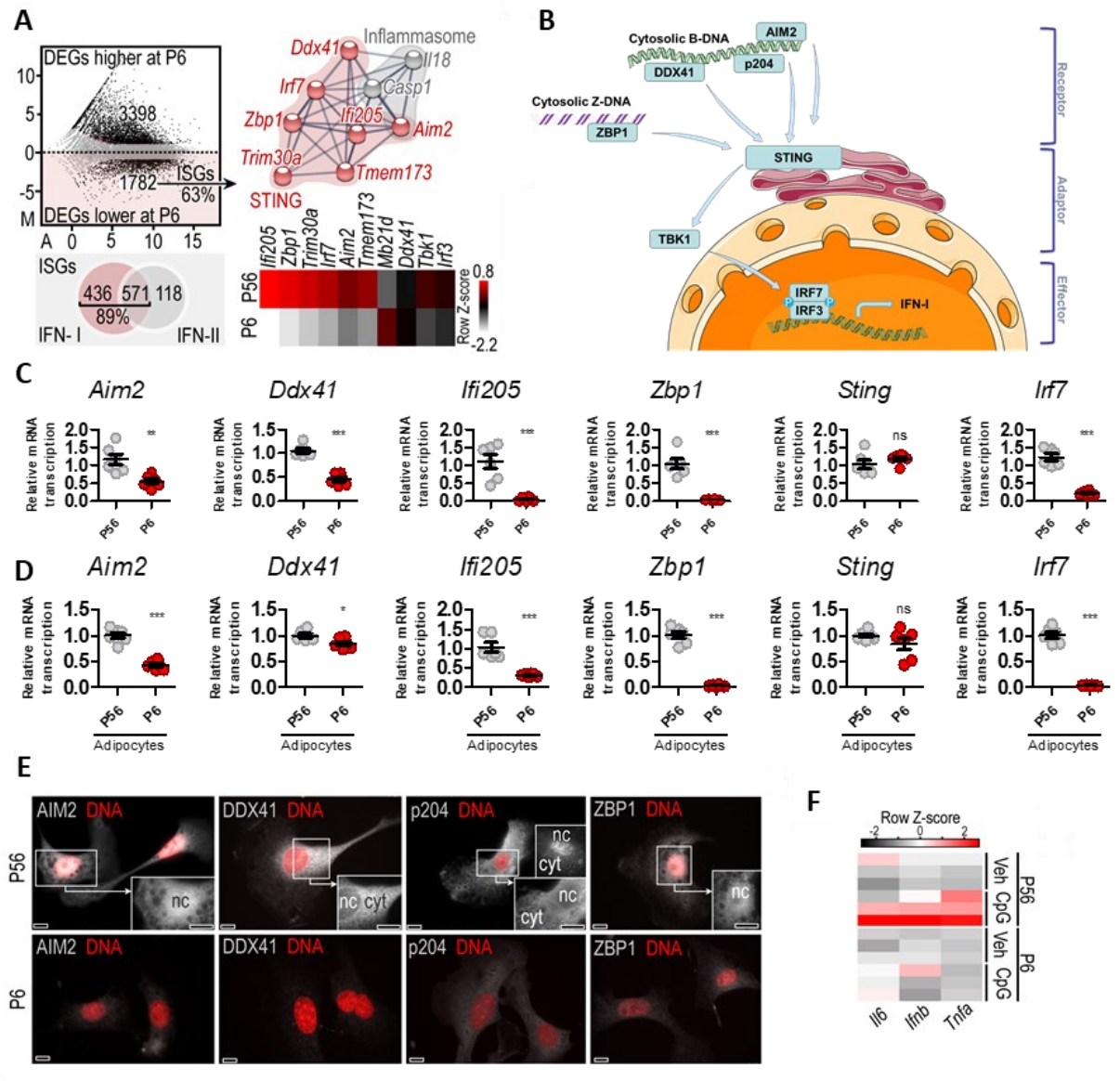

Figure 8: Underrepresented genes related to immune response in P6 iAT

(A) NGS analysis of ISGs in developing iAT with volcano plot, Venn diagram, STRING analysis and the respective heat map. (B) Investigated receptors (AIM2, DDX41, p204 and ZBP1) with respective targets, adaptors (STING and TBK1) and effectors (IRF7 and IRF3) involved in the STING pathway. NGS: next generation sequencing, AIM2: absent in melanoma 2, DDX41: DEAD-box helicase 41, p204 or IFI204: IFNγ-inducible protein 204 (BALB/C mice), ZBP1: Z-DNA-binding protein 1, STING: stimulator of interferon genes, TBK1: TANK binding kinase 1, IRF3/7: Interferon regulatory factor 3/7. (C) Relative mRNA transcription of gene members related to the STING/AIM2 pathways in P6 and P56 iAT. ** $p < 0.005$, *** $p < 0.0001$, ns: not significant, Student´s two-tailed unpaired t-test. (D) Relative mRNA transcription of gene members related to the STING/AIM2 pathways in P6 and P56 adipocytes isolated from iWAT. * $p < 0.03$, *** $p < 0.0001$, ns: not significant, Student´s two-tailed unpaired t-test. (E) DNA sensor expression in P6 and P56 adipocytes. Scale: 10 µm (F) Inflammatory gene expression in P6 and P56 adipocyte after the treatment with 1 µg/ml naked CpG for 8 hours. Source: Figure from (93), reused under license CC BY 4.0 (https://creativecommons.org/licenses/by/4.0/).

Especially, *Irf7* level was significantly higher expressed in iAT and adipocytes of P56 compared to P6 (Figure 8C,D). IRF7 activation leads to expression of genes involved in the STING/AIM2 pathway of P56 adipocytes (93). Furthermore, protein detection by immunostaining highlighted the abundance of AIM2, DDX41, IFI204 and ZBP1 proteins in the perinuclear region and cytosol of P56 adipocytes. This was in line with their functions to detect DNA fragments within the cell (135, 136). These proteins were lacking in P6 adipocytes (Figure 8E). Furthermore, adipocytes, like other cells, can detect foreign pathogens by Toll-like receptors (TLR), such as TLR8 which is located on the cell surface or in the endosomal compartments (137, 138). We exposed adult and infant adipocytes to a synthetic oligonucleotide containing unmethylated CpG dinucleotides (CpG) which was detectable through TLR8 (137). We found that P56 adipocytes were able to trigger inflammation whereas P6 adipocytes were immune suppressed towards cytosolic or endosomal DNA (Figure 8F).

Since STING transcription was present in P6 and P56 adipocytes, we treated P6 and P56 adipocytes with a STING-specific ligand to test their inflammation response. Therefore, we exposed infant and adult adipocytes with the natural STING activator 2´3´-cyclic-GMP-AMP (cGAMP). The activator entered the cell from the extracellular matrix into the cytosol through the transporter SLC19a (Figure 9E). Hereby we could prove that P56 adipocytes generated significantly higher inflammation products encoding by interferon α (*Ifna*), interferon β (*Ifnb*), tumor necrosis factor α (*Tnfa*) and IL-6 (*Il6*) (Figure 9A). The mirror experiment in infants showed that P6 adipocytes were protected from STING-induced inflammation response. In addition to that the same expression pattern of inflammation genes could be shown in iAT of P6 and P56 after cGAMP (Figure 9E). STING ligand cGAMP increased the number of autophagosomes in young adipocytes (Figure 9B-D). Autophagy is a summary term involving mitophagy, a process to reduce mitochondria content and mitochondrial DNA (mtDNA) (139). According to the literature STING is involved in the autophagy process (140) while STING inhibition impairs mitophagy in P6 adipocytes (93).

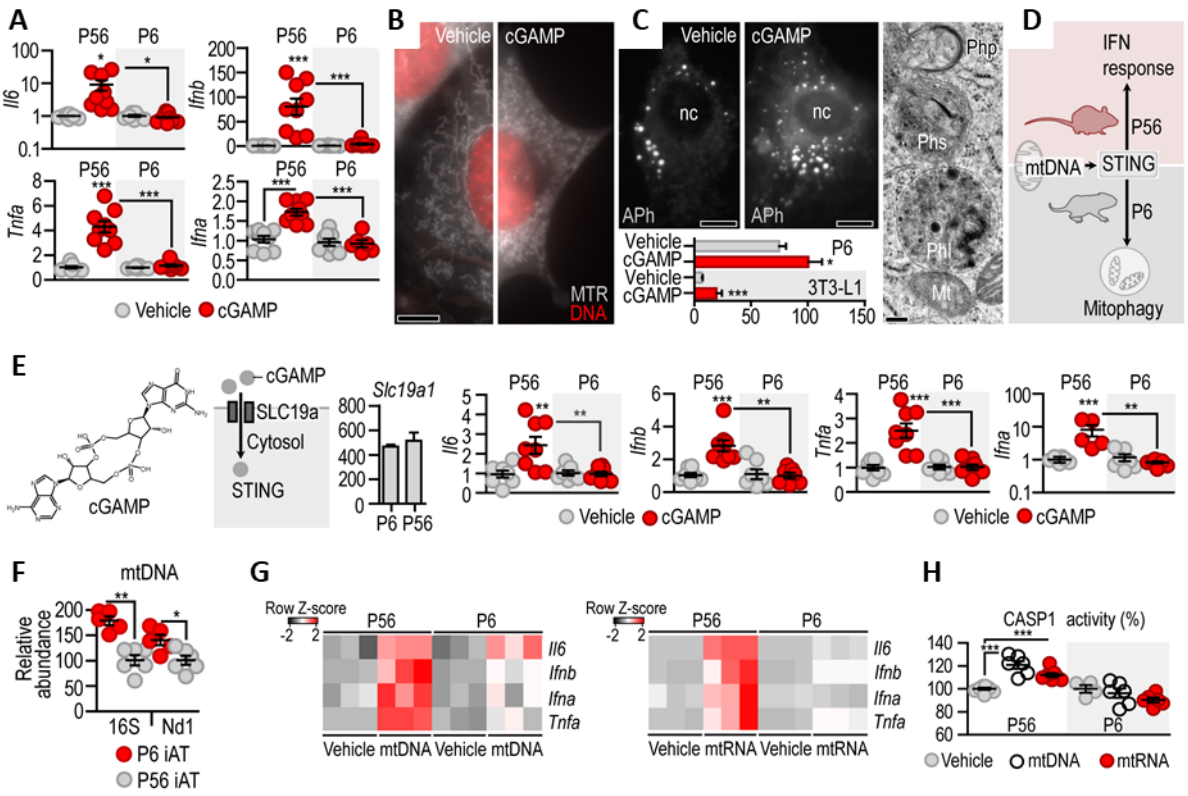

Figure 9: P6 adipocytes are protected from mtDNA-mtRNA-triggered IFN response

(A) Relative mRNA transcription of genes related to inflammation response in P6 and P56 adipocytes after 18 hours with 10 µg/ml 2´3´-cyclic-GMP-AMP (cGAMP). * $p < 0.02$, *** $p < 0.0001$, Student´s two-tailed unpaired t-test. Ifna/b: interferon α/β, Tnfa: tumor necrosis factor α, IL-6: interleukin 6. (B) MitoTracker Red (MTR) staining after 2 hours 10 µg/ml cGAMP in P6 adipocytes. (C) *Top*: Autophagosome (APh) labelling in P6 adipocytes. nc: nucleus, *Bottom*: Number of APh in P6 and 3T3-L1 adipocytes with and without 2 hours of cGAMP. TEM image of autophagosome-forming P6 adipocyte. Php: phagophore, Phs: phagosome, Phl: phagolysosome, Mt: mitochondrion. Scale: 10 µm (B,C); 0.1 µm (TEM). * $p < 0.05$, ** $p < 0.01$, *** $p < 0.001$. Student´s two-tailed unpaired t-test or one-way ANOVA with Dunnett´s post-hoc test. (D) Different functions of mtDNA-mediated STING activation in P6 and P56 iAT. (E) *Left*: A scheme of the structure of STING ligand cGAMP and its transporter into the cytosol SLC19a (141). *Slc19a1* transcription in P6 and P56 iAT. *Right*: IFN response of P6 and P56 iAT after 18 hours of 10 µg/ml cGAMP. * $p < 0.05$, ** $p < 0.01$, *** $p < 0.001$. Student´s two-tailed unpaired t-test or one-way ANOVA with Dunnett´s post-hoc test. (F) Relative abundance of mtDNA (*16S* and *Nd1*) to genomic mouse DNA in P6 and P56 iAT. (G) IFN response after the transfection of mtDNA or mtRNA (2 µg/ml, 18 hours) in P56 and P6 adipocytes. mtDNA/RNA: mitochondrial DNA/RNA. (H) Caspase-1 (CASP1) activity after 4-h challenge of cytoplasmic mtDNA or mtRNA (both 2 µg/ml) to measure inflammasome activation in P56 and P6 adipocytes. Source: Figure from (93), reused under license CC BY 4.0 (https://creativecommons.org/licenses/by/4.0/).

Since excess mitochondria were present within beige adipocytes during adipose tissue development in P6 iAT, we wanted to know if nucleic acids from the mitochondria would induce inflammation. The prevalence of mtDNA (*16S* and *Nd1*) was higher in P6 compared to P56 iAT (Figure 9F). Mitochondria can be stressed by pathogens, such as bacteria (142) or metabolic events (mitochondrial fusion and fission) (143, 144). Hence, it was not unlikely that mitochondrial content can leak into the cytosol. Furthermore it is known that mtDNA-stimulated STING activation causes type-I IFN response (145). P6 adipocytes treated with cGAMP induced mitophagy (Figure 9B-E). Therefore, P6 adipocytes were able to impair mtDNA-mediated inflammation through an active STING pathway (Figure 9G,H). Lastly, we wanted to know if mtRNA was immunogenic in adipocytes. We transfected mtRNA into the adipocytes of P6 and P56 animals which showed an impaired inflammation response in P6 adipocytes and a robust inflammation induction in P56 adipocytes (Figure 9G,H).

In summary, mtRNA and mtDNA did not evoke inflammation in P6 adipocytes which might be due to the absence of IRF7. Furthermore, mtDNA-mediated STING activation in infant adipocytes induced mitophagy.

3.7. Beige adipocyte development through the mtRNA signaling

Our data show that beige adipocytes tolerate mitochondrial content, which might be due to the lack of IRF7. Next, we tried to understand the purpose of mtRNA, since mtDNA was involved in the mitophagy process of P6 iAT. Descending from endosymbiotic bacteria, mitochondria retain features from its prokaryotic origin like a circular genome (Figure 10A). The compact genome can be transcribed bidirectional which results in overlapping transcripts leading to double-stranded RNA (dsRNA).

We found that mtRNA and mtDNA were packed within extracellular vesicles (EVs), secreted by the adipocytes (Figure 10B,C). EVs are generated through inverse budding of endosomes which leads to the formation of multivesicular bodies (MVBs) (93). By applying P6 EVs on adult adipocytes we could induce UCP1 expression (Figure 10D). Furthermore, beige marker genes (*Cidea* and *Dio2*) and mitobiogenesis genes, such as *Ppargc1a* were upregulated after 18 hours incubation with P6 EVs. Besides P6 EVs, breast milk is also known to transmit beige-inducing signal (63) and in line with that, human-derived breast milk EVs are rich in mtRNA (93). Therefore, we isolated EVs from murine breast milk and formula milk as a reference, to treat 3T3-L1

adipocytes. As it was indicated by P6 EVs, only breast milk EVs were able to beneficially regulate thermogenic, mitobiogenesis and beige genes towards beige adipocyte development (Figure 10E). Furthermore, *Il6* transcription was unaffected after the treatment with breast milk EVs. In line with our previous study showing that IL-6/STAT3 signaling induces beige adipose tissue development (63). IRF7 suppression could be achieved by the application of formula and breast milk EVs (Figure 10E).

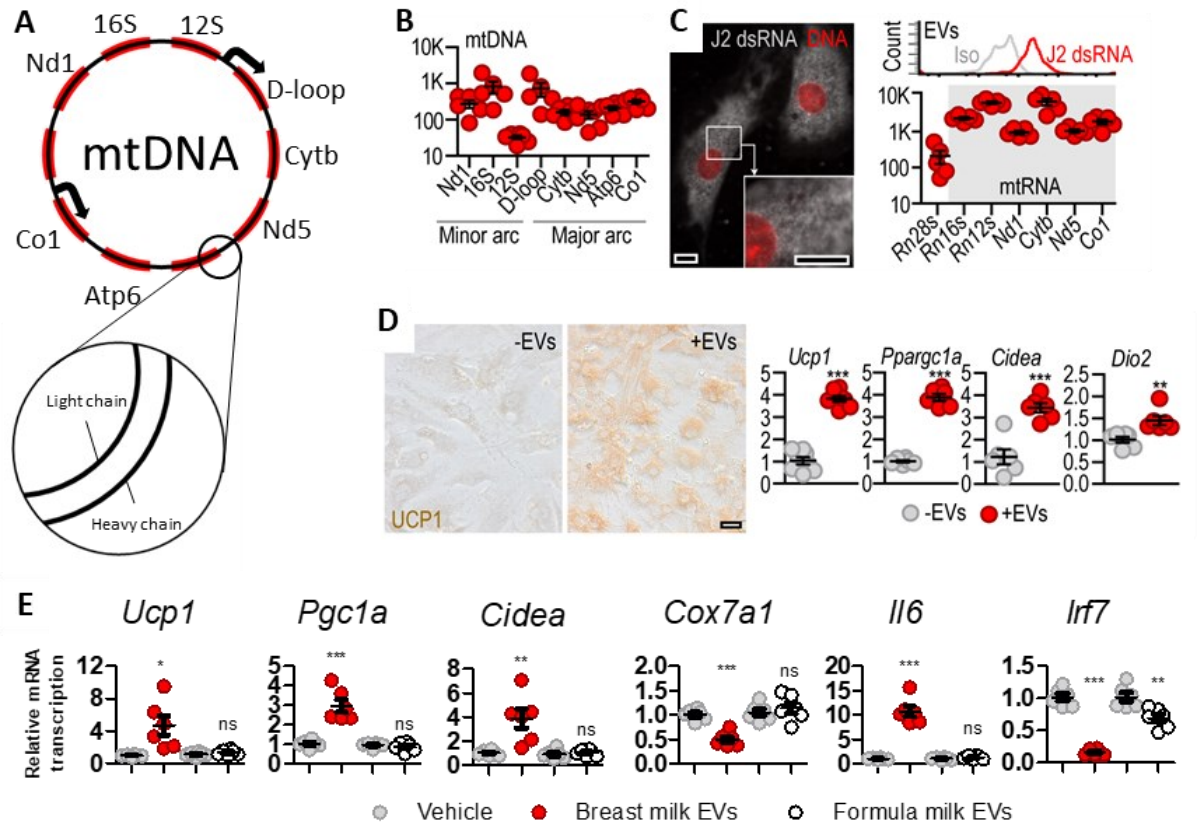

Figure 10: P6 and breast milk EVs induce beige adipocyte development

(A) Scheme of circular mtDNA with heavy and light chain. Arrows indicate transcription direction in the respective chain. (B) Level of mtDNA in extracellular vesicles (EVs) of infant adipocytes. (C) Labelling of double-stranded RNA (dsRNA) in P6 adipocytes using J2 antibodies; scale: 10 µm. Quantified RNA species in EVs of infant adipocytes. (D) *Left*: Effect of P6 EVs on the UCP1 expression on P56 adipocytes. *Right*: Relative mRNA transcription of beige and mitobiogenesis marker genes after 18 hours with P6 EVs. (E) Relative mRNA transcription of 3T3-L1 adipocyte after 18 hours with breast milk or formula milk EVs. * $p < 0.01$, ** $p < 0.005$, *** $p < 0.0001$, ns: not significant, Student´s two-tailed unpaired t-test. Source: Figure from (93), reused under license CC BY 4.0 (https://creativecommons.org/licenses/by/4.0/).

EVs from the P6 adipocytes carried dsRNA (Figure 10C) which might trigger TLR3, retinoic acid-inducible gene 1 (RIG-I) or RIG-I-like melanoma differentiation-associated gene 5 (MDA5) (146–148). We treated adipocytes with naked polyinosinic-polycytidylic acid (p(I:C)), a synthetic dsRNA, and could not mirror the effects of EVs (Figure 11A). In contrast to that, cytosolic mtRNA induction which was detected by RIG-I and MDA5 led to a robust gene transcription of beige adipocyte development (Figure 11C). Unlike mtRNA, mtDNA transfection did not affect any of these genes. The lack of RIG-I and MDA5 compromises mitobiogenesis which ultimately induces the loss of beige adipocytes (93).

Beige adipose tissue needs IL-6/STAT3 signaling (Figure 11D), especially a physiological level of IL-6 is needed which can be generated in adipocytes through the metabolism of PAF as previously described (63). Adipocyte *Il6* transcription was induced by breast milk EVs and mtRNA (Figure 10E, Figure 11E).

EV-packed nucleic acids are protected against nucleases and may serve as intracellular messengers (149). Therefore, the delivery of mtRNA into the cytosol led to mitobiogenesis, thermogenesis and the induction of beige marker genes in 3T3-L1 and P56 adipocytes (Figure 11C, E). However, in adult adipocytes mtRNA treatment, as well as other nucleic acid ligands, forced a high inflammatory response (Figure 11B) which might be caused by an active IRF7 expression. In the following, we tried to understand the mechanisms of IRF7 suppression in P6 iAT. The absence of IRF7 might be key to permit beige adipogenesis through mtRNA.

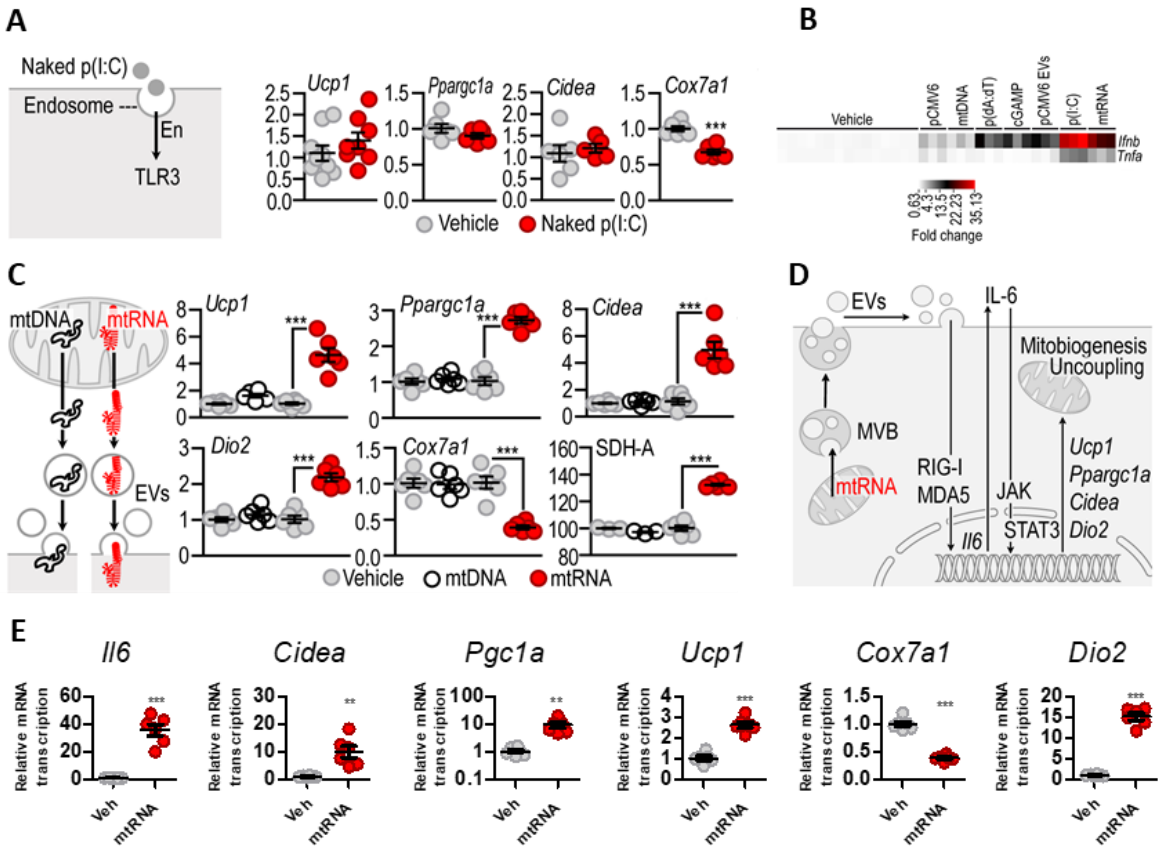

Figure 11: Beige adipocyte development through paracrine mtRNA signal

(A) Application scheme of naked polyinosinic-polycytidylic acid (p(I:C)) treatment and relative mRNA transcription of *Ucp1*, *Ppargc1a* (*Pgc1a*), *Cidea* and *Cox7a1* after 18 hours with 5 µg/ml p(I:C) on P6 adipocytes. (B) Cytosolic DNA/RNA effect on P56 adipocytes regarding *Ifnb* and *Tnfa*. P56 adipocytes receive 1 µg/ml pCMV6, 2 µg/ml mtDNA/mtRNA, 2.5 µg/ml p(dA:dT), 10 µg/ml cGAMP, 0.5 µg/ml p(I:C) or EVs containing pCMV6 (pCMV6 EVs). Exposer time was 18 hours for all treatments. pCMV6: pCMV6 plasmid transfection, pCMV6 EVs: Extracellular vesicles of pCMV6 plasmid-treated adipocytes. p(dA:dT): poly(deoxyadenylic-deoxythymidylic) acid sodium salt. (C) *Left*: Scheme of mtDNA and mtRNA transfection. *Right*: Response of 3T3-L1 adipocytes after 18 hours with 2 µg/ml mtDNA or mtRNA regarding beige gene transcription and SDH-A FACS analysis to determine mitobiogenesis. *** $p < 0.0001$, Student´s two-tailed unpaired t-test. SDH-A: Succinate Dehydrogenase Complex Flavoprotein Subunit A. (D) Scheme of mtRNA-induced signaling in P6 adipocytes. (E) Relative mRNA transcription of genes involved in the beige adipocyte development after 18 hours with 2 µg/ml mtRNA on P56 adipocytes. ** $p < 0.002$, *** $p < 0.0001$, Student´s two-tailed unpaired t-test. Source: Figure from (93), reused under license CC BY 4.0 (https://creativecommons.org/licenses/by/4.0/).

3.8. Vitamin D receptor mediated IRF7 suppression in infant adipose tissue

Active IRF7 in P56 adipocytes led to high inflammation response after cGAMP, synthetic ligands of cytosolic nucleic acid sensor proteins, mtDNA or mtRNA treatment through the activation of STING/AIM2 and RIG-I/MDA5 pathways (Figure 11B). IFNβ expression damages mitochondria in adipocytes (93). In contrast to that, IRF7-deficient adipocytes failed to induce IFNβ expression (Figure 12A,B) and they were able to keep abundant beige adipocyte content to adulthood (Figure 12C). The outcome is in line with a previous report showing that IRF7-deficient mice are protected from obesity (150). Like breast milk and formula milk EVs, P6 EVs were able to repress *Irf7* mRNA and IRF7 protein level in adipocytes (Figure 12D). Furthermore, P6 EVs did not trigger IFN-response, unlike P56 EVs which triggered IRF7 and IFNβ expression (93). Hence, a IFNβ-mediated reduction of mitochondrial content can be noticed after P56 EVs treatment (93, 151).

Our study revealed high expression of genes associated with vitamin D receptor (VDR)-controlled gene networks in P6 adipose tissue (93). Cathelicidin an antimicrobial peptide (152) encoded by *Camp* which is a known VDR-target, was abundantly expressed in P6 iAT (Figure 12E). In contrary, P6 adipocytes failed to transcribe of coronin A1 (*Coro1a*) which was a gene known to be repressed by VDR. Coronin A1 is able to reduce autophagosome formation (153). Hence, the lack of *Coro1a* due to VDR allowed P6 iAT to use STING-mediated autophagy, as described before (Figure 9B-D). P6 adipocytes were able to transcribe vitamin D metabolizing enzymes leading to vitamin D3 (Vit-D3) storage and calcitriol formation (Figure 12E) in infant iAT.

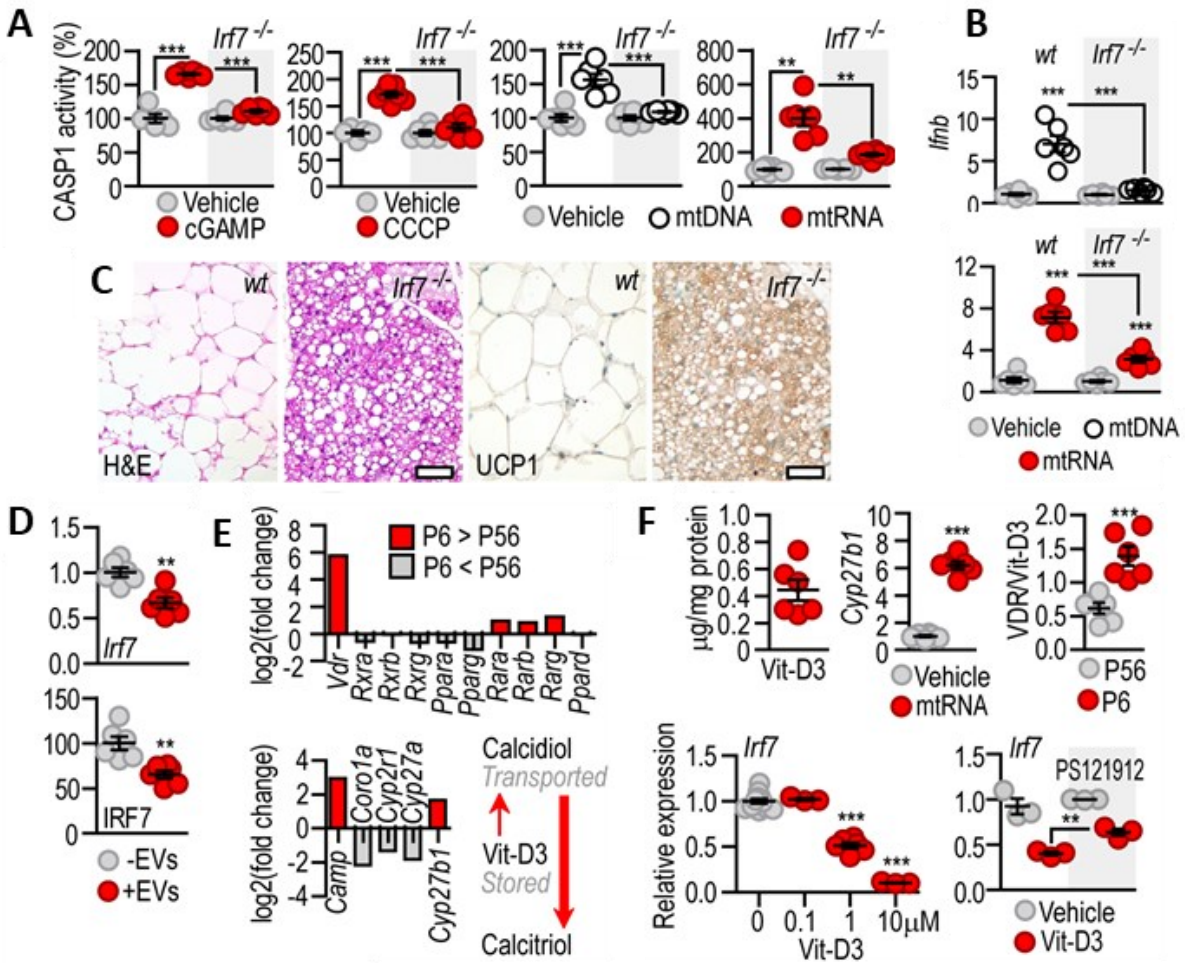

Figure 12: Absent of IRF7 supports beige adipocyte development

(A) Response of adult wild-type (*wt*) and IRF7-deficient (*Irf7*$^{-/-}$) adipocytes after cGAMP treatment, CCCP-induced (1 µM, 15 min) mitochondrial damage and mtDNA/mtRNA transfection. CCCP: carbonyl cyanide m-chlorophenyl hydrazone. (B) Relative *Ifnb* transcription after 4 hours with 2 µg/ml mtRNA/mtDNA transfection in adult adipocytes of *wt* and *Irf7*$^{-/-}$ animals. (C) Adult iAT of *wt* and *Irf7*$^{-/-}$ mice. Scale: 25 µm. H&E and UCP1 immunostaining. (D) *Irf7* transcription and IRF7 expression in mouse adipocytes after P6 EVs. (E) *Vdr* transcription level, VDR-controlled genes and genes involved in the vitamin D metabolism of P6 and P56 iAT by NGS. (F) *Top*: Vit-D3 level in P6 EVs, *Cyp27b1* transcription after mtRNA in 3T3-L1 adipocytes, VDR/Vit-D3 ratio in P6 and P56 iAT. *Bottom*: *Irf7* transcription in mouse adipocyte after 48 hours with different doses of Vit-D3. Relative *Irf7* transcription in mouse adipocytes after 1 µM Vit-D3 and Vehicle or 7.5 µM PS121912 (VDR Inhibitor) treatment (154). Source: Figure from (93), reused under license CC BY 4.0 (https://creativecommons.org/licenses/by/4.0/).

Next, we checked the availability of Vit-D3 and found that P6 EVs were rich in Vit-D3 (Figure 12F). Furthermore, mtRNA supported the transcription of the calcitriol synthesizing enzyme 1-α-hydroxylase, encoded by *Cyp27b1*. VDR expression was more prevalent in P6 iAT (Figure 12F).

After knowing the availability of Vit-D3 in the iAT, we treated 3T3-L1 adipocytes with Vit-D3 for 48 hours and found a reduction in *Irf7* transcription in a dose-dependent manner (Figure 12F). Furthermore, inhibiting VDR activity by PS121912, a selective VDR-coregulator inhibitor (154), impaired the Vit-D3-mediated *Irf7* suppression.

Diet-induced obesity compromised *Vdr* expression and upregulated the transcription of *Irf7* (Figure 13A). Correspondingly, VDR inhibition led to the loss of beige adipocytes in P10 iAT and increased IRF7 protein level (Figure 13A,B). Adipocytes pre-treated with Vit-D3 managed to decrease inflammation response to cGAMP, mtRNA and mtDNA (Figure 13C,D). Furthermore, VDR signaling did not impair mtRNA-mediated *Il6* transcription and IL-6 release in mouse and human (Figure 13D, (93)).

IRF7 is a hub gene associated to the STING pathway which triggers IFN-response upon activation (93, 155, 156). Hence, suppressing IRF7 was a potential mechanism to suppress IFN production in P6 iAT after the detection of cytosolic mtRNA or mtDNA (Figure 13D). Protected from an IFN-response through Vit-D3, mtRNA could induce mitobiogenesis, thermogenesis and beige gene expression *in vitro*. Therefore, we could show that mitochondrial nucleic acids trigger different pathways to evoke mitophagy or beige gene expression (Figure 13E).

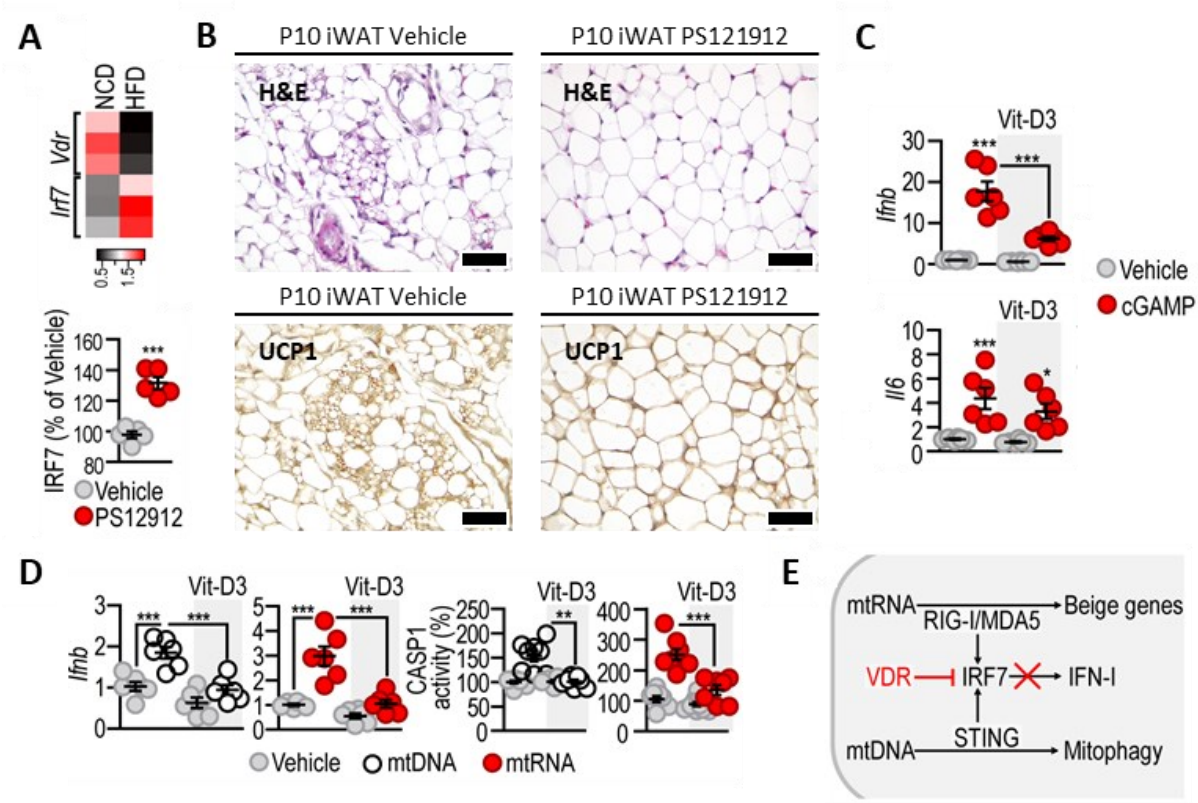

Figure 13: Vitamin D3-mediated Irf7 suppression impairs triggered IFN response

(A) *Top*: *Vdr* and *Irf7* level in iAT of normal chow diet (NCD) and high fat diet (HFD) mice. *Bottom*: IRF7 protein level after 7.5 µM P121912 in P10 iAT. (B) H&E and UCP1 immunostaining of P10 iAT after vehicle or PS121912 treatment. Scale: 25 µm. (C) *Ifnb* and *Il6* transcription after cGAMP in 1 µM Vit-D3-pretreated adipocytes. * $p < 0.05$, ** $p < 0.01$, *** $p < 0.001$, Student´s two-tailed unpaired t-test or one-way ANOVA with Dunnett´s post-hoc test. (D) *Ifnb* transcription and response of 1 µM Vit-D3-pretreated adipocytes after mtDNA or mtRNA. (E) Scheme of possible VDR role in P6 iAT. Source: Figure from (93), reused under license CC BY 4.0 (https://creativecommons.org/licenses/by/4.0/).

3.9. Obesity-driven loss of mitochondria immune tolerance in P6 adipocytes

As shown earlier in this thesis, diet-induced obesity increased *Irf7* transcription while the transcription of *Vdr* was impaired (Figure 13A,B). According to that, blocking VDR activity resulted in the loss of beige adipocytes.

In the following, we investigated a mouse model mimicking childhood obesity. Therefore, we used infant mice nursed by dams fed with normal chow diet (NCD) or high fat diet (HFD) (Figure 14A,B) (157). Animals receiving dams fed with HFD induced a robust *Irf7* transcription and an impaired *Vdr* expression in adipocytes (Figure 14C). Furthermore, mice receiving HFD-fed dams lose beige adipocytes and assisted inflammasome activation (Figure 14D,E). With an increase in IRF7 and the loss of mitochondria immune privilege, these adipocytes started to express DNA sensors associated with the AIM2/STING pathway (Figure 14F). In addition to that, they failed to build up the same mitochondrial network compared to animals nursed with NCD-fed dams. The effect of HFD-feeding was reverted by applying Vit-D3 to the infant mice (Figure 14G,H). Vit-D3 protected infant mice from diet-induced obesity *in vivo* by maintaining beige adipocytes and reducing inflammasome activity.

Earlier in this thesis we investigated the effect of Vit-D3 in a childhood obesity mouse model. Next, we want to treat diet-induced obese adult animals with mtRNA and Vit-D3 which we expected to mend mtRNA-mediated inflammation. In response to Vit-D3, IRF7 protein level was reduced even though mtRNA was transfected in the iAT of adult mice (Figure 14I-K). Vit-D3 did not impair mtRNA-driven beige-inducing effects in adult adipocytes, therefore, mtRNA could increase mitochondrial network, thermogenesis, and energy expenditure (Figure 14J-M). The Vit-D3-mtRNA-treatment induced infant-like iAT in adults. Due to that, cGAMP induction failed to active STING-mediated inflammation which allowed treated adult cells to behave like infant adipocytes (Figure 14N) regarding inflammation response and beige adipocyte development.

The combination study of mtRNA and Vit-D3 showed promising results *in vitro* and *in vivo* to reduce diet-induced obesity in adult mice. Furthermore, we could show that an immune response against mitochondria in the infant adipocytes triggered early

onset of obesity. Hence, sustaining the immune tolerance of mitochondrial content in the thermogenic fat cells in infants is important to avoid early obesity development.

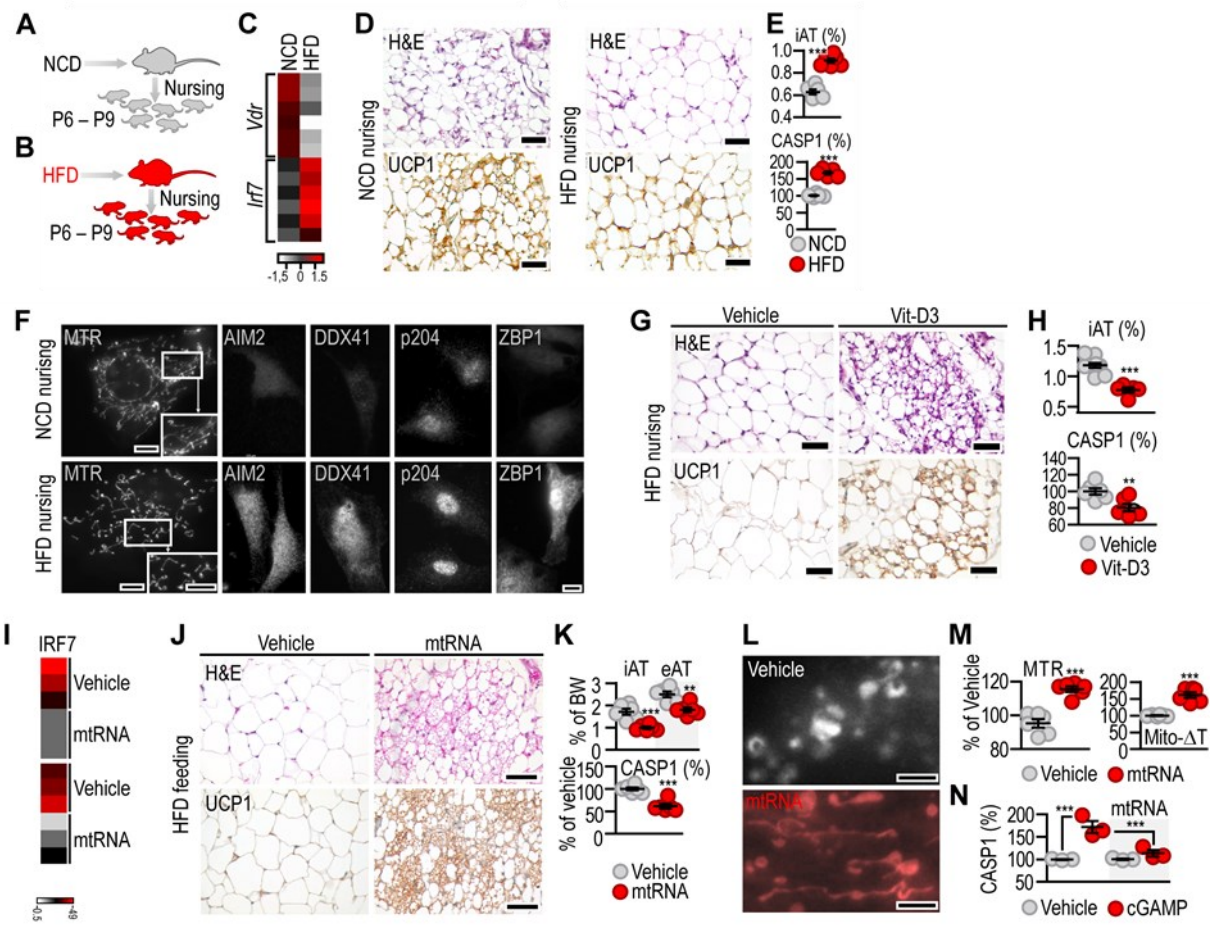

Figure 14: Treating diet-induced obese mice with cytosolic mtRNA and Vit-D3

(A,B) NCD and HFD feeding in nursing mice for 3 days after the offsprings reach postnatal day 6. Inguinal ATs of mice nursed with NCD-fed or HFD-fed dams were investigated at P10. (C) *Vdr* and *Irf7* level in iAT of NCD- and HFD-fed mice. (D) H&E and UCP1 immunostaining of iAT from NCD- and HFD-fed mice. Scale: 50 µm. (E) CASP1 activity in adipocytes and iAT/body weight ratio of NCD- or HFD-fed dams mice. (F) DNA sensor expression and mitochondrial network in adipocytes of NFD-fed or HFD-fed dams nursed animals. MTR: MitoTracker Red. Scale: 50 µm. (G) P10 iAT histology of mice receiving NCD-fed or HFD-fed dams and vehicle or Vit-D3 at P6 to P9. Scale: 100 µm. (H) CASP1 activity in adipocytes and iAT/body weight ratio (eAT: epididymal adipose tissue) of NCD- or HFD-fed dams mice with or without Vit-D3 at P6 to P9. (I) IRF7 level in adipocytes, (J) histology images, (K) CASP1 activity and iAT/body weight ration of NCD- and HFD-fed adult animals with and without mtRNA treatment. Vit-D3 was supplied to both study groups. (L) Mitochondrial network of NCD- and HFD-fed adult animals with and without mtRNA treatment. Scale: 10 µm. (M) Mitochondrial mass (relative MTR fluorescent intensity) and mitochondrial temperature change (Mito-ΔT) from isolated adipocytes of NCD- and HFD-fed adult animals with and without mtRNA treatment. (L) Vehicle- or mtRNA-treated adipocyte CASP1 activity after 4 hours with cGAMP. ** $p < 0.01$, *** $p < 0.001$, Student´s two-tailed unpaired t-test or one-way ANOVA with Dunnett´s post-hoc test. Source: Figure from (93), reused under license CC BY 4.0 (https://creativecommons.org/licenses/by/4.0/).

4. Discussion

In this thesis, we have identified gene networks and hub genes which can be seen as hallmarks of the developing BAT and WAT. In adult BAT, transcripts of thermogenesis and lipid catabolism were overrepresented. This outcome was unexpected since BAT was long considered to be functionally mature after birth and having a declining role after early postnatal life. (Figure 1A) (121) (87).Thermogenic and lipid catabolism transcripts could also be found in infant iAT. In addition to that, iAT was also able to express transcripts related to cold-induced beige adipogenesis. Our findings indicate an ongoing differentiation and maturation of infant BAT, while iAT displayed a prominent thermogenic potential.

Accordingly, we could identify beige/brite morphology and gene marker expression in young iAT. Furthermore, we could show the presence of glycogen in P6 BAT, P56 BAT and P6 iAT. Glycogen is metabolized through glycophagy in brown adipocytes to generate substrates for lipogenesis and lipid droplet formation (92). This feature allows brown and beige adipocytes to form multilocular lipid droplets which has a better lipid accessibility to perform lipolysis (158). Furthermore, pathways inducing beige adipocytes in infant and adult iAT vary from one another indicating that signals triggering thermogenic fat may be different after birth and adulthood. Altogether, these findings are impactful because they show that beige adipocytes are present in the infant fat. Like brown adipocytes, they contribute to lipolysis and thermogenesis at early age which is important for the developing adipose tissue.

In the first three years after birth, adipose tissue development has a great impact in childhood obesity (94). Losing beige adipocytes early in life is a trait known in obese children, unlike lean children who maintain their beige adipocytes in iAT until puberty (87, 95). Breast milk-derived signals, such as AKGs, can help to sustain beige adipogenesis in iAT (63). However, adipocytes from obese children lose the ability to induce lipolytic activity (88). Hence, it is likely that higher prevalence of beige adipocytes in early life is key to avoid childhood obesity development.

Our study revealed different hub genes and gene networks of P6 iAT, P6 BAT, P56 iAT and P56 BAT to discriminate them from each other. Therefore, we could identify new functions of BAT and beige adipocytes which provide new target genes and gene networks for future studies. As an example, we compared key genes and gene networks of young iAT to show their relations towards cell-cell-adhesion and cell-

matrix interaction. Therefore, we could reveal cytoskeletal protein *Krt5* as a hub gene. Present in the basal layer of skin epithelia, KRT5 can be found in keratinocytes (43). Although infant iAT and the skin are anatomically closed to each other, it is unlikely that adipocytes and keratinocytes are connected. Hence, *Krt5* expression in iAT was observed due to infant adipocytes. There are also other adipocytes able to generate KRT5 such as BAT adipocytes which derive from the keratin-rich embryonic ectoderm (72, 159). In line with the presence of *Krt5* in P6 iAT, obesity or type-I diabetes mellitus (T1DM) suppresses keratin expression including *Krt5* which lead to obesity-associated skin fragility (160, 161). Our data indicates an involvement of keratins at early fat development; however, their role and mechanism are undiscovered, yet.

Genes involved in steroidogenesis were underrepresented in infant iAT. Adipocytes belong to the steroidogenic cells, and are capable of *de novo* synthesis of pregnenolone, oxysterol, 27-hydroxycholosterol and mevalonate (43). Furthermore, it is known that the inhibition of steroidogenesis favours adipocyte differentiation (162). Human adipocyte differentiation in the subcutaneous fat increases the production of enzymes which are involved in the synthesis and inactivation of androgens (163). Therefore, the steroidogenic potential of iAT increases due to adipose tissue maturation. Due to the fact that infant iAT may contain beige adipocytes, the steroidogenic potential of infant and adult iAT is of relevance regarding childhood obesity (43). Beige adipocyte extinction is shown in obese children and as a consequence of insufficient breast milk supply (63, 95). Steroidogenesis includes sexual steroid production which is crucial for the sex-dependent organ differentiations in early life.

As an example, after birth in the first six months in boys and the first 2 months in girls, minipuberty takes places which is a sex-dependent activation of the hypothalamic-pituitary-gonadal axis (164). Minipuberty can be identified through an increase in oestradiol and testosterone which are required for sex-specific growth and maturation. Minipuberty also affects the body composition, BMI, growth velocity and body weight of infants (164). Childhood adiposity affects the obesity state in adulthood, the premature loss of thermogenic fat cells in infant iAT may affect negatively minipuberty, and in turn it may enhance obesogenic metabolism. Several studies already highlighted that insufficient breastfeeding impairs various minipuberty-related physiological functions, for instance body adiposity, cognitive and gonadal development (63, 165, 166). Hence, breastfeeding is eminent for a functional adipose

tissue in the postnatal life. Furthermore, it assists in the hormonal change which takes place during minipuberty. Altogether, these findings are impactful, because they show in another aspect that beige adipocytes are important at early life. Adiposity acquired during infancy can affect the obesity status in adulthood. Therefore, premature loss of beige adipocytes may impair minipuberty and induce obesogenic imprinting.

Our comparative assays aimed to reveal over- and underrepresented DEGs in the respective adipose tissues. Another approach to identify the different adipose tissue depots is to measure beige-, brown- and white-specific adipocyte marker genes.

This thesis highlighted two beige marker genes (*Tbx1* and *Tmem26*) which are known to be present only in adipose tissues accommodating beige adipocytes. Both genes are upregulated after β-adrenergic stimulation or cold exposure which ultimately results in an UCP1 upregulation (69). Hence, TMEM26, encoded by *Tmem26*, enhances indirectly the uncoupling process via UCP1 increase. Furthermore, TMEM26, a cell-surface protein of native beige precursors, can be detected and used to isolate beige cells from the adipose tissue (38). As mentioned before, β-adrenergic stimulation or cold exposure increase *Tbx1* and *Tmem26* expression. While *Tmem26* supports UCP1 expression, *Tbx1* is involved in the β-adrenergic sensitivity and glucose homeostasis *in vivo* (167). In addition to that, its overexpression alone does not increase beige adipocyte development, whereas its absent in iAT results in adipocyte size reduction (167). Even a comparison of brown and beige adipocytes after β-adrenergic stimulation shows a higher expression of *Tbx1* and *Tmem26* in the latter. Hence, both genes were exclusive beige marker genes.

Eva1a is known to be a BAT marker gene (69). Our data revealed that P6 iAT was able to express *Eva1a* nearly to the same degree as BAT in P6 and P56. Due to the ability that P6 iAT could perform mtDNA-driven mitophagy - which will be discussed later in detail - *Eva1a* expression in infant adipocytes was necessary to develop the autophagosome membrane (168).

WAT marker genes such as *Hoxc8* and *Hoxc9* were strongly expressed in iAT of P6 and P56 animals. *Hoxc8* and *Hoxc9* belong to the family of T-box genes which are known to play an important role in the mesoderm development (169). Comparing P6 and P56 iAT showed a higher expression of both genes in the adult iAT. As a WAT marker gene, *Hoxc8* expression increases with diet-induced obesity in mice, in turn, starvation in human reduces *Hoxc8* expression (169). Like *Hoxc8*, *Hoxc9* also increases through obesity development (170). Furthermore, *Hoxc9* is involved in the

adipogenesis by assisting *Fabp4* expression (170). *Hoxc8* is more prevalent in the subcutaneous fat, while *Hoxc9* can be found abundantly in the visceral adipose tissue (171). This is in line with our findings showing a high relative abundance of *Hoxc8* measured in iATs. Besides being WAT marker genes, both genes are known to be present in beige adipocytes at early age (172). Interestingly, *Hoxc8* and *Hoxc9* expression correlates negatively with expression of UCP1 (66). WAT maturation led to the increase of both gene expressions which would explain the decline of UCP1 expression from P6 to P56. Both genes are absent in P6 and P56 BAT which match with the high level of UCP1 measured there.

Cidea and *Dio2* were highly expressed in P56 BAT compared to P6 iAT, P6 BAT and P56 iAT. These genes were also named “browning genes”. CIDEA (encoded by *Cidea*) belongs to the cell death-inducing DNA fragmentation factor A-like effector (Cide) family which is known to play an important role in unilocular lipid droplet formation (173). BAT consists visibly adipocytes with multilocular lipid droplets which does not agree with the relative abundance of *Cidea* found in P56 BAT. Fat-specific protein of 27 β (FSP27β) is an isoform of FSP27, and a member of the Cide family, is also known to be highly expressed in BAT (173). FSP27β forms a complex with CIDEA to allow multilocular fat droplet formation, in contrast, inhibiting FSP27β in a dependent manner increases the unilocular fat droplet formation in brown adipocytes (173). The ratio of both proteins can determine uni-, and multilocular fat droplet formation. Therefore, FSP27β may decline with WAT maturation which allows the formation of one large lipid droplet within the white adipocytes.

Besides *Cidea*, *Dio2* is also a declared browning marker gene which can be measured in beige adipocytes of iAT after cold induction (121). There are two forms of thyroid hormones which are thyroxine (T_4) and the active metabolite 3,5,3´-triiodothyronine (T_3) (174). The level of T_3 and T_4 are controlled by the enzymes deiodinase iodothyronine type 1 (*Dio1*) and deiodinase iodothyronine type 2 (*Dio2*). Especially DIO2 is of interest due to its ability to convert T_4 into the active T_3 (174). T_3 in the BAT induces thermogenesis through mitochondrial uncoupling which is performed by UCP1 (175, 176). It is also known that T_3 enhances fatty acid oxidation, mitochondrial respiration, mitophagy and mitochondrial biogenesis in brown adipocytes (177). Along with *Ppargc1a* and *Ucp1*, *Dio2* expression can also be evoked by PR/SET Domain 16 (PRDM16) which is able to induce a strong brown fat-like phenotype in the WAT (178). Thus, these features could be observed in BAT of P6 and

P56, by far P56 BAT expressed a very high amount of *Dio2* compared to the others. Furthermore, we found that P6 iAT expressed more *Dio2* compared to P56 iAT proofing beige adipocytes among white adipocytes in P6 iAT. Altogether, these findings are impactful, because they show that beige adipocytes were able to express specific white, beige and brown marker genes. Due to that we can conclude that beige adipocytes can be described as a 3rd type of adipocyte in the developing fat.

BAT and iAT were also common in the expression of genes associated with the local angiotensin-kininogen system, GABA-A signaling and neuropeptide receptors in young animals. These overrepresented DEGs in young BAT and iAT were in detail NPY receptors, *Npy*, *Gal*, *Npbwr1* and several genes from the GABA-A signaling. In addition to that, adult BAT shared the same expression regarding genes from the GABA-A signaling. NPY, a orexigenic hormone, is the main ligand for NPY2R which can be expressed by the subcutaneous fat (179). Furthermore, cold stress favours the release of NPY (180). Fat-derived NPY plays an important role in young iAT development regarding angiogenesis and fat cell differentiation (180). Therefore, NPY may support adipose tissue vascularization and the expansion of iAT. Unlike being beneficial in postnatal life, excessive NPY signaling leads to obesity in adults (181, 182).

Adipocytes from P6 iAT showed an increase in the expression of *Npy4r* encoding NPY4R, the receptor for pancreatic polypeptide (PP). Pancreas-derived PP is released in response to meal ingestion and reduce appetite. Low level of PP in plasma is associated with obesity in human, in addition to that, PP level is more prevalent in men compared to women (183–185). Due to the same relation towards obesity, PP may have a similar role, like NPY, in infant adipose tissue development.

According to our data, young iAT and BAT interactome maps showed a relation between the gene network of neuropeptide signaling and genes associated with NFκB and STAT3 signaling. Among other pathways, NFκB signaling was impaired in iAT and BAT of P6 animals. NFκB suppression remained in BAT until adulthood, additionally a low level of immune cells was detected. In contrast to BAT, young iAT lose the local angiotensin-kininogen system, neuropeptide receptor and GABA-A signaling in the process of fat maturation. In turn, iAT maturation leads to the expression of genes related to inflammatory pathways. The angiotensin-kininogen system is able to control cytokine-triggered NFκB and STAT3 signaling through the activation of IκBα and the dephosphorylation of STAT3, respectively (43, 127, 186). Stress activated protein

kinases (SAPKs) belongs to the family of mitogen activated protein kinases (MAPKs) (187, 188). SAPKs can be further divided into smaller families including p38 family which consists of four members. Beige adipocytes might suppress p38-MAPK phosphorylation by the heterodimer of AGTR2 and BDRKRB2 to prevent p38-MAPK-driven adipogenesis (189–191). The gene network and hub gene comparison of P6 and P56 BAT revealed overrepresented DEGs of the *Agtr2* gene network in the infant BAT. In addition, P6 iAT overrepresented genes from the *Agtr2* gene network including angiotensin converting enzyme 2 (*Ace2*) and *Bdkrb2*. ACE2, encoded by *Ace2*, is a SARS-CoV-2 receptor, besides its main role to convert angiotensin 2 (Ang-2) to angiotensin 1-7 (Ang ((1-7)) (192, 193). *Ace2* allows virus entry in human adipocytes (193). Therefore, *Ace2* enhances the COVID-19 infection course which is more lethal for obese patients, although the expression of *Ace2* is independent form obesity (194). Nevertheless, our study revealed less *Ace2* expression in adult iAT compared to P6 iAT. Infant iAT would allow hypothetically more viral entry and due to their immune tolerance of cytosolic nucleic acids (which will be discussed later), an infection with COVID-19 for instance, proceed mostly asymptomatic or mild in young individuals (195).

Infant adipocytes have many potential strategies to control inflammation. It is known that GABA suppresses inflammatory cytokine signaling (125, 196, 197). However, the anti-inflammatory effect of GABA depends on the type of the GABA receptor, as well as the cell expressing the receptor. In addition, GABA receptors. Similarly to the neuropeptide receptors NPYR, NPBWR1 and neuropeptide FF receptor 1 (NPFFR1), GABA-B receptor is a G-protein coupled receptor (43, 198). In contrast, GABA-A receptor is an ionotropic receptor (43, 199). As an example of their functions, GABA-B receptor, present in infant and adult adipose tissue, impairs BAT functions and the inhibition of GABA-B signaling reverts obesity-induced BAT extinction (200). In contrast, activating GABA-A receptor in the lateral hypothalamus reduces food intake and body weight (201). Furthermore, GABA via GABA-B receptor can inhibit obesity-induced macrophage infiltration into the subcutaneous inguinal adipose tissue, but a GABA treatment in the visceral epididymal AT remains unaffected (202). Thereby, GABA prevents local inflammation generated by the infiltrating immune cells.

Macrophages in an obesogenic environment activate the NFκB signaling to enhance their survival within the adipose tissue (203). Accordingly, anti-inflammatory

signals, such as GABA and neuropeptides, are used to control NFκB signaling in young iAT. In the stromal vascular fraction of BAT, the level of immune cells was very low and the suppression of NFκB signaling could be retained until adulthood. Hence, the lack of immune cells in the adipose tissue may repress NFκB signaling. Therefore, GABA treatment through GABA-B receptor in the adipose tissue reduces immune cell content, but in contrary induces the loss of thermogenic fat cells due to the lack of specific inflammatory signals within the adipose tissue. According to our data, GABA-B receptor was equally expressed in P6 iAT and P56 iAT, but a lower level of the receptor was measured in P56 BAT. GABA might help to exclude immune cells in BAT from infancy to adulthood, but how BAT protects its thermogenic fat cells at the same time from the effect of GABA remains undiscovered, yet.

Excessive calorie intake leads to metabolic dysfunction of adipocytes. Therefore, the adipose tissue is dysregulated which leads to dyslipidaemia, immune cell infiltration, impaired vascular structure, and fibrosis (34). Especially, immune cell infiltration along with local inflammation contributes to fat depot expansion which in turn can be impeded by GABA via GABA-B receptor. Nevertheless, a high amount of immune cells, such as T- and B-cells, macrophages, neutrophils and mast cells, infiltrate the adipose tissue which generate a low-grade and chronic inflammation, a hallmark of obesity development (34). In contrast to that, the amount of eosinophils and Th2 cells decreases in the adipose tissue of obese patients (204). Interestingly, Th2 cytokines, such as interleukin 4 (IL-4) and interleukin 13 (IL-13), are known inducers of beige adipocyte differentiation (205, 206). Furthermore, a previous study highlighted IL-4 receptor alpha (IL4Rα) to be crucial for beige adipocyte development after cold induction. Besides Th2 cytokines, beige adipocyte development can also be evoked through inflammatory signals which are generated through pathways, such as the Janus kinase (JAK)/STAT3 signaling or the autocrine IL-6/STAT3 signaling loop (63, 207, 208). In addition to that, there are also inflammatory signals impairing the obesity-associated metabolic shift which ultimately sustain beige adipocytes (209, 210).

In line with previous findings, our study revealed cytosolic mtRNA as a potential inflammatory inducer for beige adipocyte development in infant adipocytes. The endosymbiotic origin theory describes host cell and mitochondria co-dependency regarding the metabolism and energy supply (211). The communication between mitochondria and nucleus is established by the retrograde mitochondria-to-nucleus signaling pathway which is required to transcribe genes for mitochondria maintenance

located within the nuclear genome. In our study we showed that mitochondria could emit their nucleic acid content into the cytosol. This event is in line with previous findings which describe stress-induced mitochondria content leaking due to pathogens, bacteria or metabolic events (142–144).

Due to MVBs and EVs, mtRNA and mtDNA could be transferred to other adipocytes acting like a paracrine signal. Through endocytosis, EVs can deliver their cargo into the cytosol of the recipient adipocytes. After mtRNA detection, cytosolic RNA sensors activate the autocrine IL-6/STAT3 signaling loop. The IL-6/STAT3 signaling allows gene transcription related to beige adipocyte development as it was described before (63). It is known that non-coding, mitochondrial RNA species enables the transcription of mitochondrial genes encoded by the genome located within the nucleus (212). We could also highlight mtRNA in breast milk and P6 EVs indicating mtRNA as a paracrine signal. Six days after birth mice were still dependent on their mothers and required breast milk feeding. Breast milk contain minerals, vitamins, proteins, fatty acids, antibodies and other nutrients in humans (63, 213–215). Besides the nutritional support of breast milk, it has also protective roles during P6 development (216, 217). Breast milk contains EVs to deliver relevant biological cargos (218), such as mtRNA and mtDNA, which are introduced into the recipient cell by EV-membrane fusion (219). In nature, bacteria already used the release of EVs to communicate with their host cells (220, 221). In the cytosol they are recognized by RNA or DNA sensors, respectively. In conclusion, breast milk and P6 EVs supports beige adipocyte development in infant adipose tissue through the transfer of mtRNA via EVs.

RIG-I and MDA5 are the main cytosolic sensor proteins to detect dsRNA (148). RIG-I can bind dsRNA irrespective from the 5´-triphosphate end, while MDA5 can only bind uncapped RNA (93). 5´-triphosphate end is a molecular signature for viral RNA species (222). Hence, a 5´-triphosphate end on the dsRNA is not required to be detected by RIG-I and MDA5. Therefore, mtRNA is a potential target for these RNA sensors as well. Depending on the dsRNA length, it is either bound by RIG-I or MDA5, respectively (223). Mitochondria have a prokaryotic origin; therefore, their genome and relative transcripts can be detected by the host as foreign DNA and RNA. These mtRNA species, such as ribosomal RNA, uncapped mitochondrial mRNA or non-coding mtRNA can be emitted into the cytosol to be detected by RNA sensors (224, 225). According to our data, application of p(dA:dT) to the adipocyte evokes beige adipocyte gene transcription through indirect RIG-I activation (93, 146, 147).

Furthermore, activation of MDA5 through high molecular weight p(I:C) also induce thermogenesis, mitobiogenesis and beige marker gene transcription which are not inducible by single-stranded RNA (93). In addition to that, the lack of RIG-I and MDA5 in mice lead to an impaired mtRNA-driven beige adipocyte development resulting in an early WAT maturation. As indicated by our study, we assumed that mtRNA structure should be long, double-stranded and rich in loop regions (93). These assumptions could be confirmed through *in silico* analysis by RNAfold (226) revealing in all RNA sequences multibranched, internal and hairpin loops (93).

The beneficial effects of mtRNA regarding beige adipocyte development is dose dependent, excess mitochondrial content release is a harmful signal for the cell resulting in an elevated IFN-response which ultimately damages the thermogenic fat development (83–85). This leads to mitochondrial dysfunctions or triggers adipocyte apoptosis through the mitochondrial pathway (227, 228) which ultimately enhance obesity-related metabolic diseases (229, 230).

In conclusion, our study show that infant adipocytes lack an immune response to mtRNA or mtDNA due to the lack of cytosolic DNA sensors and IRF7 expression. Regardless of an immune response, infant adipocytes were able to benefit from the presence of cytosolic mtDNA since it stimulated mitophagy. Therefore, the amount of mitochondria could be controlled by cytosolic mtDNA. This prevents inflammation, by removing excess or damaged mitochondria. Moreover, mtRNA induces mitobiogenesis. The effect of mtRNA and mtDNA, without inflammation as a side effect, can be only documented in infant adipocytes so far. The key protein is hereby IRF7 which has to be impaired to allow these features.

Infant adipocytes lose IRF7 suppression during adipocyte maturation. This may be achieved through the induction of STAT1 and NFκB signaling (43). On the contrary, IRF7 inhibition could be achieved by the application of Vit-D3. Vit-D3 is known as an immune regulating metabolite and its insufficient supply leads to autoimmune processes (231). The conversion of Vit-D3 into the active compound calcitriol was supported by mtRNA. Vit-D3 was detectable in breast milk, breast milk- and formula milk EVs, and in P6 EVs. Hence, a constant supply of Vit-D3 paired with cytosolic mtRNA sustained beige adipocyte development. Dysregulating IRF7 suppression by diet-induced inflammation impaired the immune privilege for mitochondria in infant adipocyte leading to an early loss of beige adipocyte. The innate immune response of the adipose tissue includes VDR signaling and many others (152). VDR is known to

compromise IFN-response and the expression of IRF7 (232, 233). The IRF7 promoter accommodates 4 NFκB binding sites (234). Interestingly, NFκB signaling can be impaired by VDR interaction with IκB kinase β (IKKβ), this process can be enhanced by calcitriol (235). VDR also targets subunits of NFκB, such as p65 in different organs (235, 236) or p50 in macrophages (237) which ultimately impairs NFκB-mediated inflammation. IKKβ is a subunit of IKK and needs IKKα and IKKγ to degrade IκBα (238). The degradation of IκBα leads to the canonical NFκB activation (239). IKK can be triggered through cytokines, growth factors and many other stress-inducing agents (186). As described before, a heterodimer formation of AGTR2 and BDKRB2 induces IκBα expression to inhibit NFκB signaling. Thereby, VDR can support the angiotensin-kallikrein network by the suppression of IKK formation in infant iAT.

Furthermore, VDR improves glucose uptake and prevents oxidative stress (240). Oxidative stress is known to trigger inflammation pathways and can caused chronic inflammation by constant exposure over a long time (241). Furthermore, infant iAT cannot tolerate oxidative stress due to the excess amount of mitochondria present in beige adipocytes. Reactive oxygen species damage mitochondria (242) and would force an uncontrolled mtRNA and mtDNA leaking which would ultimately support the loss of beige adipocytes. Furthermore, VDR can form homo- and heterodimers, therefore, it is able to interact with retinoid-X-receptor (RXR) (243). VDR-RXR heterodimer induces the gene expression of cathelicidin (encoded by *Camp*) and defensin beta 4 (231, 244), genes which are known to be abundantly expressed in P6 iAT (43, 152). The abundance of cathelicidin and defensin decreases due to the fat maturation and that might be mediated through the decrease of VDR expression. Accordingly, a heterodimer of VDR and RXR cannot be formed to generated antimicrobial peptides which protect the host from intracellular *Mycobacterium tuberculosis* (244). Vit-D3 also inhibited the expression of *Coro1a* which is involved in the reduction of the autophagosome formation (153). In line with the finding a strong *Eva1a* expression in P6 iAT allows the development of the autophagosomal membrane (168). Therefore, we could see mtDNA-driven STING-mediated mitophagy, an autophagy process of mitochondria, in the developing subcutaneous adipose tissue (93, 245).

Vit-D3 supplementation is routine today in postnatal care which might be the reason for the *Irf7*-suppressing effect of the formula milk EVs in our study. Obese children and adolescence develop a Vit-D3 deficiency which enhances the risk factor

for co-morbid diseases (246–248). Although Vit-D3/VDR signaling prevents weight gain in the muscle through UCP3, VDR overexpression in mice increases mouse body weight (249, 250). In line with that, formula milk was originally used to enhance Vit-D3 uptake and to increase body weight (251). In contrast to breast milk, formula milk does not consist maternal signals to sustain beige adipocyte development, moreover, it contains obesogenic signals (63). Increasing the amount of Vit-D3 in obese children will not revert obesity due to the lack of VDR signaling as a result of the metabolic disorder. In addition to that, VDR overexpression studies in adipose tissue of mice show an increase body weight and plasma lipid levels (250). Therefore, an elevated plasma FFA level can be measured which in an excessive amount is known to impair glucose transporter type 4 (GLUT4) presentation on the cell membrane (31, 252). Furthermore, excess FFA in the plasma evokes insulin secretion until exhaustion in pancreatic β-cells (lipotoxicity of the pancreas) (253, 254). Impaired glucose transport in combination with increased insulin secretion results in type 2 diabetes mellitus (T2DM) which is a co-morbidity of obesity (30). In addition to that, GABA treatment protects from T1DM-driven loss of β-cells mass (255). Hence, the overexpression of VDR or an increase of Vit-D3 supply will not help to treat obesity.

During obesity the amount of Th2 cytokines decreases while Th1 cytokines are elevated due to immune cell infiltration (34, 204). The active form of Vit-D3, calcitriol, can mend the Th2 cytokine production with its immunosuppressive effect on dendric cells (DCs) (256). Accordingly, DCs releases interleukin-12 (IL-12) which results in the production of Th1 cytokines, such as IFNγ and interleukin-2 (IL-2). Vit-D3 presence has a broad anti-inflammatory effect. In contrast, VDR knockout mice do not develop obesity after HFD induction (257, 258). Infant subcutaneous adipose tissue has lipolytic activity and was able to liberate FFA in a physiological amount to convert it immediately into heat and ATP (88), this feature declines with childhood obesity.

Nevertheless, beige adipocytes were able to use Vit-D3 via VDR to reduce mtRNA-driven IFN response. This mechanism allows to household the expanded mitochondrial network which used FFA as a fuel to generate thermogenesis and energy supply (43). Furthermore, we could show that Vit-D3 in combination with cytosolic mtRNA induce beige adipocyte development in adult and infant mice (93). A combination of both ligands reduces body weight in diet-induced obese mice which shows that the combination treatment is a potential approach to reduce obesity.

5. Conclusion

1. This thesis shows infant adipose tissue is rich in beige fat cells. Genes involved in the thermogenesis and lipid catabolism were expressed in infant iAT. Therefore, beige adipocytes in P6 iAT used fat to generate energy and heat. Lipolysis can be performed by beige and brown adipocytes and the inhibition of lipolysis results in thermogenic fat development (259). Furthermore, lipid signals induce beige and brown adipocyte differentiation (260) and breast milk-derived lipid metabolites sustain them in infants (63).
2. We also show a that a metabolic reprogramming appears during the maturation of the subcutaneous adipose tissue. The fat depot which is a fat-burning, heat- and energy generating tissue at early life, transforms into a lipid-accumulating energy storage site by adulthood. This observation is supported by the intense lipid catabolism and fatty acid release from the subcutaneous adipose tissue which is noticed in newborns of mammals and humans (40, 97, 98). In addition to that, subcutaneous fat cells can be induced into beige adipocytes upon cold exposure (74, 121). To determine and prevent childhood obesity, it is important to monitor beige adipocyte population in the subcutaneous adipose tissue of infants. Since the loss of beige adipocytes accelerates WAT maturation which results in childhood obesity.
3. We also show that there is an immune privilege of mitochondrial content in infant adipocytes. As a result, mitochondrial content is not immunogenic in the early postnatal life. This lack of immune response was due toa VDR-mediated IRF7 suppression in infant adipocytes. Furthermore, adipocyte maturation leads to a rise of IRF7 expression which can be reduced by Vit-D3. Like mice, human adipocytes are able to suppress cytosolic mtRNA- or mtDNA-driven inflammation response as long as Vit-D3 is supplied (93).
4. The thesis also shows that diet-induced obesity in infant or adult mice led to the increase of *Irf7* transcription and compromised the transcription of *Vdr*. The change of *Irf7*-*Vdr*-ratio within adipocytes led to immune response to mtRNA and mtDNA. This was due to the activation of RIG-I, MDA5 and a set of DNA sensors. STING-mediated mitophagy was induced by mtDNA while mtRNA triggered Vit-D3 conversion, IFN production and beige adipocyte development (Figure 15).

5. As of medical impact, we show here that mtRNA triggered the expression of nucleus-encoded mitochondrial genes, allowing beige adipocyte development. When VDR is active, this signaling is operative without evoking an immune response against cytosolic mtRNA (Figure 15). The therapeutic combination of mtRNA and Vit-D3 may induce mitochondria-to-nucleus signaling and protect against obesity.

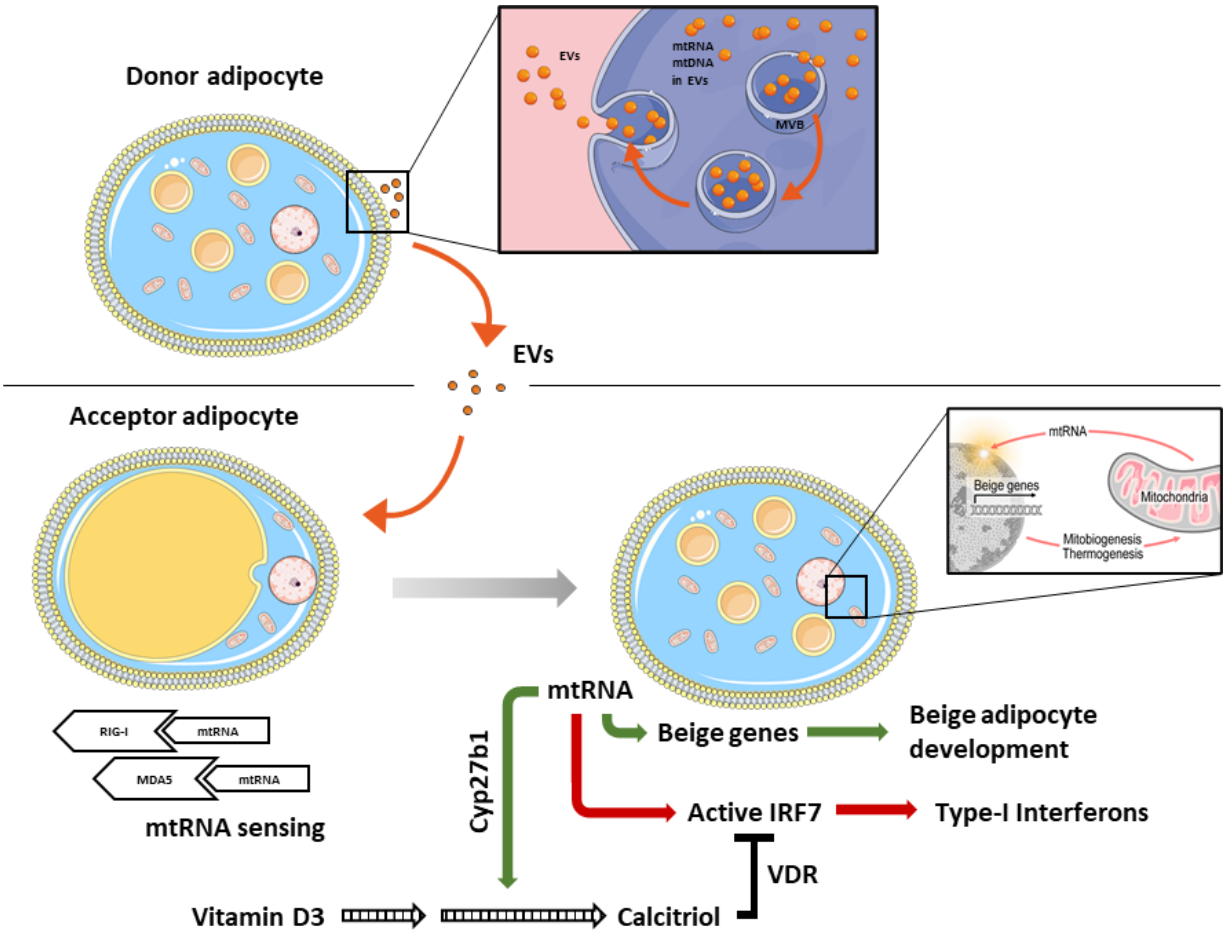

Figure 15: Role of mtRNA and Vit-D3 in the mitochondria-to-nucleus signaling

Donor adipocyte can pack mtRNA and mtDNA into EVs which are released into the extracellular matrix by MVB and exocytosis. As an endogenous signal, mtRNA can be taken up by an acceptor adipocyte. In the cytosol, mtRNA triggers the RIG-I/MDA5/ IL-6/STAT3 pathway inducing Vit-D3 metabolism, IFN production and beige adipocyte development. Acting through VDR, Vit-D3 is a potent IRF7 suppressor. Active VDR signaling is necessary to allow mtRNA-driven beige adipocyte development. Infant adipocytes are immune privileged for mitochondria which enables a retrograde mitochondria-to-nucleus signaling to induce mitobiogenesis and beige fat development. Source: Figure from (93), reused under license CC BY 4.0 (https://creativecommons.org/licenses/by/4.0/).

6. List of publications

1. **Hoang, A.C.**; Yu, H.; Röszer, T. (2021) Transcriptional landscaping identifies a beige adipocyte depot in the newborn mouse. *Cells* 2021, *10*, 2368. [IF 6.6]
2. Yu H., Dilbaz S., Coßmann J., **Hoang A.C.**, Diedrich V., Herwig A., Harauma A., Hoshi Y., Moriguchi T., Landgraf K., Körner A., Lucas C., Brodesser S., Balogh L., Thuróczy J., Karemore G., Kuefner M.S., Park E.A., Rapp C., Travers J.B., Röszer, T. (2019) Breast milk alkylglycerols sustain beige adipocytes through adipose tissue macrophages. *The Journal of Clinical Investigation*, 129:2485-2499 [IF 13.251]
3. Waqas, S.F.H., **Hoang, A.C.**, Lin, Y., Ampem, G., Azegrouz, H., Balogh, L., Thuróczy, J., Chen, J., Gerling, I.C., Nam, S., Lim, J., Martinez-Ibañez, J., Real, J.T., Paschke, S., Quillet, R., Ayachi, S., Simonin, F., Schneider, M., Brinkman, J., Lamming, D.W., Seroogy, C.M., Röszer, T. (2017) Neuropeptide FF increases M2 activation and self-renewal of adipose tissue macrophages. *The Journal of Clinical Investigation* 127:2842-2854, corrigendum 127:3559 [IF 13.250]
4. Waqas, S.F.H., Noble, A., **Hoang A.C.**, Ampem, G., Popp, M., Strauß, S., Guille, M., Röszer, T. (2017) Adipose tissue macrophages develop from bone marrow-independent progenitors in *Xenopus laevis* and mouse. *Journal of Leukocyte Biology* 102: 845-855 [IF 4.165]

As a preprint:

Hoang AC, Yu H, Lin YT, Chen JC, Chen CC, Diedrich V, Herwig A, Landgraf K, Körner A, Röszer T. Immune privilege of adipocyte mitochondria protects from obesity. In Review **2021**. *under review at Nature Metabolism.* doi:10.21203/rs.3.rs-988599/v1

7. References

1. GBD 2015 Obesity Collaborators et al. Health Effects of Overweight and Obesity in 195 Countries over 25 Years. *N Engl J Med* 2017;377(1):13–27.

2. Fruh SM. Obesity: Risk factors, complications, and strategies for sustainable long-term weight management. *J Am Assoc Nurse Pract* 2017;29(Suppl 1):S3–S14.

3. Hruby A, Hu FB. The Epidemiology of Obesity: A Big Picture. *Pharmacoeconomics* 2015;33(7):673–689.

4. Obesity and overweight [Internet]https://www.who.int/news-room/fact-sheets/detail/obesity-and-overweight. cited January 14, 2021

5. Chooi YC, Ding C, Magkos F. The epidemiology of obesity. *Metabolism* 2019;92:6–10.

6. Purnell JQ. Definitions, Classification, and Epidemiology of Obesity [Internet]. In: Feingold KR et al eds. *Endotext*. South Dartmouth (MA): MDText.com, Inc.; 2000:

7. Overweight and Obesity | NHLBI, NIH [Internet]https://www.nhlbi.nih.gov/health-topics/overweight-and-obesity. cited December 1, 2021

8. CDC. Adult Overweight & Obesity [Internet]. *Centers for Disease Control and Prevention* 2021;https://www.cdc.gov/obesity/adult/causes.html. cited December 1, 2021

9. Choquet H, Meyre D. Genetics of Obesity: What have we Learned?. *Curr Genomics* 2011;12(3):169–179.

10. Bouchard C. Defining the genetic architecture of the predisposition to obesity: a challenging but not insurmountable task. *The American Journal of Clinical Nutrition* 2010;91(1):5–6.

11. Ferraù F, Korbonits M. Metabolic comorbidities in Cushing's syndrome. *European Journal of Endocrinology* 2015;173(4):M133–M157.

12. Sam S. Obesity and Polycystic Ovary Syndrome. *Obes Manag* 2007;3(2):69–73.

13. Sanyal D, Raychaudhuri M. Hypothyroidism and obesity: An intriguing link. *Indian J Endocrinol Metab* 2016;20(4):554–557.

14. Speakman JR. Obesity and thermoregulation. *Handb Clin Neurol* 2018;156:431–443.

15. Rosen ED, Spiegelman BM. What We Talk About When We Talk About Fat. *Cell* 2014;156(1):20–44.

16. Hsu P-S, Wu C-S, Chang J-F, Lin W-N. Leptin Promotes $cPLA_2$ Gene Expression through Activation of the MAPK/NF-κB/p300 Cascade. *Int J Mol Sci* 2015;16(11):27640–27658.

17. Guan XM, Yu H, Van der Ploeg LH. Evidence of altered hypothalamic pro-opiomelanocortin/ neuropeptide Y mRNA expression in tubby mice. *Brain Res Mol Brain Res* 1998;59(2):273–279.

18. Ge TT et al. Role of leptin in the regulation of food intake in fasted mice. *J Cell Mol Med* 2020;24(8):4524–4532.

19. Chandra A et al. The relationship of body mass and fat distribution with incident hypertension: observations from the Dallas Heart Study. *J Am Coll Cardiol* 2014;64(10):997–1002.

20. Flehmig G et al. Identification of adipokine clusters related to parameters of fat mass, insulin sensitivity and inflammation. *PLoS One* 2014;9(6):e99785.

21. Csongrádi É et al. Adipokines as atherothrombotic risk factors in obese subjects: Associations with haemostatic markers and common carotid wall thickness. *Nutr Metab Cardiovasc Dis* 2017;27(6):571–580.

22. Morioka T et al. Leptin is associated with vascular endothelial function in overweight patients with type 2 diabetes. *Cardiovasc Diabetol* 2014;13:10.

23. Pereira SS, Alvarez-Leite JI. Adipokines: biological functions and metabolically healthy obese profile. *JRLCR* 2014;7:15–25.

24. Hong E-G et al. Interleukin-10 Prevents Diet-Induced Insulin Resistance by Attenuating Macrophage and Cytokine Response in Skeletal Muscle. *Diabetes* 2009;58(11):2525–2535.

25. Esposito K et al. Association of Low Interleukin-10 Levels with the Metabolic Syndrome in Obese Women. *The Journal of Clinical Endocrinology & Metabolism* 2003;88(3):1055–1058.

26. Young RW. Evolution of the human hand: the role of throwing and clubbing. *J Anat* 2003;202(1):165–174.

27. Global report on diabetes [Internet]https://www.who.int/publications-detail-redirect/9789241565257. cited November 24, 2020

28. Chobot A, Górowska-Kowolik K, Sokołowska M, Jarosz-Chobot P. Obesity and diabetes-Not only a simple link between two epidemics. *Diabetes Metab Res Rev* 2018;34(7):e3042.

29. Longo M et al. Adipose Tissue Dysfunction as Determinant of Obesity-Associated Metabolic Complications. *Int J Mol Sci* 2019;20(9):E2358.

30. Bays HE et al. Obesity, adiposity, and dyslipidemia: A consensus statement from the National Lipid Association. *Journal of Clinical Lipidology* 2013;7(4):304–383.

31. Watson RT, Pessin JE. GLUT4 translocation: the last 200 nanometers. *Cell Signal* 2007;19(11):2209–2217.

32. Huang X, Liu G, Guo J, Su Z. The PI3K/AKT pathway in obesity and type 2 diabetes. *Int J Biol Sci* 2018;14(11):1483–1496.

33. Han L et al. Free fatty acid can induce cardiac dysfunction and alter insulin signaling pathways in the heart. *Lipids Health Dis* 2018;17:185.

34. Fuster JJ, Ouchi N, Gokce N, Walsh K. Obesity-induced Changes in Adipose Tissue Microenvironment and Their Impact on Cardiovascular Disease. *Circ Res* 2016;118(11):1786–1807.

35. Hahn P, Novak M. Development of brown and white adipose tissue. *J Lipid Res* 1975;16(2):79–91.

36. Hull D. The structure and function of brown adipose tissue. *Br Med Bull* 1966;22(1):92–96.

37. Church C, Horowitz M, Rodeheffer M. WAT is a functional adipocyte?. *Adipocyte* 2012;1(1):38–45.

38. Harms M, Seale P. Brown and beige fat: development, function and therapeutic potential. *Nat Med* 2013;19(10):1252–1263.

39. Bartelt A, Heeren J. Adipose tissue browning and metabolic health. *Nat Rev Endocrinol* 2014;10(1):24–36.

40. Hardman MJ, Hull D. Fat metabolism in brown adipose tissue in vivo. *J Physiol* 1970;206(2):263–273.

41. Farkas V, Kelenyi G, Sandor A. A dramatic accumulation of glycogen in the brown adipose tissue of rats following recovery from cold exposure. *Arch Biochem Biophys* 1999;365(1):54–61.

42. Mayeuf-Louchart A. Uncovering the Role of Glycogen in Brown Adipose Tissue. *Pharm Res* 2021;38(1):9–14.

43. Hoang AC, Yu H, Röszer T. Transcriptional Landscaping Identifies a Beige Adipocyte Depot in the Newborn Mouse. *Cells* 2021;10(9):2368.

44. Novak M, Monkus E, Pardo V. Human Neonatal Subcutaneous Adipose Tissue. *NEO* 1971;19(4–6):306–321.

45. Jastroch M et al. Marsupial uncoupling protein 1 sheds light on the evolution of mammalian nonshivering thermogenesis. *Physiol Genomics* 2008;32(2):161–169.

46. Townsend K, Tseng Y-H. Brown adipose tissue. *Adipocyte* 2012;1(1):13–24.

47. Fedorenko A, Lishko PV, Kirichok Y. Mechanism of Fatty-Acid-Dependent UCP1 Uncoupling in Brown Fat Mitochondria. *Cell* 2012;151(2):400–413.

48. Aquila H, Link TA, Klingenberg M. The uncoupling protein from brown fat mitochondria is related to the mitochondrial ADP/ATP carrier. Analysis of sequence homologies and of folding of the protein in the membrane. *EMBO J* 1985;4(9):2369–2376.

49. Pei Y et al. Effect of quercetin on nonshivering thermogenesis of brown adipose tissue in high-fat diet-induced obese mice. *J Nutr Biochem* 2021;88:108532.

50. Nowack J, Giroud S, Arnold W, Ruf T. Muscle Non-shivering Thermogenesis and Its Role in the Evolution of Endothermy. *Front Physiol* 2017;8:889.

51. Golozoubova V et al. Only UCP1 can mediate adaptive nonshivering thermogenesis in the cold. *FASEB J* 2001;15(11):2048–2050.

52. Alcalá M et al. Increased inflammation, oxidative stress and mitochondrial respiration in brown adipose tissue from obese mice. *Sci Rep* 2017;7(1):16082.

53. Alcalá M, Calderon-Dominguez M, Serra D, Herrero L, Viana M. Mechanisms of Impaired Brown Adipose Tissue Recruitment in Obesity. *Frontiers in Physiology* 2019;10:94.

54. Gilsanz V, Hu HH, Kajimura S. Relevance of brown adipose tissue in infancy and adolescence. *Pediatr Res* 2013;73(1):3–9.

55. Pan R, Zhu X, Maretich P, Chen Y. Combating Obesity With Thermogenic Fat: Current Challenges and Advancements. *Front Endocrinol (Lausanne)* 2020;11:185.

56. Palmer BF, Clegg DJ. Non-shivering thermogenesis as a mechanism to facilitate sustainable weight loss. *Obes Rev* 2017;18(8):819–831.

57. Valente A, Jamurtas AZ, Koutedakis Y, Flouris AD. Molecular pathways linking non-shivering thermogenesis and obesity: focusing on brown adipose tissue development. *Biol Rev Camb Philos Soc* 2015;90(1):77–88.

58. Sanders OD, Rajagopal JA, Rajagopal L. Menthol to Induce Non-shivering Thermogenesis via TRPM8/PKA Signaling for Treatment of Obesity. *J Obes Metab Syndr* 2021;30(1):4–11.

59. Ikeda K, Maretich P, Kajimura S. The Common and Distinct Features of Brown and Beige Adipocytes. *Trends Endocrinol Metab* 2018;29(3):191–200.

60. Carobbio S, Rosen B, Vidal-Puig A. Adipogenesis: new insights into brown adipose tissue differentiation. *J Mol Endocrinol* 2013;51(3):T75-85.

61. Pilkington A-C, Paz HA, Wankhade UD. Beige Adipose Tissue Identification and Marker Specificity—Overview. *Frontiers in Endocrinology* 2021;12:8.

62. Paulo E, Wang B. Towards a Better Understanding of Beige Adipocyte Plasticity. *Cells* 2019;8(12):1552.

63. Yu H et al. Breast milk alkylglycerols sustain beige adipocytes through adipose tissue macrophages. *J Clin Invest* 2019;129(6):2485–2499.

64. Shi F, Collins S. Second messenger signaling mechanisms of the brown adipocyte thermogenic program: an integrative perspective. *Horm Mol Biol Clin Investig* 2017;31(2). doi:10.1515/hmbci-2017-0062

65. Cannon B, de Jong JMA, Fischer AW, Nedergaard J, Petrovic N. Human brown adipose tissue: Classical brown rather than brite/beige?. *Experimental Physiology* 2020;105(8):1191–1200.

66. Jespersen NZ et al. A classical brown adipose tissue mRNA signature partly overlaps with brite in the supraclavicular region of adult humans. *Cell Metab* 2013;17(5):798–805.

67. Sharp LZ et al. Human BAT Possesses Molecular Signatures That Resemble Beige/Brite Cells. *PLOS ONE* 2012;7(11):e49452.

68. Stine RR et al. EBF2 promotes the recruitment of beige adipocytes in white adipose tissue. *Mol Metab* 2016;5(1):57–65.

69. Wu J et al. Beige adipocytes are a distinct type of thermogenic fat cell in mouse and human. *Cell* 2012;150(2):366–376.

70. Röszer T. Co-Evolution of Breast Milk Lipid Signaling and Thermogenic Adipose Tissue. *Biomolecules* 2021;11(11):1705.

71. Sanchez-Gurmaches J, Guertin DA. Adipocyte lineages: tracing back the origins of fat. *Biochim Biophys Acta* 2014;1842(3):340–351.

72. Billon N et al. The generation of adipocytes by the neural crest. *Development* 2007;134(12):2283–2292.

73. Fu M et al. Neural Crest Cells Differentiate Into Brown Adipocytes and Contribute to Periaortic Arch Adipose Tissue Formation. *Arteriosclerosis, Thrombosis, and Vascular Biology* 2019;39(8):1629–1644.

74. Ravussin E, Kozak LP. Have we entered the brown adipose tissue renaissance?. *Obes Rev* 2009;10(3):265–268.

75. Gray MW. Lynn Margulis and the endosymbiont hypothesis: 50 years later. *MBoC* 2017;28(10):1285–1287.

76. Martin WF, Garg S, Zimorski V. Endosymbiotic theories for eukaryote origin. *Philos Trans R Soc Lond B Biol Sci* 2015;370(1678):20140330.

77. López-García P, Moreira D. Selective forces for the origin of the eukaryotic nucleus. *BioEssays* 2006;28(5):525–533.

78. Moreira null, Lopez-Garcia null. Symbiosis between methanogenic archaea and delta-proteobacteria as the origin of eukaryotes: the syntrophic hypothesis. *J Mol Evol* 1998;47(5):517–530.

79. Mills EL, Kelly B, O'Neill LAJ. Mitochondria are the powerhouses of immunity. *Nat Immunol* 2017;18(5):488–498.

80. Krauss S, Zhang C-Y, Lowell BB. The mitochondrial uncoupling-protein homologues. *Nat Rev Mol Cell Biol* 2005;6(3):248–261.

81. West AP et al. Mitochondrial DNA stress primes the antiviral innate immune response. *Nature* 2015;520(7548):553–557.

82. Zhong Z et al. New mitochondrial DNA synthesis enables NLRP3 inflammasome activation. *Nature* 2018;560(7717):198–203.

83. Kissig M et al. PRDM16 represses the type I interferon response in adipocytes to promote mitochondrial and thermogenic programing. *EMBO J* 2017;36(11):1528–1542.

84. Kumari M et al. IRF3 promotes adipose inflammation and insulin resistance and represses browning. *J Clin Invest* 2016;126(8):2839–2854.

85. Bai J et al. Mitochondrial stress-activated cGAS-STING pathway inhibits thermogenic program and contributes to overnutrition-induced obesity in mice. *Commun Biol* 2020;3(1):1–14.

86. Beyerlein A, Donnachie E, Jergens S, Ziegler A-G. Infections in Early Life and Development of Type 1 Diabetes. *JAMA* 2016;315(17):1899–1901.

87. Verduci E et al. Brown Adipose Tissue: New Challenges for Prevention of Childhood Obesity. A Narrative Review. *Nutrients* 2021;13(5):1450.

88. Landgraf K et al. Evidence of early alterations in adipose tissue biology and function and its association with obesity-related inflammation and insulin resistance in children. *Diabetes* 2015;64(4):1249–1261.

89. Sahoo K et al. Childhood obesity: causes and consequences. *J Family Med Prim Care* 2015;4(2):187–192.

90. Herrera E, Amusquivar E. Lipid metabolism in the fetus and the newborn. *Diabetes Metab Res Rev* 2000;16(3):202–210.

91. Whyte RK, Bayley HS. Energy metabolism of the newborn infant. *Adv Nutr Res* 1990;8:79–108.

92. Mayeuf-Louchart A et al. Glycogen Dynamics Drives Lipid Droplet Biogenesis during Brown Adipocyte Differentiation. *Cell Reports* 2019;29(6):1410-1418.e6.

93. Hoang AC et al. Immune privilege of adipocyte mitochondria protects from obesity [Internet]2021; doi:10.21203/rs.3.rs-988599/v1

94. Geserick M et al. Acceleration of BMI in Early Childhood and Risk of Sustained Obesity. *New England Journal of Medicine* 2018;379(14):1303–1312.

95. Rockstroh D et al. Direct Evidence of Brown Adipocytes in Different Fat Depots in Children. *PLOS ONE* 2015;10(2):e0117841.

96. de Jong JMA, Larsson O, Cannon B, Nedergaard J. A stringent validation of mouse adipose tissue identity markers. *Am J Physiol Endocrinol Metab* 2015;308(12):E1085-1105.

97. Novak M, Monkus E. Metabolism of subcutaneous adipose tissue in the immediate postnatal period of human newborns. 1. Developmental changes in lipolysis and glycogen content. *Pediatr Res* 1972;6(2):73–80.

98. Novak M, Penn D, Monkus E. Regulation of lipolysis in human neonatal adipose tissue. Effects of alteration in carbohydrate metabolism. *Biol Neonate* 1973;22(5):451–467.

99. Love MI, Huber W, Anders S. Moderated estimation of fold change and dispersion for RNA-seq data with DESeq2. *Genome Biology* 2014;15(12):550.

100. Kuleshov MV et al. Enrichr: a comprehensive gene set enrichment analysis web server 2016 update. *Nucleic Acids Res* 2016;44(W1):W90-97.

101. Schneider CA, Rasband WS, Eliceiri KW. NIH Image to ImageJ: 25 years of image analysis. *Nat Methods* 2012;9(7):671–675.

102. Rusinova I et al. INTERFEROME v2.0: an updated database of annotated interferon-regulated genes. *Nucleic Acids Research* 2013;41(D1):D1040–D1046.

103. Mi H, Muruganujan A, Casagrande JT, Thomas PD. Large-scale gene function analysis with the PANTHER classification system. *Nat Protoc* 2013;8(8):1551–1566.

104. SMART [Internet]. *Servier Medical Art* https://smart.servier.com/. cited March 5, 2022

105. Waqas SFH et al. Neuropeptide FF increases M2 activation and self-renewal of adipose tissue macrophages. *J Clin Invest* 2017;127(7):2842–2854.

106. Hassnain Waqas SF et al. Adipose tissue macrophages develop from bone marrow–independent progenitors in Xenopus laevis and mouse. *J Leukoc Biol* 2017;102(3):845–855.

107. Ampem G, Röszer T. Isolation and Characterization of Adipose Tissue Macrophages. *Methods Mol Biol* 2019;1966:225–236.

108. Zebisch K, Voigt V, Wabitsch M, Brandsch M. Protocol for effective differentiation of 3T3-L1 cells to adipocytes. *Analytical Biochemistry* 2012;425(1):88–90.

109. Lane N. Hot mitochondria?. *PLOS Biology* 2018;16(1):e2005113.

110. Chrétien D et al. Mitochondria are physiologically maintained at close to 50 °C. *PLOS Biology* 2018;16(1):e2003992.

111. Kim D, Langmead B, Salzberg SL. HISAT: a fast spliced aligner with low memory requirements. *Nat Methods* 2015;12(4):357–360.

112. Langmead B, Salzberg SL. Fast gapped-read alignment with Bowtie 2. *Nat Methods* 2012;9(4):357–359.

113. Langmead B, Wilks C, Antonescu V, Charles R. Scaling read aligners to hundreds of threads on general-purpose processors. *Bioinformatics* 2019;35(3):421–432.

114. Szklarczyk D et al. STRING v11: protein-protein association networks with increased coverage, supporting functional discovery in genome-wide experimental datasets. *Nucleic Acids Res* 2019;47(D1):D607–D613.

115. Waldenström A, Gennebäck N, Hellman U, Ronquist G. Cardiomyocyte Microvesicles Contain DNA/RNA and Convey Biological Messages to Target Cells. *PLOS ONE* 2012;7(4):e34653.

116. Zabeo D et al. Exosomes purified from a single cell type have diverse morphology. *J Extracell Vesicles* 2017;6(1):1329476.

117. Plank C, Rosenecker J. Magnetofection: The Use of Magnetic Nanoparticles for Nucleic Acid Delivery. *Cold Spring Harb Protoc* 2009;2009(6):pdb.prot5230.

118. Mouse Pup Appearance by Age | Laboratory Animal Resource Center (LARC) [Internet]https://larc.ucsf.edu/mouse-pup-appearance-age. cited November 21, 2021

119. Life span as a biomarker [Internet]. *The Jackson Laboratory* https://www.jax.org/research-and-faculty/research-labs/the-harrison-lab/gerontology/life-span-as-a-biomarker. cited November 21, 2021

120. Birsoy K et al. Cellular program controlling the recovery of adipose tissue mass: An in vivo imaging approach. *Proc Natl Acad Sci U S A* 2008;105(35):12985–12990.

121. Kozak LP. The genetics of brown adipocyte induction in white fat depots. *Front Endocrinol (Lausanne)* 2011;2:64.

122. Zuriaga MA, Fuster JJ, Gokce N, Walsh K. Humans and Mice Display Opposing Patterns of "Browning" Gene Expression in Visceral and Subcutaneous White Adipose Tissue Depots. *Front Cardiovasc Med* 2017;4:27.

123. Nascimento EBM et al. Genetic Markers of Brown Adipose Tissue Identity and In Vitro Brown Adipose Tissue Activity in Humans. *Obesity (Silver Spring)* 2018;26(1):135–140.

124. Perugini J et al. Zic1 mRNA is transiently upregulated in subcutaneous fat of acutely cold-exposed mice. *J Cell Physiol* 2019;234(3):2031–2036.

125. Prud'homme G, Glinka Y, Wang Q. GABA exerts anti-inflammatory and immunosuppressive effects (P5175). *The Journal of Immunology* 2013;190(1 Supplement):68.15-68.15.

126. Marcondes S, Antunes E. The plasma and tissue kininogen-kallikrein-kinin system: role in the cardiovascular system. *Curr Med Chem Cardiovasc Hematol Agents* 2005;3(1):33–44.

127. Abadir PM, Periasamy A, Carey RM, Siragy HM. Angiotensin II type 2 receptor-bradykinin B2 receptor functional heterodimerization. *Hypertension* 2006;48(2):316–322.

128. Berg AH, Lin Y, Lisanti MP, Scherer PE. Adipocyte differentiation induces dynamic changes in NF-kappaB expression and activity. *Am J Physiol Endocrinol Metab* 2004;287(6):E1178-1188.

129. Park Y-M, Myers M, Vieira-Potter VJ. Adipose Tissue Inflammation and Metabolic Dysfunction: Role of Exercise. *Mo Med* 2014;111(1):65–72.

130. Reilly SM, Saltiel AR. Adapting to obesity with adipose tissue inflammation. *Nat Rev Endocrinol* 2017;13(11):633–643.

131. Feng Z et al. Role of RAGE in obesity-induced adipose tissue inflammation and insulin resistance. *Cell Death Discov.* 2021;7(1):1–8.

132. Kristóf E et al. Interleukin-6 released from differentiating human beige adipocytes improves browning. *Exp Cell Res* 2019;377(1–2):47–55.

133. Motwani M, Pesiridis S, Fitzgerald KA. DNA sensing by the cGAS-STING pathway in health and disease. *Nat Rev Genet* 2019;20(11):657–674.

134. Shin S-I et al. Z-DNA-forming sites identified by ChIP-Seq are associated with actively transcribed regions in the human genome. *DNA Res* 2016;23(5):477–486.

135. Takaoka A et al. DAI (DLM-1/ZBP1) is a cytosolic DNA sensor and an activator of innate immune response. *Nature* 2007;448(7152):501–505.

136. Lugrin J, Martinon F. The AIM2 inflammasome: Sensor of pathogens and cellular perturbations. *Immunological Reviews* 2018;281(1):99–114.

137. Weber C et al. Toll-like receptor (TLR) 3 immune modulation by unformulated small interfering RNA or DNA and the role of CD14 (in TLR-mediated effects). *Immunology* 2012;136(1):64–77.

138. Chan CC et al. Type I interferon sensing unlocks dormant adipocyte inflammatory potential. *Nat Commun* 2020;11(1):2745.

139. Nakahira K et al. Autophagy proteins regulate innate immune responses by inhibiting the release of mitochondrial DNA mediated by the NALP3 inflammasome. *Nat. Immunol.* 2011;12(3):222–230.

140. Gui X et al. Autophagy induction via STING trafficking is a primordial function of the cGAS pathway. *Nature* 2019;567(7747):262–266.

141. Ritchie C, Cordova AF, Hess GT, Bassik MC, Li L. SLC19A1 Is an Importer of the Immunotransmitter cGAMP. *Molecular Cell* 2019;75(2):372-381.e5.

142. Wiens KE, Ernst JD. The Mechanism for Type I Interferon Induction by Mycobacterium tuberculosis is Bacterial Strain-Dependent. *PLoS Pathog* 2016;12(8):e1005809.

143. Youle RJ, van der Bliek AM. Mitochondrial fission, fusion, and stress. *Science* 2012;337(6098):1062–1065.

144. Song Y, Zhou Y, Zhou X. The role of mitophagy in innate immune responses triggered by mitochondrial stress. *Cell Communication and Signaling* 2020;18(1):186.

145. Bahat A, MacVicar T, Langer T. Metabolism and Innate Immunity Meet at the Mitochondria. *Frontiers in Cell and Developmental Biology* 2021;9:2019.

146. Ablasser A et al. RIG-I-dependent sensing of poly(dA:dT) through the induction of an RNA polymerase III-transcribed RNA intermediate. *Nat. Immunol.* 2009;10(10):1065–1072.

147. Chiu Y-H, Macmillan JB, Chen ZJ. RNA polymerase III detects cytosolic DNA and induces type I interferons through the RIG-I pathway. *Cell* 2009;138(3):576–591.

148. Kato H et al. Differential roles of MDA5 and RIG-I helicases in the recognition of RNA viruses. *Nature* 2006;441(7089):101–105.

149. Abels ER, Breakefield XO. Introduction to Extracellular Vesicles: Biogenesis, RNA Cargo Selection, Content, Release, and Uptake. *Cell Mol Neurobiol* 2016;36(3):301–312.

150. Wang X-A et al. Interferon regulatory factor 7 deficiency prevents diet-induced obesity and insulin resistance. *American Journal of Physiology-Endocrinology and Metabolism* 2013;305(4):E485–E495.

151. Meyer A et al. IFN-β-induced reactive oxygen species and mitochondrial damage contribute to muscle impairment and inflammation maintenance in dermatomyositis. *Acta Neuropathol* 2017;134(4):655–666.

152. Zhang L et al. Innate immunity. Dermal adipocytes protect against invasive Staphylococcus aureus skin infection. *Science* 2015;347(6217):67–71.

153. Seto S, Tsujimura K, Koide Y. Coronin-1a inhibits autophagosome formation around Mycobacterium tuberculosis-containing phagosomes and assists mycobacterial survival in macrophages. *Cell Microbiol* 2012;14(5):710–727.

154. Sidhu PS et al. Anticancer Activity of VDR-Coregulator Inhibitor PS121912. *Cancer Chemother Pharmacol* 2014;74(4):787–798.

155. Suschak JJ, Wang S, Fitzgerald KA, Lu S. A cGAS-Independent STING/IRF7 Pathway Mediates the Immunogenicity of DNA Vaccines. *J Immunol* 2016;196(1):310–316.

156. Cheng Y et al. IRF7 Is Involved in Both STING and MAVS Mediating IFN-β Signaling in IRF3-Lacking Chickens. *The Journal of Immunology* 2019;203(7):1930–1942.

157. Masuyama H, Hiramatsu Y. Additive Effects of Maternal High Fat Diet during Lactation on Mouse Offspring. *PLOS ONE* 2014;9(3):e92805.

158. Nishimoto Y, Tamori Y. CIDE Family-Mediated Unique Lipid Droplet Morphology in White Adipose Tissue and Brown Adipose Tissue Determines the Adipocyte Energy Metabolism. *J Atheroscler Thromb* 2017;24(10):989–998.

159. Iwatsuki H, Suda M. Transient expression of keratin during neuronal development in the adult rabbit spinal ganglion. *Anat Sci Int* 2010;85(1):46–55.

160. Aoki M, Murase T. Obesity-associated insulin resistance adversely affects skin function. *PLOS ONE* 2019;14(10):e0223528.

161. Okano J et al. Hyperglycemia Induces Skin Barrier Dysfunctions with Impairment of Epidermal Integrity in Non-Wounded Skin of Type 1 Diabetic Mice. *PLOS ONE* 2016;11(11):e0166215.

162. Li J, Daly E, Campioli E, Wabitsch M, Papadopoulos V. De novo synthesis of steroids and oxysterols in adipocytes. *J Biol Chem* 2014;289(2):747–764.

163. Blouin K et al. Pathways of adipose tissue androgen metabolism in women: depot differences and modulation by adipogenesis. *Am J Physiol Endocrinol Metab* 2009;296(2):E244-255.

164. Becker M, Hesse V. Minipuberty: Why Does it Happen?. *Horm Res Paediatr* 2020;93(2):76–84.

165. Ortega-García JA et al. Breastfeeding Duration and Anogenital Distance in 2-Year-Old Infants. *Breastfeed Med* 2016;11:350–355.

166. Stewart CJ et al. Temporal development of the gut microbiome in early childhood from the TEDDY study. *Nature* 2018;562(7728):583–588.

167. Markan KR et al. Adipose TBX1 regulates β-adrenergic sensitivity in subcutaneous adipose tissue and thermogenic capacity in vivo. *Mol Metab* 2020;36:100965.

168. Hu J et al. TMEM166/EVA1A interacts with ATG16L1 and induces autophagosome formation and cell death. *Cell Death Dis* 2016;7(8):e2323.

169. Yamamoto Y et al. Adipose Depots Possess Unique Developmental Gene Signatures. *Obesity (Silver Spring)* 2010;18(5):872–878.

170. Dommel S et al. The Fabp4-Cre-Model is Insufficient to Study Hoxc9 Function in Adipose Tissue. *Biomedicines* 2020;8(7):184.

171. Lee KY et al. Developmental and functional heterogeneity of white adipocytes within a single fat depot. *EMBO J* 2019;38(3):e99291.

172. Basse AL et al. Global gene expression profiling of brown to white adipose tissue transformation in sheep reveals novel transcriptional components linked to adipose remodeling. *BMC Genomics* 2015;16(1):215.

173. Nishimoto Y et al. Cell death-inducing DNA fragmentation factor A-like effector A and fat-specific protein 27β coordinately control lipid droplet size in brown adipocytes. *J Biol Chem* 2017;292(26):10824–10834.

174. Bianco AC, Kim BW. Deiodinases: implications of the local control of thyroid hormone action. *J Clin Invest* 2006;116(10):2571–2579.

175. Silva JE. The thermogenic effect of thyroid hormone and its clinical implications. *Ann Intern Med* 2003;139(3):205–213.

176. Bianco AC, Maia AL, da Silva WS, Christoffolete MA. Adaptive activation of thyroid hormone and energy expenditure. *Biosci Rep* 2005;25(3–4):191–208.

177. Yau WW et al. Thyroid hormone (T3) stimulates brown adipose tissue activation via mitochondrial biogenesis and MTOR-mediated mitophagy. *Autophagy* 2019;15(1):131–150.

178. Seale P et al. Transcriptional Control of Brown Fat Determination by PRDM16. *Cell Metabolism* 2007;6(1):38–54.

179. Kos K et al. Secretion of neuropeptide Y in human adipose tissue and its role in maintenance of adipose tissue mass. *Am J Physiol Endocrinol Metab* 2007;293(5):E1335-1340.

180. Kuo LE et al. Neuropeptide Y acts directly in the periphery on fat tissue and mediates stress-induced obesity and metabolic syndrome. *Nat Med* 2007;13(7):803–811.

181. Yan C et al. Peripheral-specific Y1 receptor antagonism increases thermogenesis and protects against diet-induced obesity. *Nat Commun* 2021;12(1):2622.

182. Park S et al. NPY Deficiency Prevents Postmenopausal Adiposity by Augmenting Estradiol-Mediated Browning. *J Gerontol A Biol Sci Med Sci* 2020;75(6):1042–1049.

183. Koska J, DelParigi A, Courten B de, Weyer C, Tataranni PA. Pancreatic Polypeptide Is Involved in the Regulation of Body Weight in Pima Indian Male Subjects. *Diabetes* 2004;53(12):3091–3096.

184. Lassmann V, Vague P, Vialettes B, Simon M-C. Low Plasma Levels of Pancreatic Polypeptide in Obesity. *Diabetes* 1980;29(6):428–430.

185. Tong J et al. Plasma pancreatic polypeptide levels are associated with differences in body fat distribution in human subjects. *Diabetologia* 2007;50(2):439–442.

186. Israël A. The IKK complex, a central regulator of NF-kappaB activation. *Cold Spring Harb Perspect Biol* 2010;2(3):a000158.

187. Manieri E, Sabio G. Stress kinases in the modulation of metabolism and energy balance. *J Mol Endocrinol* 2015;55(2):R11-22.

188. Sabio G, Davis RJ. TNF and MAP kinase signalling pathways. *Semin Immunol* 2014;26(3):237–245.

189. Engelman JA, Lisanti MP, Scherer PE. Specific inhibitors of p38 mitogen-activated protein kinase block 3T3-L1 adipogenesis. *J Biol Chem* 1998;273(48):32111–32120.

190. Aouadi M et al. p38MAP Kinase activity is required for human primary adipocyte differentiation. *FEBS Lett* 2007;581(29):5591–5596.

191. Engelman JA et al. Constitutively active mitogen-activated protein kinase kinase 6 (MKK6) or salicylate induces spontaneous 3T3-L1 adipogenesis. *J Biol Chem* 1999;274(50):35630–35638.

192. Iwai M, Horiuchi M. Devil and angel in the renin-angiotensin system: ACE-angiotensin II-AT1 receptor axis vs. ACE2-angiotensin-(1-7)-Mas receptor axis. *Hypertens Res* 2009;32(7):533–536.

193. Yang J et al. Molecular interaction and inhibition of SARS-CoV-2 binding to the ACE2 receptor. *Nat Commun* 2020;11(1):4541.

194. Al-Benna S. Association of high level gene expression of ACE2 in adipose tissue with mortality of COVID-19 infection in obese patients. *Obes Med* 2020;19:100283.

195. Elahi S. Neonatal and Children's Immune System and COVID-19: Biased Immune Tolerance versus Resistance Strategy. *J Immunol* 2020;205(8):1990–1997.

196. Bhat R et al. Inhibitory role for GABA in autoimmune inflammation. *PNAS* 2010;107(6):2580–2585.

197. Kelley JM, Hughes LB, Bridges SL. Does gamma-aminobutyric acid (GABA) influence the development of chronic inflammation in rheumatoid arthritis?. *J Neuroinflammation* 2008;5:1.

198. Frangaj A, Fan QR. Structural biology of GABAB receptor. *Neuropharmacology* 2018;136(Pt A):68–79.

199. Barker JS, Hines RM. Regulation of GABAA Receptor Subunit Expression in Substance Use Disorders. *International Journal of Molecular Sciences* 2020;21(12):4445.

200. Ikegami R et al. Gamma-Aminobutyric Acid Signaling in Brown Adipose Tissue Promotes Systemic Metabolic Derangement in Obesity. *Cell Rep* 2018;24(11):2827-2837.e5.

201. Turenius CI et al. GABAA receptors in the lateral hypothalamus as mediators of satiety and body weight regulation. *Brain Research* 2009;1262:16–24.

202. Hwang I et al. GABA-stimulated adipose-derived stem cells suppress subcutaneous adipose inflammation in obesity. *PNAS* 2019;116(24):11936–11945.

203. Hill AA et al. Activation of NF-κB drives the enhanced survival of adipose tissue macrophages in an obesogenic environment. *Mol Metab* 2015;4(10):665–677.

204. Cildir G, Akıncılar SC, Tergaonkar V. Chronic adipose tissue inflammation: all immune cells on the stage. *Trends Mol Med* 2013;19(8):487–500.

205. Qiu Y et al. Eosinophils and type 2 cytokine signaling in macrophages orchestrate development of functional beige fat. *Cell* 2014;157(6):1292–1308.

206. Guo D-H et al. Beige adipocytes mediate the neuroprotective and anti-inflammatory effects of subcutaneous fat in obese mice. *Nat Commun* 2021;12(1):4623.

207. Babaei R et al. Jak-TGFβ cross-talk links transient adipose tissue inflammation to beige adipogenesis. *Sci Signal* 2018;11(527):eaai7838.

208. Derecka M et al. Tyk2 and Stat3 regulate brown adipose tissue differentiation and obesity. *Cell Metab* 2012;16(6):814–824.

209. Cao W et al. p38 Mitogen-Activated Protein Kinase Is the Central Regulator of Cyclic AMP-Dependent Transcription of the Brown Fat Uncoupling Protein 1 Gene. *Mol Cell Biol* 2004;24(7):3057–3067.

210. Alsaggar M, Mills M, Liu D. Interferon beta overexpression attenuates adipose tissue inflammation and high-fat diet-induced obesity and maintains glucose homeostasis. *Gene Ther* 2017;24(1):60–66.

211. Youle RJ. Mitochondria-Striking a balance between host and endosymbiont. *Science* 2019;365(6454):eaaw9855.

212. Ro S et al. The mitochondrial genome encodes abundant small noncoding RNAs. *Cell Res* 2013;23(6):759–774.

213. Atyeo C, Alter G. The multifaceted roles of breast milk antibodies. *Cell* 2021;184(6):1486–1499.

214. Van de Perre P. Transfer of antibody via mother's milk. *Vaccine* 2003;21(24):3374–3376.

215. Martin CR, Ling P-R, Blackburn GL. Review of Infant Feeding: Key Features of Breast Milk and Infant Formula. *Nutrients* 2016;8(5):279.

216. Verhasselt V et al. Breast milk–mediated transfer of an antigen induces tolerance and protection from allergic asthma. *Nat Med* 2008;14(2):170–175.

217. Ziegler MM, MacNeill C, Rupnick M. Breast Milk Protection Against Enterocolitis. *Pediatr Res* 1984;18(4):218–218.

218. Kupsco A et al. Human milk extracellular vesicle miRNA expression and associations with maternal characteristics in a population-based cohort from the Faroe Islands. *Sci Rep* 2021;11(1):5840.

219. Prada I, Meldolesi J. Binding and Fusion of Extracellular Vesicles to the Plasma Membrane of Their Cell Targets. *Int J Mol Sci* 2016;17(8):1296.

220. Bitto NJ et al. Bacterial membrane vesicles transport their DNA cargo into host cells. *Sci Rep* 2017;7(1):7072.

221. Toyofuku M, Nomura N, Eberl L. Types and origins of bacterial membrane vesicles. *Nat Rev Microbiol* 2019;17(1):13–24.

222. Abbas YM, Pichlmair A, Górna MW, Superti-Furga G, Nagar B. Structural basis for viral 5'-PPP-RNA recognition by human IFIT proteins. *Nature* 2013;494(7435):60–64.

223. Kato H et al. Length-dependent recognition of double-stranded ribonucleic acids by retinoic acid-inducible gene-I and melanoma differentiation-associated gene 5. *J. Exp. Med.* 2008;205(7):1601–1610.

224. Eberle F, Sirin M, Binder M, Dalpke AH. Bacterial RNA is recognized by different sets of immunoreceptors. *Eur J Immunol* 2009;39(9):2537–2547.

225. Eigenbrod T, Dalpke AH. Bacterial RNA: An Underestimated Stimulus for Innate Immune Responses. *The Journal of Immunology* 2015;195(2):411–418.

226. Gruber AR, Lorenz R, Bernhart SH, Neuböck R, Hofacker IL. The Vienna RNA Websuite. *Nucleic Acids Research* 2008;36(suppl_2):W70–W74.

227. Bai J, Liu F. The cGAS-cGAMP-STING Pathway: A Molecular Link Between Immunity and Metabolism. *Diabetes* 2019;68(6):1099–1108.

228. Gkirtzimanaki K et al. IFNα Impairs Autophagic Degradation of mtDNA Promoting Autoreactivity of SLE Monocytes in a STING-Dependent Fashion. *Cell Rep* 2018;25(4):921-933.e5.

229. Tian Y, Jennings J, Gong Y, Sang Y. Viral Infections and Interferons in the Development of Obesity. *Biomolecules* 2019;9(11):E726.

230. Birk RZ, Rubinstein M. IFN-alpha induces apoptosis of adipose tissue cells. *Biochem Biophys Res Commun* 2006;345(2):669–674.

231. Blumberg JM et al. Complex role of the vitamin D receptor and its ligand in adipogenesis in 3T3-L1 cells. *J. Biol. Chem.* 2006;281(16):11205–11213.

232. Cippitelli M, Santoni A. Vitamin D3: a transcriptional modulator of the interferon-γ gene. *European Journal of Immunology* 1998;28(10):3017–3030.

233. Stoppelenburg AJ, von Hegedus JH, Huis in't Veld R, Bont L, Boes M. Defective control of vitamin D receptor-mediated epithelial STAT1 signalling predisposes to severe respiratory syncytial virus bronchiolitis. *The Journal of Pathology* 2014;232(1):57–64.

234. Ning S, Pagano JS, Barber GN. IRF7: activation, regulation, modification and function. *Genes Immun* 2011;12(6):399–414.

235. Chen Y-H et al. Vitamin D3 inhibits lipopolysaccharide-induced placental inflammation through reinforcing interaction between vitamin D receptor and nuclear factor kappa B p65 subunit. *Sci Rep* 2015;5(1):1–14.

236. Xu S et al. Vitamin D3 pretreatment regulates renal inflammatory responses during lipopolysaccharide-induced acute kidney injury. *Sci Rep* 2015;5(1):1–13.

237. Ma D et al. 1, 25(OH)2D3-induced interaction of vitamin D receptor with p50 subunit of NF-κB suppresses the interaction between KLF5 and p50, contributing to inhibition of LPS-induced macrophage proliferation. *Biochem Biophys Res Commun* 2017;482(2):366–374.

238. Sun S-C, Ley SC. New insights into NF-kappaB regulation and function. *Trends Immunol* 2008;29(10):469–478.

239. Liu T, Zhang L, Joo D, Sun S-C. NF-κB signaling in inflammation. *Sig Transduct Target Ther* 2017;2(1):1–9.

240. Manna P, Achari AE, Jain SK. Vitamin D supplementation inhibits oxidative stress and upregulate SIRT1/AMPK/GLUT4 cascade in high glucose-treated 3T3L1 adipocytes and in adipose tissue of high fat diet-fed diabetic mice. *Archives of Biochemistry and Biophysics* 2017;615:22–34.

241. Hussain T et al. Oxidative Stress and Inflammation: What Polyphenols Can Do for Us?. *Oxid Med Cell Longev* 2016;2016:7432797.

242. Guo C, Sun L, Chen X, Zhang D. Oxidative stress, mitochondrial damage and neurodegenerative diseases. *Neural Regen Res* 2013;8(21):2003–2014.

243. Ma F et al. Retinoid X receptor α attenuates host antiviral response by suppressing type I interferon. *Nat Commun* 2014;5(1):1–12.

244. Liu PT et al. Toll-like receptor triggering of a vitamin D-mediated human antimicrobial response. *Science* 2006;311(5768):1770–1773.

245. Saito T, Sadoshima J. Molecular Mechanisms of Mitochondrial Autophagy/Mitophagy in the Heart. *Circulation Research* 2015;116(8):1477–1490.

246. Roth CL, Elfers C, Kratz M, Hoofnagle AN. Vitamin d deficiency in obese children and its relationship to insulin resistance and adipokines. *J Obes* 2011;2011:495101.

247. de Oliveira LF, de Azevedo LG, da Mota Santana J, de Sales LPC, Pereira-Santos M. Obesity and overweight decreases the effect of vitamin D supplementation in adults: systematic review and meta-analysis of randomized controlled trials. *Rev Endocr Metab Disord* 2020;21(1):67–76.

248. Pramono A, Jocken JWE, Blaak EE. Vitamin D deficiency in the aetiology of obesity-related insulin resistance. *Diabetes/Metabolism Research and Reviews* 2019;35(5):e3146.

249. Fan Y et al. Vitamin D3/VDR resists diet-induced obesity by modulating UCP3 expression in muscles. *Journal of Biomedical Science* 2016;23(1):56.

250. Xu Y, Lou Y, Kong J. VDR regulates energy metabolism by modulating remodeling in adipose tissue.. *European journal of pharmacology* [published online ahead of print: 2019]; doi:10.1016/j.ejphar.2019.172761

251. Biggs KV et al. Formula Milk Supplementation on the Postnatal Ward: A Cross-Sectional Analytical Study. *Nutrients* 2018;10(5):608.

252. Lekli I et al. Protective mechanisms of resveratrol against ischemia-reperfusion-induced damage in hearts obtained from Zucker obese rats: the role of GLUT-4 and endothelin. *American Journal of Physiology-Heart and Circulatory Physiology* 2008;294(2):H859–H866.

253. Boden G. Free fatty acids, insulin resistance, and type 2 diabetes mellitus. *Proc Assoc Am Physicians* 1999;111(3):241–248.

254. Maassen JA, Romijn JA, Heine RJ. Fatty acid-induced mitochondrial uncoupling in adipocytes as a key protective factor against insulin resistance and beta cell dysfunction: a new concept in the pathogenesis of obesity-associated type 2 diabetes mellitus. *Diabetologia* 2007;50(10):2036–2041.

255. Soltani N et al. GABA exerts protective and regenerative effects on islet beta cells and reverses diabetes. *PNAS* 2011;108(28):11692–11697.

256. Szodoray P et al. The Complex Role of Vitamin D in Autoimmune Diseases. *Scandinavian Journal of Immunology* 2008;68(3):261–269.

257. Narvaez CJ, Matthews D, Broun E, Chan M, Welsh J. Lean phenotype and resistance to diet-induced obesity in vitamin D receptor knockout mice correlates with induction of uncoupling protein-1 in white adipose tissue. *Endocrinology* 2009;150(2):651–661.

258. Weber K, Erben RG. Differences in triglyceride and cholesterol metabolism and resistance to obesity in male and female vitamin D receptor knockout mice. *J Anim Physiol Anim Nutr (Berl)* 2013;97(4):675–683.

259. Lodhi IJ et al. Inhibiting Adipose Tissue Lipogenesis Reprograms Thermogenesis and PPARγ Activation to Decrease Diet-induced Obesity. *Cell Metab* 2012;16(2):189–201.

260. Park H, He A, Lodhi IJ. Lipid Regulators of Thermogenic Fat Activation. *Trends Endocrinol Metab* 2019;30(10):710–723.

8. Appendix

8.1. Publication and preprint presented in the thesis

Hoang, A.C.; Yu, H.; Röszer, T. (2021) Transcriptional landscaping identifies a beige adipocyte depot in the newborn mouse. *Cells* **2021**, *10*, 2368. [IF 6.6]

Paper available under https://doi.org/10.3390/cells10092368.

Reprinted under license CC BY 4.0 (https://creativecommons.org/licenses/by/4.0/).

Hoang AC, Yu H, Lin YT, Chen JC, Chen CC, Diedrich V, Herwig A, Landgraf K, Körner A, Röszer T. Immune privilege of adipocyte mitochondria protects from obesity. Under Review **2021**.

Preprint available under https://doi.org/10.21203/rs.3.rs-988599/v1.

Reprinted under license CC BY 4.0 (https://creativecommons.org/licenses/by/4.0/).

cells

MDPI

Article

Transcriptional Landscaping Identifies a Beige Adipocyte Depot in the Newborn Mouse

Anh Cuong Hoang, Haidong Yu and Tamás Röszer*

Institute of Neurobiology, Ulm University, 89081 Ulm, Germany; anh.hoang@uni-ulm.de (A.C.H.); haidong.yu@uni-ulm.de (H.Y.)

* Correspondence: tamas.roeszer@uni-ulm.de; Tel.: +49-(0)-731-50-22629

Abstract: The present study sought to identify gene networks that are hallmarks of the developing inguinal subcutaneous adipose tissue (iWAT) and the interscapular brown adipose tissue (BAT) in the mouse. RNA profiling revealed that the iWAT of postnatal (P) day 6 mice expressed thermogenic and lipid catabolism transcripts, along with the abundance of transcripts associated with the beige adipogenesis program. This was an unexpected finding, as thermogenic BAT was believed to be the only site of nonshivering thermogenesis in the young mouse. However, the transcriptional landscape of BAT in P6 mice suggests that it is still undergoing differentiation and maturation, and that the iWAT temporally adopts thermogenic and lipolytic potential. Moreover, P6 iWAT and adult (P56) BAT were similar in their expression of immune gene networks, but P6 iWAT was unique in the abundant expression of antimicrobial proteins and virus entry factors, including a possible receptor for SARS-CoV-2. In summary, postnatal iWAT development is associated with a metabolic shift from thermogenesis and lipolysis towards fat storage. However, transcripts of beige-inducing signal pathways including β-adrenergic receptors and interleukin-4 signaling were underrepresented in young iWAT, suggesting that the signals for thermogenic fat differentiation may be different in early postnatal life and in adulthood.

Keywords: adipose tissue; adipogenesis; brown fat; thermogenesis; obesity

check for updates

Citation: Hoang, A.C.; Yu, H.; Röszer, T. Transcriptional Landscaping Identifies a Beige Adipocyte Depot in the Newborn Mouse. *Cells* **2021**, *10*, 2368. https://doi.org/10.3390/cells10092368

Academic Editor: Bruce A. Bunnell

Received: 9 August 2021
Accepted: 5 September 2021
Published: 9 September 2021

Publisher's Note: MDPI stays neutral with regard to jurisdictional claims in published maps and institutional affiliations.

Copyright: © 2021 by the authors. Licensee MDPI, Basel, Switzerland. This article is an open access article distributed under the terms and conditions of the Creative Commons Attribution (CC BY) license (https://creativecommons.org/licenses/by/4.0/).

1. Introduction

The field of adipose tissue biology is gaining ever more attention, largely driven by the alarming worldwide incidence of obesity and related diseases. Indeed, obesity is projected to affect ~60% of the global adult population by 2030 [1], and the prevalence of metabolic diseases associated with obesity—including insulin resistance, diabetes, metabolic syndrome and other immune-metabolic diseases—is also rising rapidly [2]. Beyond its traditional role as a lipid storage site, adipose tissue is pivotal in regulating the systemic metabolism [3]. Subcutaneous fat depots also serve as thermal insulation layers, and modulate endocrine and immune functions by producing and secreting various hormones, adipokines and cytokines [3]. These signals, in turn, affect the metabolic health of distant organs/tissues such as liver, muscle, endocrine pancreas, and the cardiovascular and skeletal systems [2]. Excess adipose tissue development leads to obesity, which can ultimately result in various chronic, incurable diseases such as coronary heart disease, non-alcoholic fatty liver disease, renal and retinal vascular complications, insulin resistance and diabetes [1,4,5]. Depending on its anatomical location, adipose tissue may serve additional functions; for example, it supports the subcutaneous connective layers and shapes body surfaces (e.g., Bichat fat pad at the cheek [6]), it helps to reduce mechanical stress on muscles and protect deep nerves, and it forms fat pads in the plantar and gluteal regions to support locomotion [7]. Adipose tissue also helps manual abilities and to firmly fix small objects by forming fat pads on the palmar surface of the hand [8].

Traditionally, two types of adipose tissue have been distinguished based on their cell morphology and functions: white adipose tissue (WAT) and brown adipose tissue

(BAT) [9,10]. Adipocytes of the WAT are adapted for the long-term storage of fat and have the capacity to accumulate neutral lipids in a large droplet, which are broken down in response to hormonal signals under starvation [3]. By contrast, adipocytes of the BAT actively break down fat and oxidize fatty acids into ATP or heat [11–13]. BAT adipocytes are rich in mitochondria, and lipids are found in multiple small droplets surrounded by mitochondria [10,14–16]. BAT is also rich in glycogen, which, in addition to neutral lipids, serves as a metabolic fuel in cold-challenged BAT adipocytes [10,14–16]. Primordial fat cells in WAT and BAT depots contain glycogen and neutral lipids at birth [17–19], and these energy reserves comprise 1% and 16% of the body weight, respectively, in a newborn human [18]. Adipocyte lipolysis occurs rapidly after birth, followed by de novo fatty acid synthesis and lipogenesis that is accompanied by the catabolism of glycogen (so-called glycophagy) [20]. Glycophagy promotes lipid droplet formation, and lipid droplets are formed within glycogen clusters in developing BAT adipocytes [17]. The build-up of lipid stores continues during infancy, and is fueled by lipids consumed from breast milk or formula milk [21]. It is plausible that the scattered and small nature of lipid droplets in BAT increases their accessibility for mitochondrial β-oxidation [9,22]. Indeed, the difference in lipid droplet morphology is a distinguishing hallmark of WAT and BAT, and WAT adipocytes are often termed as unilocular (meaning "with one site" of fat storage) while BAT adipocytes are multilocular (meaning "many sites" of fat storage) [9,10,20,23]. WAT is present in all extant vertebrates, whereas BAT develops only in mammals, and is a less prevalent fat depot than WAT [24]. BAT is also typically located in the interscapular region [13], although thermogenic fat is present in the supraclavicular region, around large arteries and in the kidney capsule [25–27]. Obesity develops as a result of the expansion of WAT and decreases the amount of BAT [28–30]. Pediatric obesity is a current public health challenge, and it is thought that the decline in BAT during growth accelerates the development of obesity in children and adolescents [31].

Recent studies have described a third type of adipose tissue, the so-called brown-in-white adipose tissue ("brite"), also named "diffuse BAT" (reviewed in [11]). It contains both multilocular and unilocular fat cells, has a higher degree of fat oxidation than WAT, and can generate heat through uncoupled electron transport activity, resembling the function of the BAT [32]. The multilocular, thermogenic and fat-oxidizing adipocytes of the brown-in-white adipose tissue are often termed as beige adipocytes [27,33]. Cold exposure, Th2 cytokines and β-adrenergic stimuli, high-caloric diet, thiazolidinedione, and certain lipid species can evoke beige adipocyte traits in WAT [27,34–38]. Notably, thermogenic fat depots in the supraclavicular region, around the large arteries and in the kidney capsule, have been recently considered to be formed from beige adipocytes rather from BAT [39–41]. It is still debated whether beige adipocytes develop from BAT preadipocytes within WAT depots [42], as suggested by the term "brite", or through unique differentiation programs of the adipocyte precursors to produce fat storing or fat oxidizing/thermogenic fat cells [43]. The resulting beige adipocytes are distributed among fat-storing white adipocytes [44]. Single-cell RNA sequencing has revealed considerable differences between the individual fat cells in terms of their thermogenic potential [45], and the distinct fat depots contain ontogenetically-heterogenous adipocyte populations [46,47]. The unique metabolic characteristics of beige adipocytes—including their ability to burn off lipids as heat—make them attractive candidates in the treatment of obesity, and the development of therapeutic beige adipocytes is an intensive area of research [32,34–36,48].

Newborn mammals have the ability to dissipate the energy in lipids as heat, which is necessary to maintain their body temperature [25,49]. Indeed, the clade of mammals and their evolutionary forerunners are termed "thermolipials", which means "animals with warm fat" [50]. Certain fat depots of infant mammals were traditionally described as BAT [9,10,25,26]; however, as our understanding of adipose tissue development and function has grown, it is clear that newborn mammals and human infants have BAT only in some specific anatomical sites (e.g., in the interscapular region, buccal fat pad, around the large thoracic arteries), which disappears or regresses by adulthood [11,31,51]. The ther-

mogenic potential of the subcutaneous adipose tissue has also been shown in infancy [20], which is sustained by breast milk-derived lipid signals, and is rapidly lost when breast-feeding is discontinued [38]. Of note, the loss of the thermogenic fat in the subcutaneous fat depots is accelerated in childhood obesity [52], and obesity reduces the potential of beige adipocyte differentiation [53]. As thermogenic fat also has lipolytic activity and provides free fatty acids for energy production by the liver and by the BAT, the presence of thermogenic cells in the subcutaneous fat depot contributes to the intense fat oxidation observed after birth in mammals [14,19,25,54]. The similarities between subcutaneous WAT in the newborn and BAT make it plausible that the infant subcutaneous fat depot is actually composed of beige fat cells. Beige adipocytes have been mostly studied under induction conditions in adults [27,33,55], and much less is known about beige adipocytes in infancy. Moreover, while there are abundant data on the transcriptional changes of the adult adipose tissue induced by cold stress or thermoneutral environment [32,45], including at the single-cell level [45], there is a paucity of similar studies in newborns.

To question whether newborn WAT is similar to beige adipocytes and to BAT, the present study was designed to survey the transcriptional landscape in the developing fat depots of mice, and to define hallmark gene networks and hub genes. The data presented here help to define a new form of fat depot, which appears in early postnatal development, and is markedly distinct from BAT. Obesity in childhood is associated with a loss of thermogenic fat cells, and a similar loss has been observed in a mouse model of childhood obesity [38,56]. Our study shows that the BAT-independent subcutaneous fat depot is a relevant thermogenic/fat-oxidizing adipose tissue in early postnatal development in the mouse.

2. Materials and Methods

2.1. Animals and Cells

We used male C57BL/6 mice (Charles River Laboratories, Wilmington, MA, USA), housed under specific pathogen free conditions. Legislation of tissue collection from animals was approved by the regional governmental ethics and animal welfare committee in Tübingen, Germany (#1206; #1441; #1492; #o.189-20; #o.232-1,2,4,5). Primary mouse preadipocytes from inguinal WAT (iWAT) were isolated by collagenase digestion and cell separation and were subsequently cultured, as described [57,58]. To ensure the depletion of adipose tissue macrophages (ATMs) from the harvested preadipocytes, we used magnetic bead cell purification of the stromal vascular fraction with an antibody against the F4/80 antigen (Miltenyi Biotec, Bergisch Gladbach, Germany) [59]. Preadipocytes were maintained in cell culture medium supplemented with 20 µg/mL insulin. To induce white adipogenic differentiation of the preadipocytes of the stromal vascular fraction, we treated the cells with 50 µM IBMX, 1 µM dexamethasone, 1 µM rosiglitazone and 20 µg/mL insulin (all from Merck Sigma-Aldrich, St. Louis, MO, USA), as described [38]. The 3T3-L1 preadipocyte cell line was obtained from the ATCC (Merck Sigma-Aldrich) and maintained as described [60].

2.2. Histology and Image Analysis

Adipose tissue samples from iWAT and interscapular BAT were fixed with 4% paraformaldehyde and embedded in paraffin, as described (1). Sections were stained with hematoxylin and eosin, or with periodic acid Schiff (PAS)-reagent (Carl Roth, Karlsruhe, Germany). Immunohistochemistry was performed on paraffin-embedded tissue sections, using a mouse/human UCP1 antibody raised in rabbit (Thermo Fisher Scientific, Rockford, IL, USA) or an anti-mouse/human GABA-A receptor raised in rabbit (Alomone Labs, Jerusalem, Israel). Beige fat area was measured with our custom-developed image analysis software (BeAR, [38]).

2.3. Flow Cytometry Analysis

Immune cells of iWAT and BAT were isolated by collagenase digestion and cell separation and were analyzed as described [57,58]. ATMs were labeled for CD11b and F4/80 antigen and mast cells were labeled for CD117 and FCεR1a. FACS analysis was performed on a BD LSR II cytometer [59]. Flow Repository identifier of raw FACS data: #FR-FCM-Z236.

2.4. mRNA Analysis and Next-Generation Sequencing

Extraction of total RNA was performed as described [57] using samples obtained from at least three animals (Figure S1). Quality of the isolated total cellular RNA was controlled with denaturing gel electrophoresis to label ribosomal RNAs. Quantitative (q) PCR assays were performed on the Quantabio platform (Beverly, MA, USA), using *Bactin*, *Gapdh* and *Ppia* as references [38]. Next-generation sequencing (NGS) analysis was performed on the BGISEQ-500 platform by BGI Genomics Inc. (Cambridge, MA, USA), generating ~26.2 million reads per sample. Sequencing reads were checked to remove low-quality, adaptor-polluted and unknown base reads before downstream analyses. After filtering, the clean reads were mapped to the reference genome using HISAT [61]. On average, 96.8% of reads were mapped, and the uniformity of the mapping result for each sample suggested that the samples were comparable. We mapped clean reads to reference transcripts using Bowtie2, then calculated the gene expression level for each sample with RSEM [62,63]. Sequencing data saturation analysis was used to measure whether the depth of sequencing data was sufficient for bioinformatics analysis. Based on their gene expression levels, we identified differentially-expressed genes (DEGs) between sample groups. We used the DEseq2 algorithm to detect the DEGs [64]. We performed Gene Ontology (GO) classification and functional enrichment for biological function, pathway and biological process. For annotation of transcripts, such as enrichment of predicted transcription factor sites and additional pathway analysis, we used EnrichR, Panther and Interferome-2.0 [65–67]. Interactome maps of the DEGs were generated with the STRING Functional Protein Associations Network [68]. To reflect the gene expression correlation between samples, we calculated the Pearson correlation coefficients for all gene expression levels between each two samples. All samples were submitted to hierarchical clustering by the expression level of all genes. Materials and data are available for secondary use upon request. Raw NGS data are deposited at GEO with the accession number #GSE133500. For secondary analysis, we used our previously published NGS dataset, with accession number #GSE125405.

2.5. Data Representation and Statistics

Gene expression data are represented as mean ± s.e.m. in bar graphs. To visualize gene transcription differences between samples, transcript levels are indicated relative to reference genes, or the relative abundance of the transcripts. We used Venn diagrams to display uniquely expressed genes of the different sample groups and to visualize the number of genes specifically expressed in a given sample group or expressed in multiple samples groups. Volcano or scatter plots were used to show the number of DEGs in the various sample groups. In the volcano plots the X-axis represents the $\log_2$ transformed fold change of the DEGs; the Y-axis represents the $-\log_{10}$ transformed significance. In the scatter plots, the X-axis represents value A ($\log_2$ transformed mean expression level), and the Y-axis represents value M ($\log_2$ transformed fold change). Red data points represent upregulated DEGs. Blue data points represent downregulated DEGs. Gray data points represent non-DEGs. The applied statistical tests are indicated in the respective figure legends.

3. Results

3.1. Gene Networks and Hub Genes of Fat Depots during Early Life and in Adulthood

We isolated adipose tissue depots from mice at postnatal day 6 (P6) and P56 for NGS analysis of the iWAT and the interscapular BAT. At P6, the iWAT was rich in multilocular

fat cells and expressed uncoupling protein 1 (UCP1) (Figure 1a), the main hallmark of thermogenic fat. By contrast, P56 iWAT lacked multilocular fat cells and UCP1 expression (Figure 1a). Interscapular BAT was composed of multilocular cells at both P6 and P56 and showed strong UCP1 expression (Figures 1a and S2). The cytoplasmic content of the fat cells in P6 iWAT, P6 BAT and P56 BATstained positive for PAS, indicating the presence of glycogen (Figure 1a), particularly in the multilocular adipocytes, in accordance with previous observations [17,69]. The extracellular matrix stained positive for PAS in all tested adipose tissue depots (Figure 1a).

Hierarchical clustering analysis revealed that the transcriptional landscapes of iWAT and BAT were distinct at both P6 and P56 (Figure 1b). The least similarity was found between P6 iWAT and P56 BAT (Figure 1b), although both tissues contained multilocular adipocytes and expressed UCP1 (Figure 1a). The gene networks of each tissue were generated using GO terms and the Kyoto Encyclopedia of Genes and Genomes (KEGG) pathway assignment. The gene networks are accessible in an interactive format in Figure S3. P6 iWAT had less than 1K unique gene products, which were expressed specifically by this fat depot and not by the other depots analyzed (Figure 1b). We performed pairwise comparisons of P6 iWAT and P56 iWAT, and P6 BAT and P56 BAT to define DEGs that have a restricted expression in infancy and in adulthood (Figure 1c–f). When we compared P6 and P56 iWAT, we found that the former had >3.3K overrepresented DEGs and 1.7K underrepresented DEGs compared with P56 iWAT (Figure 1c). The most overrepresented DEG was *Krt5*, encoding keratin 5. Interactome analysis identified *Krt5* as a hub gene, interconnecting three extensive gene networks: a gene network of cadherins, a gene network of caveolin-3, and a gene network of keratins (Figure 1e, Table S1, *Krt5* network). Members of these networks were equally overrepresented in P6 iWAT. GO analysis indicated their involvement in vinculin binding and in cell−cell adhesion. The most underrepresented DEG in P6 iWAT was *Mup2*, encoding for major urinary protein 2, and it appeared to be a hub gene of a gene network of steroidogenesis (Figure 1f, Table S2, *Mup2* network). GO analysis indicated that the underrepresented DEGs of this network had a function in steroid hydrolase activity and in arachidonic acid metabolism.

The pairwise comparison analysis of P6 BAT and P56 BAT (Figure 1d) revealed that 2.4K DEGs were overrepresented in P6 BAT, with *Agtr2*, encoding angiotensin II receptor type 2, having the highest expression level (Figure 1g,h). The networks associated with *Agtr2* included chemokine ligands (CCLs) and CXC chemokine receptors (CXCRs), and also elements of angiotensin- and kininogen-signaling (Figure 1i, Table S3, *Agtr2* network). Genes of these networks were also overrepresented in P6 BAT, and their GO terms were associated with neutrophil granulocyte chemotaxis. The most underrepresented DEG in P6 BAT was *H2-Q9*, which belongs to the H-2 and class I histocompatibility antigens network (Figure 1j, Table S4, *H2-Q9* network). Members of this network were underrepresented in P6 BAT and had GO terms associated with MHC class I protein binding.

The above two comparisons aimed to define hub genes and gene networks associated with the postnatal development of iWAT and BAT. We next sought to define hub genes and gene networks which were specific to the BAT, irrespective of postnatal age. We thus compared P6 BAT with P6 iWAT (Figure 1k) and P56 BAT with P56 iWAT (Figure 1f). We found that 1.1K DEGs were overrepresented in P6 BAT, with *Ucp1* showing the highest expression level (Figure 1l). Notably, *Ucp1* was not associated with extensive gene networks and was not defined as a hub gene; rather, it was a member of a small network of mitobiogenesis genes that were overrepresented in P6 BAT (Figure 1m, Table S5, *Ucp1* network), and with roles in fat cell differentiation and fatty acid catabolism (Figure 1m). A total of 1.8K DEGs were underrepresented at P6, with *Krt71* (keratin 71) showing the lowest expression level (Figure 1l). *Krt71* belongs to a small network of keratins, with GO terms associated with keratin filament binding and bioactive lipid receptor activity (Figure 1n, Table S6, *Krt71* network). Lastly, we compared P56 BAT with P56 iWAT (Figure 1o), which revealed 1.6K DEGs overrepresented and 2.3K DEGs underrepresented in P56 BAT (Figure 1p). The most overrepresented DEG was *Fabp3*, encoding fatty acid-binding protein 3, which was not

positioned as a hub gene but belongs to a small network of fatty acid-binding proteins (FABPs) with functions in fatty acid transport and lipid catabolism (Figure 1q, Table S7, *Fabp3* network). The most underrepresented DEG was a pseudogene of the innate immune system, termed *Glycam1* (glycosylation-dependent cell adhesion molecule 1), belonging to a gene network of leukocyte tethering and adhesion (Figure 1r, Table S8, *Glycam1* network).

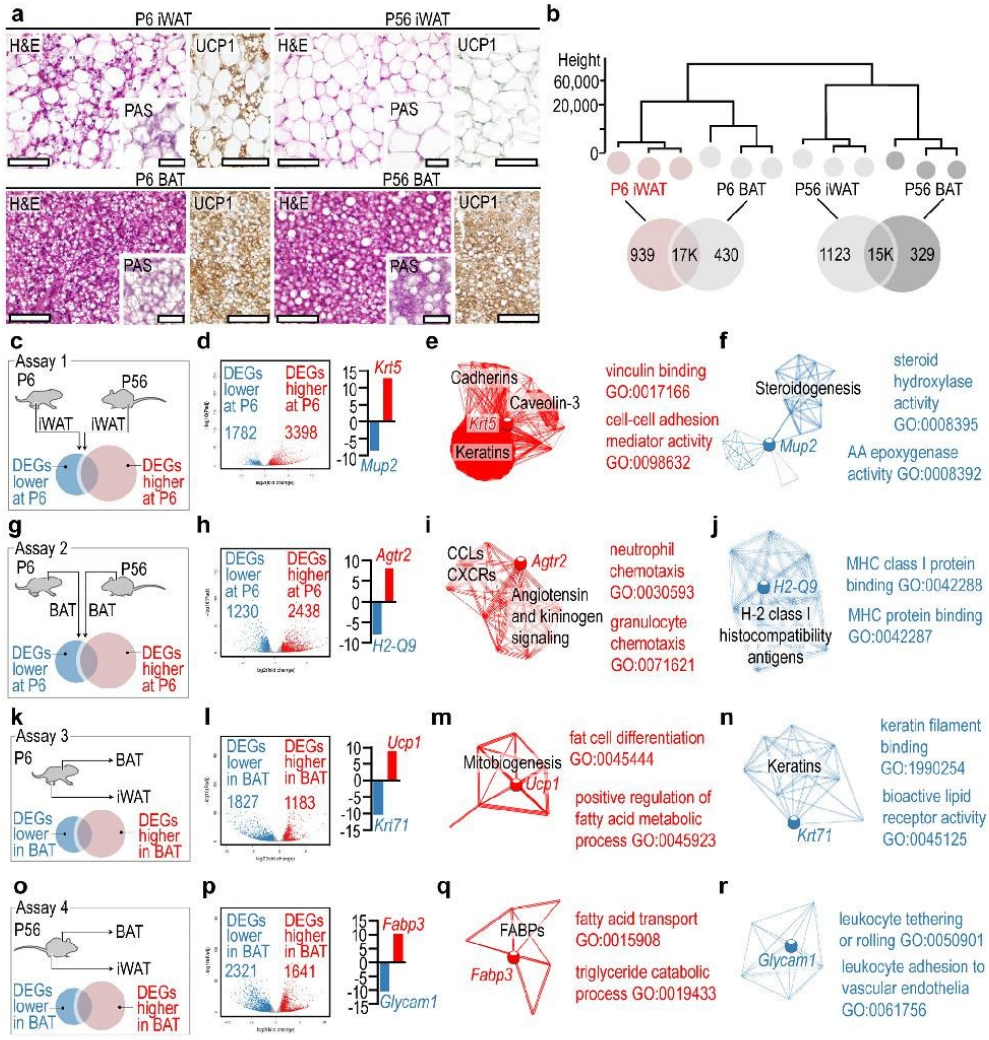

Figure 1. Gene networks and hub genes of the developing iWAT and BAT. (**a**) Hematoxylin and eosin (H&E) stained sections, and UCP1 immunostaining of BAT and iWAT at P6 and P56. Insets show periodic acid Schiff (PAS)-stained sections. Scale 50 µm. (**b**) Hierarchical clustering of samples. The closer the samples were to each other, the more similar their transcriptional landscapes were. (**c**) In assay 1, gene expression profiles of P6 and P56 iWAT were compared. (**d**) Volcano plot of DEGs. (**e**) Interactome map and most significant GO terms of DEGs overrepresented in P6 iWAT in assay 1. (**f**) Interactome

map and most significant GO terms of underrepresented DEGs in P6 iWAT in assay 1. (**g**) In assay 2, gene expression profiles of P6 and P56 BAT were compared. (**h**) Volcano plot of DEGs. (**i**) Interactome map and most significant GO terms of DEGs overrepresented in P6 BAT in assay 1. (**j**) Interactome map and most significant GO terms of underrepresented DEGs in P6 BAT in assay 1. (**k**) In assay 3, gene expression profiles of P6 BAT and P6 iWAT were compared. (**l**) Volcano plot of DEGs. (**m**) Interactome map and most significant GO terms of DEGs overrepresented in P6 BAT in assay 3. (**n**) Interactome map and most significant GO terms of underrepresented DEGs in P6 BAT in assay 1. (**o**) In assay 4, gene expression profiles of P56 BAT and P56 iWAT were compared. (**p**) Volcano plot of DEGs. (**q**) Interactome map and most significant GO terms of DEGs overrepresented in P56 BAT in assay 4. (**r**) Interactome map and most significant GO terms of underrepresented DEGs in P56 BAT in assay 4.

3.2. Cell Cycle and Myogenesis Genes Are Hallmarks of the Developing BAT

The analysis of gene networks suggested that there was a greater gene expression difference between P6 BAT and P56 BAT than between iWAT and BAT, pointing to a high degree of transcriptional changes associated with the postnatal development of BAT. Accordingly, we further analyzed the transcriptional landscape of BAT at P6 and P56. We identified only 0.2K genes that were unique to P56 BAT and 1.7K genes that were unique to P6 BAT (Figure 2a). Genes expressed only by the P56 BAT were associated with neuropeptide signaling, urea cycle, and metabolic processes of lipid-soluble vitamins and blood coagulation. Comprehensive analysis revealed that these genes were associated with neuropeptide Y (NPY), galanin and prostaglandin signaling, and with vitamin K-dependent protein C and coagulation factor XII (Hageman factor) (Figure 2b). Moreover, the genes characteristic to P56 BAT had an enriched predicted binding for peroxisome proliferator activator receptor gamma coactivator-1a (PPARGC1A) (Figure 2b). By contrast the P6-specific genes were associated with synaptic transmission, neuron differentiation, neuropeptide signaling and cell adhesion, and had predicted binding sites for various transcription factors, such as RE1-silencing transcription factor (REST), homeobox protein CDX-2 (CDX2) and T-box transcription factor 2 (TBX2) (Figure 2b), which may be associated with adipogenesis [70].

The most overrepresented DEGs of P6 BAT were associated with skeletal muscle development, such as myosin 3 *(Myh3)*, myosin 8 *(Myh8)*, microfibril-associated protein 4 *(Mfap4)*, sarcolipin *(Sln)*, fibrillin-2 *(Fbn2)* and many other genes of actin binding and microtubule binding (Figure 2c). These genes formed three interconnected networks, which were associated with cell cycle and DNA replication, myogenesis, insulin-like growth factor (IGF) signaling, collagen synthesis and gap junctions (Figure 2d). The transcriptional landscape of P6 BAT was associated with ongoing cell proliferation and tissue differentiation processes, with a notable overrepresentation of genes involved in skeletal muscle differentiation. While the demand of thermogenesis is higher in early postnatal life than in adulthood, we found similar levels of thermogenic genes and of genes associated with mitobiogenesis and fat catabolism between young and adult BAT.

3.3. Neuropeptide and GABA Signaling Networks Are Similarly Overrepresented in Adult BAT and Young iWAT

Our results revealed that DEGs associated with neuropeptide signaling were overrepresented in P56 BAT. We next aimed to define these genes. Neuropeptide signaling-associated DEGs were overrepresented in P6 iWAT, making it similar to P56 BAT (Figure 3a). Specifically, the DEGs were associated with pancreatic polypeptide (PP) signaling, neuropeptide Y (NPY) signaling and gamma aminobutyric acid (GABA) receptor signaling. Further comparisons of P6 iWAT with P6 BAT, P56 iWAT with P56 BAT, P6 iWAT with P56 iWAT, and P6 iWAT with P56 BAT revealed that the genes of neuropeptide signaling and GABA receptor activity were overrepresented in both P56 BAT and P6 iWAT.

The DEGs included NPY and PP receptors (*Npy2r*, *Npy4r*, and the pseudogene *Npy6r*), neuropeptide B/W receptor *(Npbwr1)*, NPY *(Npy)*, galanin *(Gal)* and several components of GABA-A receptor signaling. GABA-A receptors were overrepresented in P56 BAT and P6 iWAT and minimally expressed in P56 iWAT, whereas GABA-B receptors were stably ex-

pressed at P6 and P56, and showed higher levels in iWAT than in BAT (Figures 3b and S4). Interactome analysis of the DEGs overrepresented in P6 iWAT revealed their association with three interconnected networks: GABA receptor signaling, G_0 protein-coupled neuropeptide signaling, and NFκB, STAT3, and interferon regulatory factor (IRF)-signaling (Figure 3c). Functional annotation of the DEGs indicated that they were all involved in inhibitory signaling towards NFκB, STAT3 and IRFs, suggesting a potential immune suppressor or anti-inflammatory role of these neuropeptides and GABA in P6 iWAT and P56 BAT (Figure 3d). In this line, inflammatory genes, interferon-regulated genes and the NFκB pathway were all underrepresented in P56 BAT (Figure 3e).

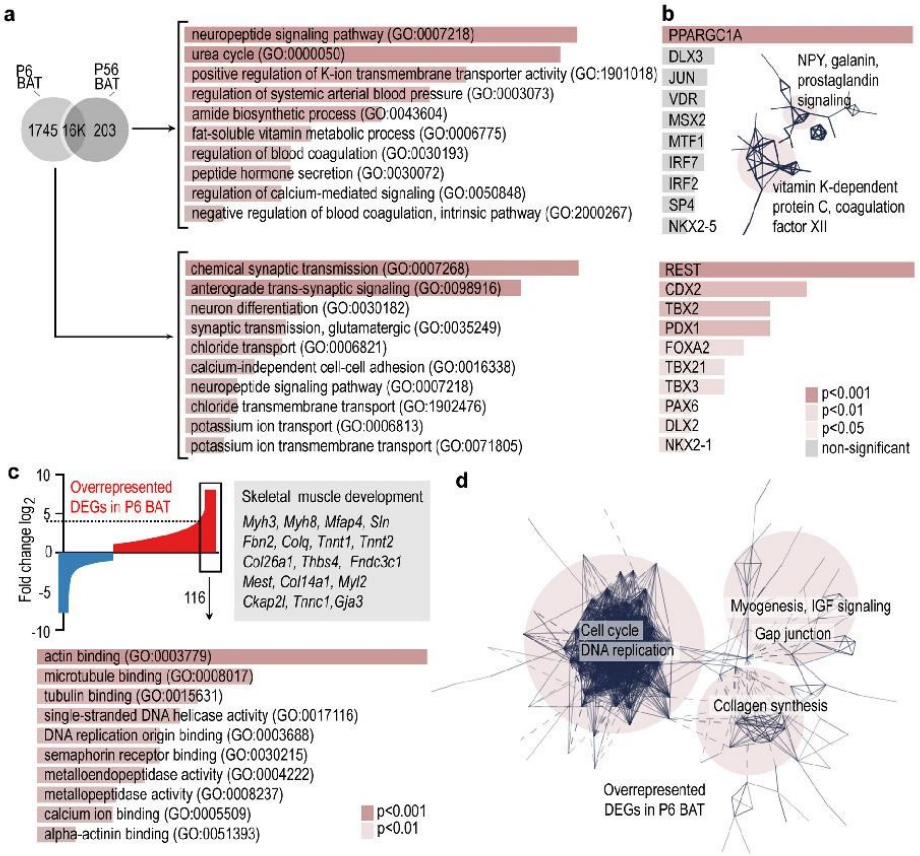

Figure 2. Gene ontology analysis and gene networks of BAT-specific transcripts. (**a**) Venn diagram showing uniquely expressed genes in P6 BAT or P56 BAT. GO terms associated with P6-, and P56-specific transcripts. (**b**) Transcription factor-binding prediction for P6-, and P56-specific transcripts. Inset shows gene networks of P56-specific transcripts. Combined *p*-values of the enrichment are shown in color codes in panels a and b. (**c**) Top: Gene expression profiles of P6 and P56 BAT were compared, and the differences were visualized on the Y-axis as $\log_2$ of fold change of DEGs. DEGs overrepresented at P6 are indicated in red, and underrepresented DEGs are shown in blue. The 116 DEGs which were ≥4.5-fold overrepresented in P6 were analyzed further. Bottom: GO terms of the 116 most overrepresented DEGs. (**d**) Interactome map of DEGs overrepresented in P6 BAT. PPI enrichment *p*-value < 1.0×10^{-16}.

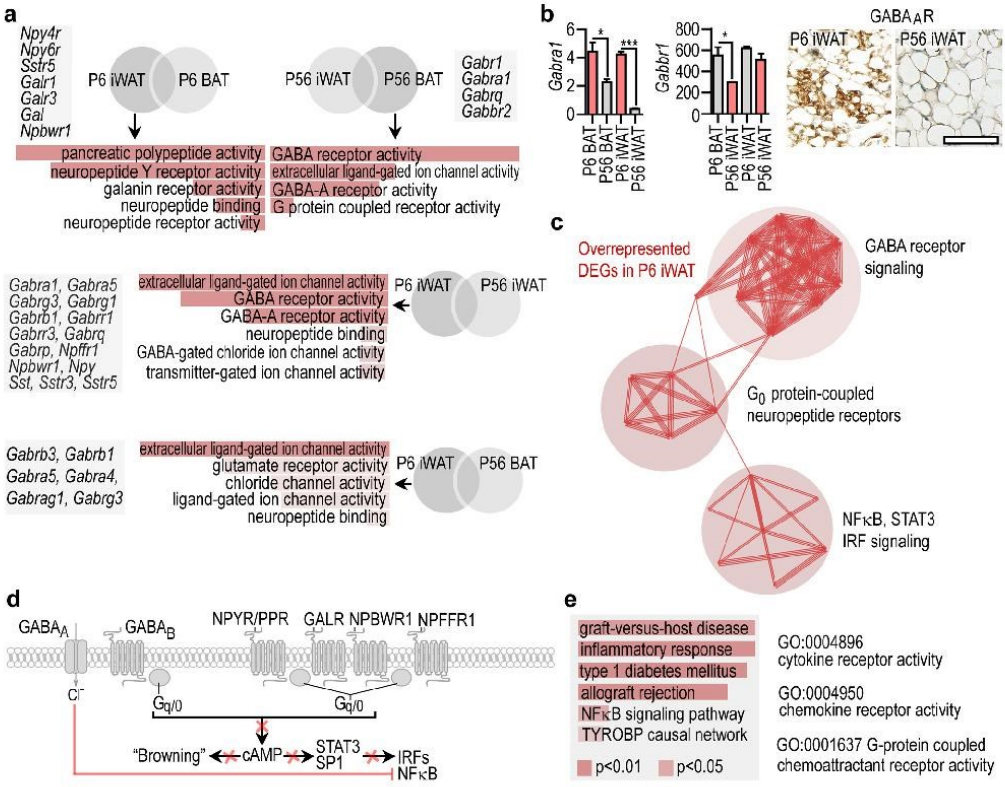

Figure 3. Gene expression pattern shared by P56 BAT and P6 iWAT. (**a**) GO analysis and representative gene transcripts specific to P6 iWAT and P56 BAT. (**b**) Left: Expression level of *Gabra1*, encoding GABA-A receptor, and *Gabbr1*, encoding GABA-B receptor in P6 iWAT, P6 BAT, P56 iWAT and P56 BAT. * $p < 0.05$, *** $p < 0.001$, Student's two-tailed unpaired t-test. Right: Immunostaining of GABA-A in iWAT at P6 and P56, scale 50 µm. (**c**) Interactome map of DEGs overrepresented in P6 iWAT. PPI enrichment *p*-value < 1.0×10^{-16}. (**d**) Scheme showing cell compartment association of DEGs overrepresented in P6 iWAT. cAMP is a known signal for transformation of WAT into beige adipocyte-rich depots, in the so-called adipose tissue "browning" process [35]. Red cross denotes inhibition of the respective pathways. (**e**) GO analysis of cellular functions and biological processes of immune-related transcripts in P56 BAT. Combined *p*-values are indicated with color codes. TYROBP: TYRO protein tyrosine kinase-binding protein.

3.4. Transcriptional Landscapes of Immune Genes in the Developing Fat Depots

We further explored the expression of immune signaling genes in BAT and found that P56 BAT and P56 iWAT had distinct transcriptional profiles of interferon-stimulated genes (ISGs, Figure 4a, GO analysis and KEGG pathways are available in the Supplemental Material). Indeed, 44% of the DEGs overrepresented in P56 BAT were ISGs, including thermogenic genes such as *Ucp1*, mitobiogenesis genes such as *Cox7a1*, *Cidea*, *Cpt1b* and *Dio2*, encoding cytochrome c oxidase subunit 7A1, cell death inducing DFFA-like effector A, carnitine palmitoyltransferase 1B and iodothyronine deiodinase 2, respectively [71,72] (Figure 4b). Other ISGs that were overrepresented in BAT included M2 macrophage-activation genes such as arginase 2 *(Arg2)* and transforming growth factor beta *(Tgfb2)*, the M1 macrophage activation gene gamma interferon receptor *(Ifngr2)*, macrophage proliferation gene NDRG family member 2 *(Ndrg2)*, and the ubiquitin ligase ring-finger protein 128

(Rnf128) [57,73]. RNF128 is known to increase the ubiquitination and proteasomal degradation of phosphorylated STAT6, and hence can impede M2 activation of macrophages and Th2 signaling of lymphocytes [74]. Some virus entry factors and antiviral ISGs such as Coxsackievirus and adenovirus receptor *(Cxadr)*, and self-tolerance genes such as milk fat globule EGF and factor V/VIII domain containing protein *(Mfge8)*, were overrepresented in P56 BAT (Figure 4b).

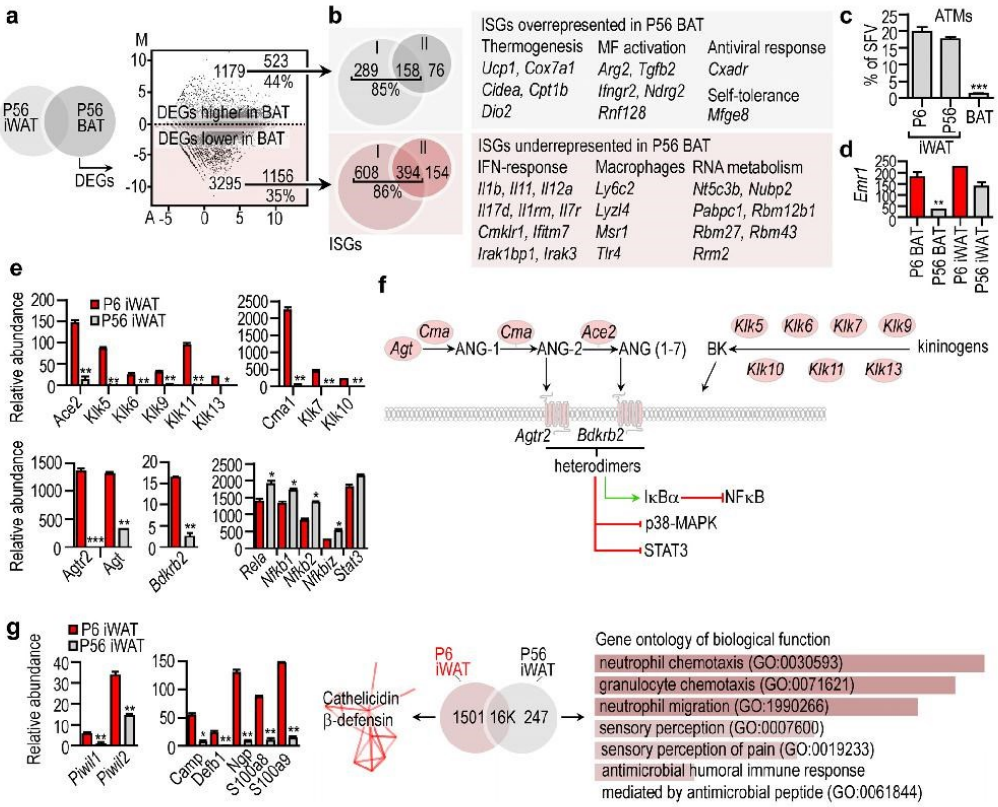

Figure 4. Immune-related gene transcripts in the BAT and in the iWAT. (**a**) P56 iWAT and P56 BAT were compared, and the DEGs were visualized in a scatter plot. Number of DEGs, and the percentage of interferon-stimulated genes (ISGs) are shown. (**b**) Representative ISGs overrepresented or underrepresented in BAT. (**c**) Percentage of adipose tissue macrophages (ATMs) within the stromal vascular fraction (SVF) of P6 iWAT, P56 iWAT and P56 BAT. *** $p < 0.001$, two-way ANOVA with Dunnett's post hoc test, using P6 BAT as reference group (**d**) Expression level of the macrophage marker *Emr1*, encoding F4/80 antigen. ** $p < 0.01$, two-way ANOVA with Dunnett's post hoc test, using P6 BAT as reference group. (**e**) Expression level of genes associated with the local angiotensin and kininogen system. * $p < 0.05$, ** $p < 0.01$, *** $p < 0.001$, Student's two-tailed unpaired t-test. (**f**) Scheme summarizing the cell compartment association of the gene products associated with the local angiotensin and kininogen system. All indicated gene products were overrepresented in P6 iWAT. (**g**) Left: Expression level of PIWI protein-encoding genes, and genes encoding cathelicidin and β-defensins. * $p < 0.05$, ** $p < 0.001$, Student's two-tailed unpaired t-test. Middle: Cathelicidin and β-defensin gene network overrepresented in P6 iWAT. PPI enrichment p-value $< 1.0 \times 10^{-16}$. Right: Gene ontology of DEGs overrepresented in P56 iWAT. Combined p-value < 0.01.

In turn, 35% of the underrepresented DEGs in P56 BAT were ISGs, including the IFN-response genes interleukin 1b *(Il1b)*, *Il11*, *Il12a*, interleukin-7-receptor *(Il7r)*, and

macrophage genes such as lymphocyte antigen 6 *(Ly6c2)*, lysozyme like 4 *(Lyzl4)* and macrophage scavenger receptor 1 *(Msr1)*. The ISGs were type I and type II interferon target genes. RNA metabolism genes were also underrepresented in P56 BAT (Figure 4b). The evident lack of expressed macrophage genes in BAT was consistent with the paucity of adipose tissue macrophages (ATMs) (Figure 4c,d).

When we extended our analysis to iWAT, we found that the *Agtr2* gene network was overrepresented in P6 iWAT, along with angiotensin converting enzyme 2 (*Ace2*) and bradykinin receptor 2 (*Bdkrb2*) (Figure 4e). ACE2 is a receptor for SARS-CoV-2 [75] and is believed to enhance virus entry into human adipocytes, which may account for the increased disease severity in patients with COVID-19 and obesity [76]. NGS analysis showed that *Ace2* was minimally expressed in iWAT at P56, but robustly expressed at P6. The *Agtr2* network included *Ace2*, angiotensin (*Ang*), chymase (*Cma1*) and genes encoding kallikreins (Figure 4f). As a gene network, these genes form a tissue hormone signaling niche and convert angiotensinogen into ANG-2 and ANG (1–7) [77] (Figure 4f). Heterodimers of AGTR2 and BDKRB2 phosphorylate IκBα and dephosphorylate STAT3 and p38-MAPK, and induce nitric oxide production in endothelial cells [78]. This signaling potentially inhibits NFκB and STAT3 signaling (Figure 4f). Coherently, iWAT maturation was associated with an increase of DEGs of neutrophil chemotaxis and the expression of inflammatory genes (Figure 4g). This indicates that the P56 iWAT environment is inflammatory, which is in line with previous observations showing that adipogenesis is associated with the upregulated expression of NFκB subunits [79] (Figure 4e). By contrast, P6 iWAT had a robust gene expression of the antimicrobial peptides cathelicidin and β-defensin (Figure 4g). Altogether, a local angiotensin and kininogen-kallikrein system along with the abundance of AGTR2 and BDKRB2 can be used as a hallmark of P6 iWAT, distinguishing it from both P56 iWAT and BAT.

3.5. Transcription of Beige Marker Genes in the Developing BAT and iWAT

We then focused on the expression of the so-called brown and beige marker genes. These genes have been identified by transcriptional profiling of the adipose tissue in mice challenged with cold. The most relevant thermogenic gene of mammals is *Ucp1*, and its expression was abundant in both P6 and P56 BAT. *Ucp1* was minimally expressed in iWAT, relative to its levels measured in BAT, but it was a prevalent transcript in P6 iWAT (Figure 5a). The key mitobiogenesis gene *Ppargc1a* was highly expressed in P6 and P56 BAT, and had a moderate and similar level in P6 and P56 iWAT. Other genes associated with adipose tissue "browning", such as *Cidea*, *Cox7a1* and *Dio2* [72], were abundantly expressed in P56 BAT. Unexpectedly, however, they were much less prevalent in P6 BAT, and were minimally expressed in P56 iWAT. For example, higher levels of *Dio2* were found in P6 iWAT than in P56 iWAT. *Tmem26* and *Tbx1*, which have been previously described as markers of beige adipocytes [40], were abundantly expressed in P6 iWAT (Figure 5a), were less prevalent in P56 iWAT, were minimally expressed in P6 BAT, and were absent in P56 BAT (Figure 5a). These genes were, therefore, unique hallmarks of P6 iWAT. *Eva1a* (encoding Eva-1 homolog A), a transcript previously denoted as a marker of BAT [40,80], was abundant in P6 and P56 BAT, and also in P6 iWAT (Figure 5b), and was significantly less prevalent in P56 iWAT. This gene product is, hence, a shared transcript of BAT and P6 iWAT.

The majority of brown adipocytes develop from a myogenic factor 5 $(Myf5)^+$ cell lineage [47]. We found that the level of *Myf5* was highest in P6 BAT, and was minimally expressed in P56 BAT and P56 iWAT (Figure 5b). Its level was also significantly higher in P6 iWAT than in P56 iWAT (Figure 5b). Another BAT-specific transcript, *Lhx8*, encoding LIM homeobox 8, was most abundant in P6 BAT, less prevalent in P56 BAT, and moderately expressed in P6 and P56 iWAT. There was no difference between *Lhx8* levels in P6 and P56 iWAT (Figure 5b).

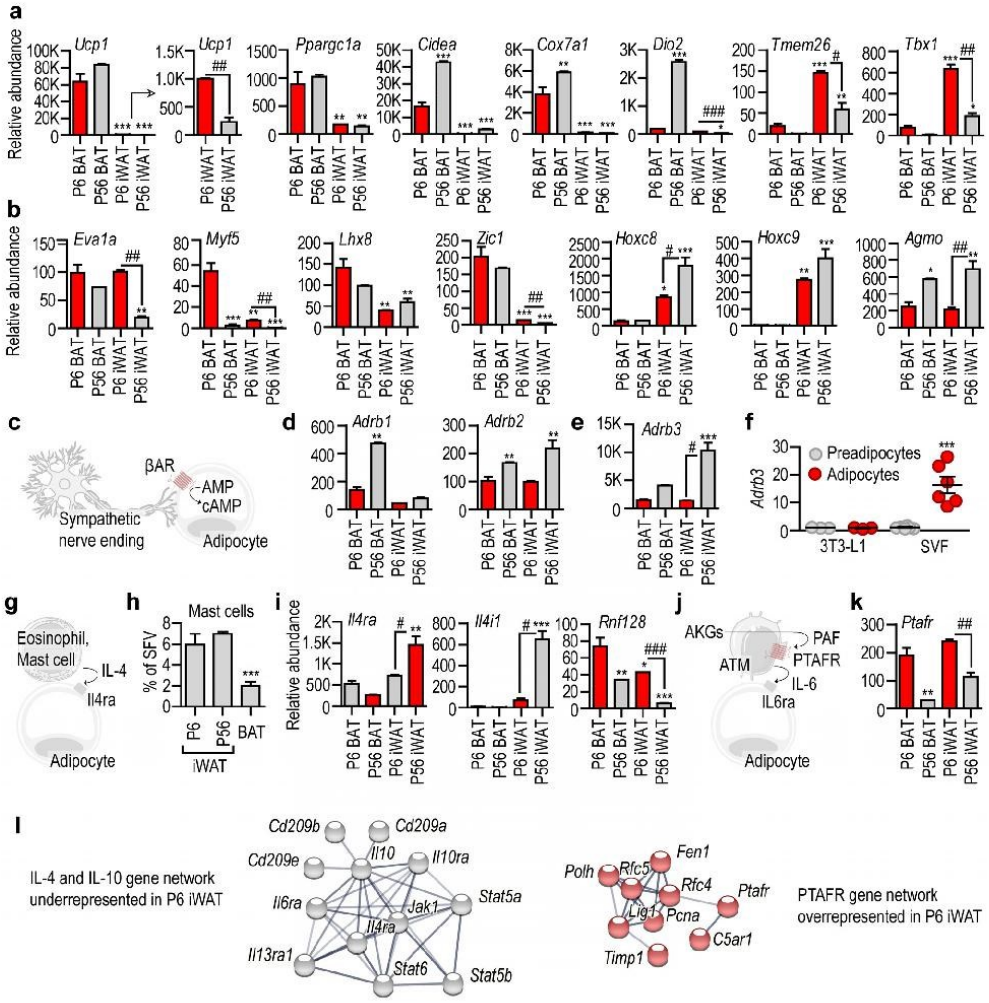

Figure 5. Transcription of beige-marker genes and beige-inducing signal pathways. (**a**,**b**) Transcript level of genes previously defined as markers of BAT and beige adipocytes. *Ucp1* is key for nonshivering thermogenesis; *Ppargc1a* is a regulator of mitobiogenesis; *Cidea*, *Cox7a1*, *Dio2*, *Tmem26* and *Tbx1* are markers of beige adipocytes; *Eva1a* is a marker of BAT; *Myf5* is expressed by progenitors of BAT adipocytes; *Lhx8* and *Zic1* are markers of BAT. The levels of *Hoxc8* and *Hoxc9* increase during WAT adipocyte development. *Agmo* is responsible for the degradation of beige adipocyte-inducing lipid species, so-called alkylglycerols (AKGs). (**c**) Scheme of beige induction by β-adrenergic stimuli of the sympathetic nervous system. (**d**) Level of β-adrenergic receptors. (**e**) Level of *Adrb3* in the various fat depots. (**f**) *Adrb3* level in 3T3-L1 preadipocytes and in in vitro cultured primary preadipocytes of the iWAT stromal vascular fraction (SVF). Adipocyte development was chemically induced. (**g**) Scheme of IL-4-induced adipose tissue browning. (**h**) Percentage of mast cells in the SVF of iWAT and BAT. (**i**) Expression level of IL-4 signaling in the various fat depots. (**j**) Scheme of adipose tissue browning induced in postnatal life by the AKG–PAF–IL-6 axis. (**k**) Expression of *Paftr*. (**l**) Underrepresented gene network of IL-4 signaling in P6 iWAT. Overrepresented gene network of PAF signaling in P6 iWAT. PPI enrichment p-value < 1.0×10^{-16}. * $p < 0.05$, ** $p < 0.01$, *** $p < 0.001$, two-way ANOVA with Dunnett´s post hoc test, using P6 BAT as reference group, # $p < 0.05$, ## $p < 0.01$, ### $p < 0.001$, Student's unpaired, two-tailed t-test.

It has been shown that acute cold stress triggers the expression of *Zic1*, encoding zinc finger protein 1, in the subcutaneous fat of mice [40,81]. The level of *Zic1* was prominent in P6 and P56 BAT, and was minimal in P6 and P56 iWAT. Nonetheless, the level of *Zic1* was significantly higher in P6 iWAT than in P56 iWAT (Figure 5b). Two homeobox genes, *Hoxc8* and *Hoxc9*, show increased gene expression during WAT differentiation [40]. We found that both genes were prominently expressed in P56 iWAT, were less expressed in P6 iWAT, and were minimally expressed or lacking in BAT (Figure 5b).

We also tested for two other potential markers of thermogenic fat development: *Prdm16* and *Cited1*, encoding PR/SET domain 16 and the transcriptional coactivator Cbp/p300-interacting transactivator with Glu/Asp-rich carboxy-terminal domain 1, respectively. PRDM16 promotes BAT differentiation and supports thermogenic adipocyte development [82,83] and "browning" [84], and also maintains BAT in adult mice [85]. We found that *Prdm16* was mostly expressed by P56 BAT, and was expressed to a greater level in P6 iWAT than in P56 iWAT (Figure S2). *Cited1* was originally identified as a beige adipocyte marker [41]; however, whether beige and white adipocytes differ in their *Cited1* expression levels has recently been challenged [33,55]. P6 BAT and P6 iWAT had the strongest *Cited1* expression, and P56 BAT had a low *Cited1* level (Figure S2).

We recently showed that ether lipids, the so-called alkylglycerols (AKGs), sustain beige adipogenesis in the subcutaneous adipose tissue of newborn mice, and that AKG monooxygenase (AGMO) inhibits their function by metabolizing them [38]. We found that the level of *Agmo* was high in P56 BAT and P56 iWAT, and was moderate in P6 BAT and P6 iWAT (Figure 5b).

We next analyzed the transcription of cell membrane receptor genes that are required for brown and beige adipogenesis. Cold stress induces beige adipogenesis through β-adrenergic receptors (Figure 5c). We found that these receptors were expressed mostly by P56 BAT and P56 iWAT (Figure 5d). Indeed, *Adrb3*, encoding ADRB3, an adrenergic receptor involved in cold-induced adipose tissue browning, was highly expressed in P56 iWAT, and was moderately detectable in P6 iWAT and in P56 BAT (Figure 5e). The mouse 3T3-L1 preadipocyte line lacked *Adrb3* expression, and this remained unchanged during adipocyte differentiation (Figure 5f), which accords with the lack of beige induction in 3T3-L1 cells by certain stimuli [86]. Unexpectedly, however, primary mouse preadipocytes also lacked *Adrb3* expression, although its expression was strongly increased during adipocyte differentiation (Figure 5f). Genes of the β-adrenergic signaling pathway were not expressed in P6 iWAT or in nondifferentiated preadipocytes, suggesting that beige induction by noradrenaline is a trait of adult adipose tissue.

It is known that the Th2 cytokines IL-4 and IL-13 induce beige adipocyte differentiation, and that IL-4 receptor alpha (IL4Rα) is necessary for cold-induced beige adipocyte development [87]. It is thought that the Th2 cytokines are released into the adipose tissue stroma by mast cells or eosinophils in response to cold (Figure 5g) [87,88]. However, mast cells were scarce in BAT (Figure 5h), and a similar paucity of eosinophils in BAT has been reported previously [58]. Moreover, *Il4ra* was moderately expressed by P6 BAT, P56 BAT and P6 iWAT, whereas P56 iWAT showed abundant *Il4ra* expression (Figure 5i). The expression level of *Il4i1*, encoding interleukin 4-induced 1 protein, had a similar, even stronger pattern: P56 iWAT showed abundant *Il4i1* expression, whereas P6 BAT, P56 BAT and P6 iWAT had negligible *Il4i1* levels (Figure 5i). The expression level of *Rnf128*, which is responsible for the inactivation of the downstream IL4Rα signaling [57], had an inverse pattern, with the highest level in P6 BAT and the lowest level in P56 iWAT (Figure 5i). These data reveal that the IL-4/IL4Rα/STAT6 signaling is repressed in BAT and P6 iWAT.

The above two signaling mechanisms have been established in adult mice, and are known as inducers of beige adipogenesis under cold stress. Much less is known about the signals that induce thermogenic fat in newborns. We have shown recently that signaling through the platelet-activating factor (PAF) receptor (PTAFR) maintains beige adipogenesis in newborn mice (Figure 5j) [38]. In line with this, *Ptafr* expression was highest in P6 BAT

and P6 iWAT, with minimal or moderate expression in P56 BAT and P56 iWAT, respectively (Figure 5k,l).

In summary, our findings reveal that receptors for beige adipogenesis are distinctly expressed in adult and in infant adipose tissue. β-adrenergic signaling is predominant in P56 iWAT. Functional IL-4 signaling is evident in P56 iWAT, but not in P6 iWAT (Figure 5l). Lastly, the necessary genes for the recently described AKG-, and PAF-mediated beige adipogenesis program are highly expressed in P6 iWAT (Figure 5b,k,l).

4. Discussion

In the present study we have identified gene networks and hub genes that are hallmarks of the developing BAT and iWAT. We found that the transcriptional landscapes of young and adult BAT are markedly different, with an overrepresentation of thermogenic and lipid catabolism transcripts in adult BAT. This is an unexpected finding, as thermogenic BAT is morphologically mature at birth (Figure 1a) [72], and it was thought to be relevant for thermogenesis of the infant [31]. We also found that young iWAT expresses thermogenic and lipid catabolism transcripts together with an abundance of transcripts associated with cold-induced beige adipogenesis. This indicates that BAT is still undergoing differentiation and maturation in newborn mice, and that iWAT temporally adopts thermogenic potential. In line with this, we found that iWAT of young mice has a beige/brite morphology and a gene expression landscape of beige/brite fat. However, the beige-inducing signal pathways are distinct in adult and young iWAT, highlighting that the signals for thermogenic fat differentiation may be different in early postnatal life and in adulthood.

Adipose tissue development in the first three years of life is known to be key for determining childhood obesity [89]. It is also known that obese children lose their thermogenic fat cells early on, whereas lean children maintain them in their subcutaneous fat depots until puberty [31,56]. Breast milk-derived signals play a key role in triggering and maintaining beige adipogenesis in infant fat [38]. Moreover, the subcutaneous adipose tissue of the infant has lipolytic activity and releases free fatty acids, but this process declines in childhood obesity [52]. It is thus key to maintain the infant-type features of the adipose tissue, including its beige adipocyte-like traits in early postnatal life to prevent childhood obesity.

We have identified novel hub genes and gene networks that can be used to discriminate between both young and adult BAT and iWAT. Because obesity reduces BAT mass, and a premature loss of beige adipocytes may contribute to obesity [38,56], adequate animal models and experimental approaches are needed to study the mechanisms which sustain BAT and beige adipocytes. The novel hub genes and gene networks not only decipher as yet unexplored functions of the BAT and beige adipocytes, but will also aid future studies by providing target genes and gene networks to analyze by transcriptional profiling or single-cell sequencing.

Hallmark genes and gene networks of the young iWAT were associated with cell−cell adhesion and cell−matrix interaction, with the cytoskeletal protein *Krt5* acting as a hub gene. KRT5 is a protein of the basal layer of the skin epithelia. While there is close proximity between iWAT and the skin, it is unlikely that keratinocytes are connected to the developing fat. However, some fat cell lineages, including BAT adipocytes, are derived from the embryonic ectoderm [90], which is rich in keratin expression [91]. Moreover, *Krt5* is expressed by myoepithelial progenitors [92], and BAT fat cells have been shown to develop from myoepithelial cells in the mammary gland [93] where epithelium-to-adipocyte transdifferentiation might occur [94,95]. It is known that *Krt19* is expressed by mouse preadipocytes, and in vitro adipocyte differentiation is associated with an increment in *Krt19* expression [46]. *Krt19* was overrepresented in P6 iWAT and belonged to the *Krt5* gene network. Moreover, the levels of *Krt5* and several keratin and desmosome genes are suppressed in obesity and in type 1 diabetes in the mouse, leading to obesity-associated skin fragility [96,97]. Keratin also increases the adipogenic differentiation of adipose tissue

stem cells [98]. Our findings suggest that early fat development may be associated with keratins through as yet unknown mechanisms.

Steroidogenesis genes were underrepresented in P6 iWAT. Adipocytes are steroidogenic cells, and are capable of de novo production of pregnenolone and the oxysterol 27-hydroxycholesterol from cholesterol and its precursor, mevalonate. The inhibition of steroidogenesis induces adipocyte differentiation [99]. Adipocyte differentiation in human subcutaneous fat is associated with an increase in the mRNA levels of enzymes synthesizing and inactivating androgens [100], and iWAT acquires its steroidogenic potential during its maturation. As young iWAT shows features of beige adipocytes, the marked difference in the steroidogenic potential of young and adult iWAT has relevance for childhood obesity. The premature loss of beige adipocytes has been observed in obese children, and as a result of insufficient breastfeeding [38,56]. Steroidogenesis, in particular the level of sexual steroids, is key in the early life imprinting of the sex-dependent differentiation of organs. In the first six months of life in boys, and during the first two years in girls, there is a transient sex-specific activation of the hypothalamic−pituitary−gonadal axis, which is called minipuberty [101]. Minipuberty is associated with the rise in estradiol and testosterone, and is thought to determine sex-specific growth and maturation in later life. Moreover, minipuberty influences body composition [101]. As adiposity in infancy has an impact on obesity status in adulthood, the premature loss of beige adipocytes may compromise minipuberty and trigger obesogenic imprinting during metabolic development. Insufficient breastfeeding impairs several physiological functions that are associated with minipuberty, such as body adiposity, cognitive development and gonadal development [38,102,103]. It is plausible that breastfeeding is required for postnatal adipose tissue functions, which contribute to the hormonal changes of the minipuberty.

Young BAT and young iWAT shared a similar expression of a local angiotensin-kininogen system, inhibitory G-protein-linked neuropeptide receptors and GABA-A signaling. Specifically, NPY receptors, *Npy*, *Gal*, *Npbwr1* and various components of the GABA-A receptor signaling were overrepresented DEGs in young BAT and iWAT. GABA-A receptors were also overrepresented in adult BAT. NPY2R is the receptor for NPY, which is an important central orexigenic hormone that is also produced by the subcutaneous fat [104], and cold stress induces NPY release [105]. It is therefore important that young iWAT expresses higher levels of *Npy* and *Npy2r* than adult iWAT or BAT, suggesting that fat-derived NPY may have a role in the postnatal development of the adipose tissue. NPY induces angiogenesis and fat cell differentiation through NPY2R [105], making it plausible that NPY may be responsible for early vascularization and expansion of iWAT. In adults, however, excessive NPY signaling leads to obesity [106,107] and NPY increases adipocyte size in hyperinsulinemic conditions [104]. Young iWAT also showed elevated expression of *Npy4r*, which encodes NPY4R, a receptor for PP. PP is released from the pancreas in response to meal ingestion and reduces appetite. Low plasma PP levels have been observed in human obesity [108,109], and PP levels are higher in men than in women [110]. It is plausible that PP, similarly to NPY, has a role in early fat development. The transcript of the *Npy6r* pseudogene was also enriched in young iWAT, however, its gene product has no ligand binding for NPY or PP [111]. Young iWAT also showed increased expression of the neuropeptide receptors NPBWR and NPFFR1. NPBWR is a receptor for the neuropeptide W and neuropeptide B. Ablation of this receptor in mice leads to obesity [112], and NPBWR signaling has a role in the central regulation of energy balance [113]. Similarly, NPFF in the hypothalamus suppresses appetite [114], and protects from obesity-induced inflammation, and obesity is associated with decreased plasma NPFF levels [57,115].

Interactome maps of the neuropeptide signaling gene networks of young iWAT and BAT pointed to their association with NFκB and STAT3 signaling. Suppressed chemotaxis for granulocytes and underrepresented NFκB signaling were shared features of young BAT and iWAT. This immune-suppressed state was retained in adult BAT, which showed very little immune cell content. By contrast, maturation of iWAT was associated with the overrepresentation of inflammatory pathways and the decline in the expression of the

local angiotensin-kininogen system, inhibitory G-protein linked neuropeptide receptors and GABA-A signaling. GABA has a role in suppressing inflammatory cytokine signaling [116–118]; however, its effects are dependent on the GABA receptor engaged. For instance, the GABA-B receptor, which showed a stable expression in young and adult adipose tissue, worsens BAT function, and inhibition of this signaling axis restores BAT in obese mice [119]. Unexpectedly, young iWAT had a strongly expressed innate immune gene network, involving cathelicidin and β-defensin [120]. Young iWAT was also unique in the expression of PIWI genes, which are involved in the neutralization of transposable elements, safeguard genome integrity and ensure the adaptation of the immune response to rapidly evolving viruses [121].

We also identified some unexplored traits of adult BAT, which uniquely expressed vitamin K-dependent protein C and coagulation factor XII (Hageman factor). Vitamin K-dependent protein C is an anticoagulation factor, and is activated by the thrombin-thrombomodulin complex to degrade the activated forms of coagulation factors V and VIII. Mutations in the gene are associated with thrombophilia, neonatal purpura fulminans, and recurrent venous thrombosis [122,123]. Hageman factor activates the intrinsic pathway of the blood coagulation cascade, and is also involved in fibrinolysis. Of relevance, obesity is associated with metainflammation and hyperlipidemia, which both contribute to thrombotic disorders and the dysregulation of endogenous anticoagulant mechanisms [124]. For instance, unsaturated fatty acids and long-chain fatty acids are known to activate the Hageman factor [125,126], while metainflammation is associated with an increased risk of thrombosis [127]. BAT may have an as yet unexplored role in hemostasis, and this may be impaired by the loss of BAT in obesity.

5. Conclusions

We found that the iWAT of young mice is rich in beige fat cells and can be defined as a "bona fide" beige adipocyte depot (Figure 6). Metabolic genes including thermogenic and lipid catabolism genes were expressed in young iWAT, which likely means that this fat depot functions to break down fat to produce energy and heat. Lipolysis is a trait of beige adipocytes and BAT, and the inhibition of lipolysis favors thermogenic fat development [37], with lipid metabolites functioning as key signals for beige adipocyte, and BAT differentiation [36]. Breast milk-derived lipid mediators are known to sustain thermogenic fat in the infant [38,128]. By contrast, the transcriptional landscape of adult iWAT is associated with lipid storage, and the inactivation of beige adipocyte-inducing lipid species [38].

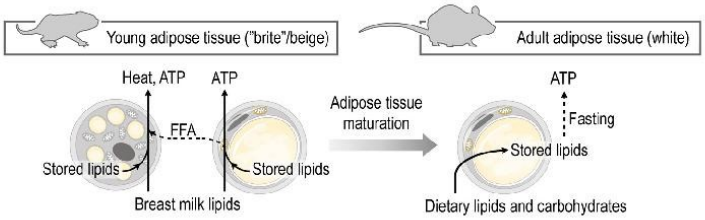

Figure 6. Maturation of the subcutaneous adipose tissue entails a shift from fat catabolism and thermogenesis to fat storage. The subcutaneous adipose tissue in early postnatal life shows hallmarks of beige adipocytes, and supports the catabolism of dietary lipids, mostly breast milk lipids. At this developmental stage the fat is catabolized by the adipocytes to elaborate free fatty acids (FFA), produce energy and heat. Breast milk lipid mediators maintain beige adipocytes. In adulthood, however, the subcutaneous adipose tissue is predominantly a lipid storage site.

Our findings indicate the probable existence of metabolic reprogramming during the maturation of subcutaneous adipose tissue, shifting from the burning of fat as heat

and energy to the accumulation of lipids as energy storage. This metabolic shift is in good agreement with the previously observed intensive lipid catabolism and fatty acid release from the subcutaneous adipose tissue in newborn mammals, including human infants [14,19,25,54], and the potential of the subcutaneous adipose tissue-derived adipocytes to transform into beige adipocytes in response to cold stress [44,72].

Indeed, the expression of beige adipocyte genes and the multilocular appearance of fat cells in the subcutaneous adipose tissue of human infants support the presence of subcutaneous beige adipocytes in humans [38,56]. The existence of a subcutaneous beige adipocytes is relevant in the early life determination of obesity, as signals triggering the premature loss of beige adipocytes may be the roots of a premature expansion of the WAT, leading to childhood obesity.

Supplementary Materials: The following are available online at https://www.mdpi.com/article/10.3390/cells10092368/s1, Figure S1: Workflow of our NGS analysis and correlation heatmap of the samples analyzed, Figure S2: Area of beige fat in the iWAT at P6 and P56, Figure S3: Interactive maps of gene networks, Figure S4: Immunostaining of $GABA_BR$ in P6 and P56 iWAT, Table S1: *Krt5* network, Table S2: *Mup2* network, Table S3: *Agtr2* network, Table S4: *H2-Q9* network, Table S5: *Ucp1* network, Table S6: *Krt71* network, Table S7: *Fabp3* network, Table S8: *Glycam1* network.

Author Contributions: Conceptualization, methodology, writing, and funding acquisition, T.R., investigation, A.C.H., H.Y. All authors have read and agreed to the published version of the manuscript.

Funding: This research was funded by the German Research Fund (DFG, RO 4856), and the European Foundation for the Study of Diabetes on New Targets for Type 2 Diabetes, Supported by MSD (No. 96403). The APC was funded by the German Research Fund (DFG, RO 4856), and by the Ulm University.

Institutional Review Board Statement: Research involving animals was approved by the regional governmental ethics and animal welfare committee in Tübingen, Germany (#1206; #1441; #1492; #o.189-20; #o.232-1,2,4,5). All applicable international, national, and/or institutional guidelines for the care and use of animals were followed. This article does not contain any studies with human participants performed by the authors.

Informed Consent Statement: Not applicable.

Data Availability Statement: Raw NGS data are deposited at GEO with the accession number #GSE133500. For secondary analysis, we used our previously published NGS dataset, with accession number #GSE125405. Flow Repository identifier of raw FACS data: #FR-FCM-Z236.

Acknowledgments: Vincent Pflüger provided technical help. Kenneth McCreath edited the manuscript.

Conflicts of Interest: The authors declare no conflict of interest.

References

1. Hruby, A.; Hu, F.B. The Epidemiology of Obesity: A Big Picture. *Pharmacoeconomics* **2015**, *33*, 673–689. [CrossRef]
2. Murray, C.J.L. Health Effects of Overweight and Obesity in 195 Countries over 25 Years. *N. Engl. J. Med.* **2017**, *377*, 13–27. [CrossRef]
3. Rosen, E.D.; Spiegelman, B.M. What we talk about when we talk about fat. *Cell* **2014**, *156*, 20–44. [CrossRef] [PubMed]
4. WHO. *Global Report on Diabetes*; WHO Press: Geneve, Switzerland, 2016.
5. Chobot, A.; Górowska-Kowolik, K.; Sokołowska, M.; Jarosz-Chobot, P. Obesity and diabetes—Not only a simple link between two epidemics. *Diabetes Metab. Res. Rev.* **2018**, *34*, e3042. [CrossRef] [PubMed]
6. Kahn, J.L.; Sick, H.; Laude, M.; Koritke, J.G. Bichat's fat pad: Anatomy and imaging. *Arch. Anat. Histol. Embryol. Norm. Exp.* **1988**, *71*, 57–83.
7. Braus, H. *Anatomie des Menschen: Ein Lehrbuch für Studierende und Ärzte (Band 1): Bewegungsapparat*; Springer: Berlin/Heidelberg, Germany, 1921; Volume 3.
8. Young, R.W. Evolution of the human hand: The role of throwing and clubbing. *J. Anat.* **2003**, *202*, 165–174. [CrossRef] [PubMed]
9. Hahn, P.; Novak, M. Development of brown and white adipose tissue. *J. Lipid Res.* **1975**, *16*, 79–91. [CrossRef]
10. Hull, D. The structure and function of brown adipose tissue. *Br. Med. Bull.* **1966**, *22*, 92–96. [CrossRef]
11. Harms, M.; Seale, P. Brown and beige fat: Development, function and therapeutic potential. *Nat. Med.* **2013**, *19*, 1252–1263. [CrossRef]
12. Bartelt, A.; Heeren, J. Adipose tissue browning and metabolic health. *Nat. Rev. Endocrinol.* **2014**, *10*, 24–36. [CrossRef]

13. Bligh, J. Hibernation. In *Temperature Regulation in Mammals and Other Vertebrates*; Bigh, J., Ed.; North-Holland Research Monographs: Amsterdam, The Netherlands; American Elsevier: New York, NY, USA, 1973.
14. Hardman, M.J.; Hull, D. Fat metabolism in brown adipose tissue in vivo. *J. Physiol.* **1970**, *206*, 263–273. [CrossRef]
15. Farkas, V.; Kelenyi, G.; Sandor, A. A dramatic accumulation of glycogen in the brown adipose tissue of rats following recovery from cold exposure. *Arch. Biochem. Biophys.* **1999**, *365*, 54–61. [CrossRef]
16. Mayeuf-Louchart, A. Uncovering the Role of Glycogen in Brown AdiposeTissue. *Pharm. Res.* **2021**, *38*, 9–14. [CrossRef] [PubMed]
17. Mayeuf-Louchart, A.; Lancel, S.; Sebti, Y.; Pourcet, B.; Loyens, A.; Delhaye, S.; Duhem, C.; Beauchamp, J.; Ferri, L.; Thorel, Q.; et al. Glycogen Dynamics Drives Lipid Droplet Biogenesis during Brown Adipocyte Differentiation. *Cell Rep.* **2019**, *29*, 1410–1418.e6. [CrossRef] [PubMed]
18. Persson, B. Carbohydrate and Lipid Metabolism in the Newborn Infant. *Acta Anaesthesiol. Scand.* **1974**, *18*, 50–57. [CrossRef] [PubMed]
19. Novak, M.; Monkus, E. Metabolism of Subcutaneous Adipose Tissue in the Immediate Postnatal Period of Human Newborns. 1. Developmental Changes in Lipolysis and Glycogen Content. *Pediatr. Res.* **1972**, *6*, 73–80. [CrossRef]
20. Novak, M.; Monkus, E.; Pardo, V. Human neonatal subcutaneous adipose tissue. Function and ultrastructure. *Biol. Neonate* **1971**, *19*, 306–321. [CrossRef]
21. Herrera, E.; Amusquivar, E. Lipid metabolism in the fetus and the newborn. *Diabetes Metab. Res. Rev.* **2000**, *16*, 202–210. [CrossRef]
22. De Robertis, E.D.P.; Nowinski, W.W.; Saez, A.F. Morphlogy of the mitochondria. In *Cell Bilogy*, 4th ed.; W. B. Saunders: London, UK, 1965.
23. Aherne, W.; Hull, D. Brown adipose tissue and heat production in the newborn infant. *J. Pathol. Bacteriol.* **1966**, *91*, 223–234. [CrossRef]
24. Jastroch, M.; Withers, K.W.; Taudien, S.; Frappell, P.B.; Helwig, M.; Fromme, T.; Hirschberg, V.; Heldmaier, G.; McAllan, B.M.; Firth, B.T.; et al. Marsupial uncoupling protein 1 sheds light on the evolution of mammalian nonshivering thermogenesis. *Physiol. Genom.* **2008**, *32*, 161–169. [CrossRef]
25. Stave, U. *Perinatal Physiology*; Plenum Medical Company: New York, NY, USA; London, UK, 1970.
26. Clara, M. *Entwicklungsgeschichte des Menschen*; Georg Thieme Verlag: Leipzig, Germany, 1955.
27. Carobbio, S.; Rosen, B.; Vidal-Puig, A. Adipogenesis: New insights into brown adipose tissue differentiation. *J. Mol. Endocrinol.* **2013**, *51*, T75–T85. [CrossRef] [PubMed]
28. Alcalá, M.; Calderon-Dominguez, M.; Bustos, E.; Ramos, P.; Casals, N.; Serra, D.; Viana, M.; Herrero, L. Increased inflammation, oxidative stress and mitochondrial respiration in brown adipose tissue from obese mice. *Sci. Rep.* **2017**, *7*, 16082. [CrossRef]
29. Alcalá, M.; Calderon-Dominguez, M.; Serra, D.; Herrero, L.; Viana, M. Mechanisms of Impaired Brown Adipose Tissue Recruitment in Obesity. *Front. Physiol.* **2019**, *10*, 94. [CrossRef] [PubMed]
30. Gilsanz, V.; Hu, H.H.; Kajimura, S. Relevance of brown adipose tissue in infancy and adolescence. *Pediatr. Res.* **2013**, *73*, 3–9. [CrossRef]
31. Verduci, E.; Calcaterra, V.; Di Profio, E.; Fiore, G.; Rey, F.; Magenes, V.C.; Todisco, C.F.; Carelli, S.; Zuccotti, G.V. Brown Adipose Tissue: New Challenges for Prevention of Childhood Obesity. A Narrative Review. *Nutrients* **2021**, *13*, 1450. [CrossRef] [PubMed]
32. Ikeda, K.; Maretich, P.; Kajimura, S. The Common and Distinct Features of Brown and Beige Adipocytes. *Trends Endocrinol. Metab.* **2018**, *29*, 191–200. [CrossRef] [PubMed]
33. Pilkington, A.-C.; Paz, H.A.; Wankhade, U.D. Beige Adipose Tissue Identification and Marker Specificity—Overview. *Front. Endocrinol.* **2021**, *12*, 599134. [CrossRef] [PubMed]
34. Paulo, E.; Wang, B. Towards a Better Understanding of Beige Adipocyte Plasticity. *Cells* **2019**, *8*, 1552. [CrossRef]
35. Shi, F.; Collins, S. Second messenger signaling mechanisms of the brown adipocyte thermogenic program: An integrative perspective. *Horm. Mol. Biol. Clin. Investig.* **2017**, *31*, 20170062. [CrossRef]
36. Park, H.; He, A.; Lodhi, I.J. Lipid Regulators of Thermogenic Fat Activation. *Trends Endocrinol. Metab.* **2019**, *30*, 710–723. [CrossRef]
37. Lodhi, I.J.; Yin, L.; Jensen-Urstad, A.P.L.; Funai, K.; Coleman, T.; Baird, J.H.; El Ramahi, M.K.; Razani, B.; Song, H.; Fu-Hsu, F.; et al. Inhibiting adipose tissue lipogenesis reprograms thermogenesis and PPARγ activation to decrease diet-induced obesity. *Cell Metab.* **2012**, *16*, 189–201. [CrossRef]
38. Yu, H.; Dilbaz, S.; Coßmann, J.; Hoang, A.C.; Diedrich, V.; Herwig, A.; Harauma, A.; Hoshi, Y.; Moriguchi, T.; Landgraf, K.; et al. Breast milk alkylglycerols sustain beige adipocytes through adipose tissue macrophages. *J. Clin. Investig.* **2019**, *129*, 2485–2499. [CrossRef]
39. Cannon, B.; de Jong, J.M.A.; Fischer, A.W.; Nedergaard, J.; Petrovic, N. Human brown adipose tissue: Classical brown rather than brite/beige? *Exp. Physiol.* **2020**, *105*, 1191–1200. [CrossRef]
40. Jespersen, N.Z.; Larsen, T.J.; Peijs, L.; Daugaard, S.; Homøe, P.; Loft, A.; de Jong, J.; Mathur, N.; Cannon, B.; Nedergaard, J.; et al. A classical brown adipose tissue mRNA signature partly overlaps with brite in the supraclavicular region of adult humans. *Cell Metab.* **2013**, *17*, 798–805. [CrossRef] [PubMed]
41. Sharp, L.Z.; Shinoda, K.; Ohno, H.; Scheel, D.W.; Tomoda, E.; Ruiz, L.; Hu, H.; Wang, L.; Pavlova, Z.; Gilsanz, V.; et al. Human BAT possesses molecular signatures that resemble beige/brite cells. *PLoS ONE* **2012**, *7*, e49452. [CrossRef]
42. Stine, R.R.; Shapira, S.N.; Lim, H.-W.; Ishibashi, J.; Harms, M.; Won, K.-J.; Seale, P. EBF2 promotes the recruitment of beige adipocytes in white adipose tissue. *Mol. Metab.* **2016**, *5*, 57–65. [CrossRef]

43. Wu, J.; Bostrom, P.; Sparks, L.M.; Ye, L.; Choi, J.H.; Giang, A.H.; Khandekar, M.; Virtanen, K.A.; Nuutila, P.; Schaart, G.; et al. Beige adipocytes are a distinct type of thermogenic fat cell in mouse and human. *Cell* **2012**, *150*, 366–376. [CrossRef]
44. Ravussin, E.; Kozak, L.P. Have we entered the brown adipose tissue renaissance? *Obes. Rev.* **2009**, *10*, 265–268. [CrossRef]
45. Song, A.; Dai, W.; Jang, M.J.; Medrano, L.; Li, Z.; Zhao, H.; Shao, M.; Tan, J.; Li, A.; Ning, T.; et al. Low- and high-thermogenic brown adipocyte subpopulations coexist in murine adipose tissue. *J. Clin. Investig.* **2020**, *130*, 247–257. [CrossRef] [PubMed]
46. Lee, K.Y.; Luong, Q.; Sharma, R.; Dreyfuss, J.M.; Ussar, S.; Kahn, C.R. Developmental and functional heterogeneity of white adipocytes within a single fat depot. *EMBO J.* **2019**, *38*, e99291. [CrossRef] [PubMed]
47. Sanchez-Gurmaches, J.; Guertin, D.A. Adipocyte lineages: Tracing back the origins of fat. *Biochim. Biophys. Acta* **2014**, *1842*, 340–351. [CrossRef]
48. Sidossis, L.; Kajimura, S. Brown and beige fat in humans: Thermogenic adipocytes that control energy and glucose homeostasis. *J. Clin. Investig.* **2015**, *125*, 478–486. [CrossRef]
49. Whyte, R.K.; Bayley, H.S. Energy Metabolism of the Newborn Infant. In *Advances in Nutritional Research*; Draper, H.H., Ed.; Springer: Boston, MA, USA, 1990; pp. 79–108.
50. Hayward, J.S.; Lisson, P.A. Evolution of brown fat: Its absence in marsupials and monotremes. *Can. J. Zool.* **1992**, *70*, 171–179. [CrossRef]
51. Cinti, S. Adipose Organ Development and Remodeling. *Compr. Physiol.* **2018**, *8*, 1357–1431. [CrossRef] [PubMed]
52. Landgraf, K.; Rockstroh, D.; Wagner, I.V.; Weise, S.; Tauscher, R.; Schwartze, J.T.; Löffler, D.; Bühligen, U.; Wojan, M.; Till, H.; et al. Evidence of early alterations in adipose tissue biology and function and its association with obesity-related inflammation and insulin resistance in children. *Diabetes* **2015**, *64*, 1249–1261. [CrossRef] [PubMed]
53. Carey, A.L.; Vorlander, C.; Reddy-Luthmoodoo, M.; Natoli, A.K.; Formosa, M.F.; Bertovic, D.A.; Anderson, M.J.; Duffy, S.J.; Kingwell, B.A. Reduced UCP-1 content in in vitro differentiated beige/brite adipocytes derived from preadipocytes of human subcutaneous white adipose tissues in obesity. *PLoS ONE* **2014**, *9*, e91997. [CrossRef] [PubMed]
54. Novak, M.; Penn, D.; Monkus, E. Regulation of lipolysis in human neonatal adipose tissue. Effects of alteration in carbohydrate metabolism. *Biol. Neonate* **1973**, *22*, 451–467. [CrossRef] [PubMed]
55. De Jong, J.M.; Larsson, O.; Cannon, B.; Nedergaard, J. A stringent validation of mouse adipose tissue identity markers. *Am. J. Physiol. Endocrinol. Metab.* **2015**, *308*, E1085–E1105. [CrossRef] [PubMed]
56. Rockstroh, D.; Landgraf, K.; Wagner, I.V.; Gesing, J.; Tauscher, R.; Lakowa, N.; Kiess, W.; Bühligen, U.; Wojan, M.; Till, H.; et al. Direct evidence of brown adipocytes in different fat depots in children. *PLoS ONE* **2015**, *10*, e0117841. [CrossRef]
57. Waqas, S.F.H.; Hoang, A.; Lin, Y.; Ampem, G.; Azegrouz, H.; Balogh, L.; Thuróczy, J.; Chen, J.C.; Gerling, I.C.; Nam, S.; et al. Neuropeptide FF increases M2 activation and self-renewal of adipose tissue macrophages. *J. Clin. Investig.* **2017**, *127*, 2842–2854. [CrossRef]
58. Waqas, S.F.H.; Noble, A.; Hoang, A.; Ampem, G.; Popp, M.; Strauß, S.; Guille, M.; Röszer, T. Adipose tissue macrophages develop from bone marrow-independent progenitors in *Xenopus laevis* and mouse. *J. Leukoc. Biol.* **2017**, *102*, 845–855. [CrossRef]
59. Ampem, G.; Röszer, T. Isolation and Characterization of Adipose Tissue Macrophages. In *Nuclear Receptors: Methods and Experimental Protocols*; Badr, M.Z., Ed.; Springer: New York, NY, USA, 2019; pp. 225–236.
60. Zebisch, K.; Voigt, V.; Wabitsch, M.; Brandsch, M. Protocol for effective differentiation of 3T3-L1 cells to adipocytes. *Anal. Biochem.* **2012**, *425*, 88–90. [CrossRef]
61. Kim, D.; Langmead, B.; Salzberg, S.L. HISAT: A fast spliced aligner with low memory requirements. *Nat. Methods* **2015**, *12*, 357–360. [CrossRef] [PubMed]
62. Langmead, B.; Salzberg, S.L. Fast gapped-read alignment with Bowtie 2. *Nat. Methods* **2012**, *9*, 357–359. [CrossRef] [PubMed]
63. Langmead, B.; Wilks, C.; Antonescu, V.; Charles, R. Scaling read aligners to hundreds of threads on general-purpose processors. *Bioinformatics* **2018**, *35*, 421–432. [CrossRef] [PubMed]
64. Love, M.I.; Huber, W.; Anders, S. Moderated estimation of fold change and dispersion for RNA-seq data with DESeq2. *Genome Biol.* **2014**, *15*, 550. [CrossRef]
65. Chen, E.Y.; Tan, C.M.; Kou, Y.; Duan, Q.; Wang, Z.; Meirelles, G.V.; Clark, N.R.; Ma'ayan, A. Enrichr: Interactive and collaborative HTML5 gene list enrichment analysis tool. *BMC Bioinform.* **2013**, *14*, 128. [CrossRef]
66. Kuleshov, M.V.; Jones, M.R.; Rouillard, A.D.; Fernandez, N.F.; Duan, Q.; Wang, Z.; Koplev, S.; Jenkins, S.L.; Jagodnik, K.M.; Lachmann, A.; et al. Enrichr: A comprehensive gene set enrichment analysis web server 2016 update. *Nucleic Acids Res.* **2016**, *44*, W90–W97. [CrossRef]
67. Rusinova, I.; Forster, S.; Yu, S.; Kannan, A.; Masse, M.; Cumming, H.; Chapman, R.; Hertzog, P.J. Interferome v2.0: An updated database of annotated interferon-regulated genes. *Nucleic Acids Res.* **2013**, *41*, D1040–D1046. [CrossRef]
68. Szklarczyk, D.; Gable, A.L.; Lyon, D.; Junge, A.; Wyder, S.; Huerta-Cepas, J.; Simonovic, M.; Doncheva, N.T.; Morris, J.H.; Bork, P.; et al. STRING v11: Protein-protein association networks with increased coverage, supporting functional discovery in genome-wide experimental datasets. *Nucleic Acids Res.* **2019**, *47*, D607–D613. [CrossRef]
69. Birsoy, K.; Soukas, A.; Torrens, J.; Ceccarini, G.; Montez, J.; Maffei, M.; Cohen, P.; Fayzikhodjaeva, G.; Viale, A.; Socci, N.D.; et al. Cellular program controlling the recovery of adipose tissue mass: An in vivo imaging approach. *Proc. Natl. Acad. Sci. USA* **2008**, *105*, 12985–12990. [CrossRef]
70. Hilton, C.; Karpe, F.; Pinnick, K.E. Role of developmental transcription factors in white, brown and beige adipose tissues. *Biochim. Biophys. Acta Mol. Cell Biol. Lipids* **2015**, *1851*, 686–696. [CrossRef]

71. Maurer, S.F.; Fromme, T.; Grossman, L.I.; Hüttemann, M.; Klingenspor, M. The brown and brite adipocyte marker Cox7a1 is not required for non-shivering thermogenesis in mice. *Sci. Rep.* **2015**, *5*, 17704. [CrossRef]
72. Kozak, L.P. The genetics of brown adipocyte induction in white fat depots. *Front. Endocrinol.* **2011**, *2*, 64. [CrossRef]
73. Röszer, T. Understanding the Mysterious M2 Macrophage through Activation Markers and Effector Mechanisms. *Mediat. Inflamm.* **2015**, *2015*, 816460. [CrossRef]
74. Sahoo, A.; Alekseev, A.; Obertas, L.; Nurieva, R. Grail controls Th2 cell development by targeting STAT6 for degradation. *Nat. Commun.* **2014**, *5*, 4732. [CrossRef] [PubMed]
75. Yang, J.; Petitjean, S.J.L.; Koehler, M.; Zhang, Q.; Dumitru, A.C.; Chen, W.; Derclaye, S.; Vincent, S.P.; Soumillion, P.; Alsteens, D. Molecular interaction and inhibition of SARS-CoV-2 binding to the ACE2 receptor. *Nat. Commun.* **2020**, *11*, 4541. [CrossRef]
76. Al-Benna, S. Association of high level gene expression of ACE2 in adipose tissue with mortality of COVID-19 infection in obese patients. *Obes. Med.* **2020**, *19*, 100283. [CrossRef] [PubMed]
77. Marcondes, S.; Antunes, E. The plasma and tissue kininogen-kallikrein-kinin system: Role in the cardiovascular system. *Curr. Med. Chem. Cardiovasc. Hematol. Agents* **2005**, *3*, 33–44. [CrossRef] [PubMed]
78. Abadir, P.M.; Periasamy, A.; Carey, R.M.; Siragy, H.M. Angiotensin II Type 2 Receptor—Bradykinin B Receptor Functional Heterodimerization. *Hypertension* **2006**, *48*, 316–322. [CrossRef] [PubMed]
79. Berg, A.H.; Lin, Y.; Lisanti, M.P.; Scherer, P.E. Adipocyte differentiation induces dynamic changes in NF-κB expression and activity. *Am. J. Physiol. Endocrinol. Metab.* **2004**, *287*, E1178–E1188. [CrossRef]
80. Nascimento, E.B.M.; Sparks, L.M.; Divoux, A.; van Gisbergen, M.W.; Broeders, E.P.M.; Jörgensen, J.A.; Schaart, G.; Bouvy, N.D.; van Marken Lichtenbelt, W.D.; Schrauwen, P. Genetic Markers of Brown Adipose Tissue Identity and In Vitro Brown Adipose Tissue Activity in Humans. *Obesity* **2018**, *26*, 135–140. [CrossRef]
81. Perugini, J.; Bordoni, L.; Venema, W.; Acciarini, S.; Cinti, S.; Gabbianelli, R.; Giordano, A. Zic1 mRNA is transiently upregulated in subcutaneous fat of acutely cold-exposed mice. *J. Cell. Physiol.* **2019**, *234*, 2031–2036. [CrossRef] [PubMed]
82. Seale, P.; Bjork, B.; Yang, W.; Kajimura, S.; Chin, S.; Kuang, S.; Scimè, A.; Devarakonda, S.; Conroe, H.M.; Erdjument-Bromage, H.; et al. PRDM16 controls a brown fat/skeletal muscle switch. *Nature* **2008**, *454*, 961–967. [CrossRef]
83. Kissig, M.; Ishibashi, J.; Harms, M.J.; Lim, H.-W.; Stine, R.R.; Won, K.-J.; Seale, P. PRDM16 represses the type I interferon response in adipocytes to promote mitochondrial and thermogenic programing. *EMBO J.* **2017**, *36*, 1528–1542. [CrossRef] [PubMed]
84. Cohen, P.; Levy, J.D.; Zhang, Y.; Frontini, A.; Kolodin, D.P.; Svensson, K.J.; Lo, J.C.; Zeng, X.; Ye, L.; Khandekar, M.J.; et al. Ablation of PRDM16 and beige adipose causes metabolic dysfunction and a subcutaneous to visceral fat switch. *Cell* **2014**, *156*, 304–316. [CrossRef] [PubMed]
85. Harms, M.J.; Ishibashi, J.; Wang, W.; Lim, H.-W.; Goyama, S.; Sato, T.; Kurokawa, M.; Won, K.-J.; Seale, P. Prdm16 is required for the maintenance of brown adipocyte identity and function in adult mice. *Cell Metab.* **2014**, *19*, 593–604. [CrossRef]
86. Morrison, S.; McGee, S.L. 3T3-L1 adipocytes display phenotypic characteristics of multiple adipocyte lineages. *Adipocyte* **2015**, *4*, 295–302. [CrossRef] [PubMed]
87. Qiu, Y.; Nguyen, K.D.; Odegaard, J.I.; Cui, X.; Tian, X.; Locksley, R.M.; Palmiter, R.D.; Chawla, A. Eosinophils and type 2 cytokine signaling in macrophages orchestrate development of functional beige fat. *Cell* **2014**, *157*, 1292–1308. [CrossRef] [PubMed]
88. Finlin, B.S.; Zhu, B.; Confides, A.L.; Westgate, P.M.; Harfmann, B.D.; Dupont-Versteegden, E.E.; Kern, P.A. Mast Cells Promote Seasonal White Adipose Beiging in Humans. *Diabetes* **2017**, *66*, 1237–1246. [CrossRef]
89. Geserick, M.; Vogel, M.; Gausche, R.; Lipek, T.; Spielau, U.; Keller, E.; Pfaffle, R.; Kiess, W.; Korner, A. Acceleration of BMI in Early Childhood and Risk of Sustained Obesity. *N. Engl. J. Med.* **2018**, *379*, 1303–1312. [CrossRef] [PubMed]
90. Billon, N.; Iannarelli, P.; Monteiro, M.C.; Glavieux-Pardanaud, C.; Richardson, W.D.; Kessaris, N.; Dani, C.; Dupin, E. The generation of adipocytes by the neural crest. *Development* **2007**, *134*, 2283–2292. [CrossRef] [PubMed]
91. Iwatsuki, H.; Suda, M. Transient expression of keratin during neuronal development in the adult rabbit spinal ganglion. *Anat. Sci. Int.* **2010**, *85*, 46–55. [CrossRef]
92. Sekiguchi, R.; Martin, D.; Yamada, K.M. Single-Cell RNA-seq Identifies Cell Diversity in Embryonic Salivary Glands. *J. Dent. Res.* **2020**, *99*, 69–78. [CrossRef]
93. Li, L.; Li, B.; Li, M.; Niu, C.; Wang, G.; Li, T.; Król, E.; Jin, W.; Speakman, J.R. Brown adipocytes can display a mammary basal myoepithelial cell phenotype in vivo. *Mol. Metab.* **2017**, *6*, 1198–1211. [CrossRef]
94. Prokesch, A.; Smorlesi, A.; Perugini, J.; Manieri, M.; Ciarmela, P.; Mondini, E.; Trajanoski, Z.; Kristiansen, K.; Giordano, A.; Bogner-Strauss, J.G.; et al. Molecular Aspects of Adipoepithelial Transdifferentiation in Mouse Mammary Gland. *Stem Cells* **2014**, *32*, 2756–2766. [CrossRef]
95. Sugathan, S.; Lee, S.-J.; Shiwani, S.; Singh, N.K. Transdifferentiation of bovine epithelial cells towards adipocytes in the presence of myoepithelium. *Asian-Australas. J. Anim. Sci.* **2020**, *33*, 349–359. [CrossRef]
96. Aoki, M.; Murase, T. Obesity-associated insulin resistance adversely affects skin function. *PLoS ONE* **2019**, *14*, e0223528. [CrossRef]
97. Okano, J.; Kojima, H.; Katagi, M.; Nakagawa, T.; Nakae, Y.; Terashima, T.; Kurakane, T.; Kubota, M.; Maegawa, H.; Udagawa, J. Hyperglycemia Induces Skin Barrier Dysfunctions with Impairment of Epidermal Integrity in Non-Wounded Skin of Type 1 Diabetic Mice. *PLoS ONE* **2016**, *11*, e0166215. [CrossRef]
98. Wu, Y.L.; Lin, C.W.; Cheng, N.C.; Yang, K.C.; Yu, J. Modulation of keratin in adhesion, proliferation, adipogenic, and osteogenic differentiation of porcine adipose-derived stem cells. *J. Biomed. Mater. Res. Part B Appl. Biomater.* **2017**, *105*, 180–192. [CrossRef]

99. Li, J.; Daly, E.; Campioli, E.; Wabitsch, M.; Papadopoulos, V. De Novo Synthesis of Steroids and Oxysterols in Adipocytes. *J. Biol. Chem.* **2014**, *289*, 747–764. [CrossRef]
100. Blouin, K.; Nadeau, M.; Mailloux, J.; Daris, M.; Lebel, S.; Luu-The, V.; Tchernof, A. Pathways of adipose tissue androgen metabolism in women: Depot differences and modulation by adipogenesis. *Am. J. Physiol. Endocrinol. Metab.* **2009**, *296*, E244–E255. [CrossRef]
101. Becker, M.; Hesse, V. Minipuberty: Why Does it Happen? *Horm. Res. Paediatr.* **2020**, *93*, 76–84. [CrossRef] [PubMed]
102. Ortega-García, J.A.; Olano-Soler, H.A.; Martínez-Álvarez, A.; Campillo-López, F.; Gomariz-Peñalver, V.; Mendiola-Olivares, J.; Iglesias-Gómez, C.; Escribano-Muñoz, A. Breastfeeding Duration and Anogenital Distance in 2-Year-Old Infants. *Breastfeed. Med.* **2016**, *11*, 350–355. [CrossRef] [PubMed]
103. Stewart, C.J.; Ajami, N.J.; O'Brien, J.L.; Hutchinson, D.S.; Smith, D.P.; Wong, M.C.; Ross, M.C.; Lloyd, R.E.; Doddapaneni, H.; Metcalf, G.A.; et al. Temporal development of the gut microbiome in early childhood from the TEDDY study. *Nature* **2018**, *562*, 583–588. [CrossRef] [PubMed]
104. Kos, K.; Harte, A.L.; James, S.; Snead, D.R.; O'Hare, J.P.; McTernan, P.G.; Kumar, S. Secretion of neuropeptide Y in human adipose tissue and its role in maintenance of adipose tissue mass. *Am. J. Physiol. Endocrinol. Metab.* **2007**, *293*, E1335–E1340. [CrossRef] [PubMed]
105. Kuo, L.E.; Kitlinska, J.B.; Tilan, J.U.; Li, L.; Baker, S.B.; Johnson, M.D.; Lee, E.W.; Burnett, M.S.; Fricke, S.T.; Kvetnansky, R.; et al. Neuropeptide Y acts directly in the periphery on fat tissue and mediates stress-induced obesity and metabolic syndrome. *Nat. Med.* **2007**, *13*, 803–811. [CrossRef]
106. Yan, C.; Zeng, T.; Lee, K.; Nobis, M.; Loh, K.; Gou, L.; Xia, Z.; Gao, Z.; Bensellam, M.; Hughes, W.; et al. Peripheral-specific Y1 receptor antagonism increases thermogenesis and protects against diet-induced obesity. *Nat. Commun.* **2021**, *12*, 2622. [CrossRef] [PubMed]
107. Park, S.; Nayantai, E.; Komatsu, T.; Hayashi, H.; Mori, R.; Shimokawa, I. NPY Deficiency Prevents Postmenopausal Adiposity by Augmenting Estradiol-Mediated Browning. *J. Gerontol. Ser. A Biol. Sci. Med. Sci.* **2020**, *75*, 1042–1049. [CrossRef]
108. Koska, J.; DelParigi, A.; de Courten, B.; Weyer, C.; Tataranni, P.A. Pancreatic Polypeptide Is Involved in the Regulation of Body Weight in Pima Indian Male Subjects. *Diabetes* **2004**, *53*, 3091–3096. [CrossRef] [PubMed]
109. Lassmann, V.; Vague, P.; Vialettes, B.; Simon, M.C. Low plasma levels of pancreatic polypeptide in obesity. *Diabetes* **1980**, *29*, 428–430. [CrossRef]
110. Tong, J.; Utzschneider, K.M.; Carr, D.B.; Zraika, S.; Udayasankar, J.; Gerchman, F.; Knopp, R.H.; Kahn, S.E. Plasma pancreatic polypeptide levels are associated with differences in body fat distribution in human subjects. *Diabetologia* **2007**, *50*, 439–442. [CrossRef] [PubMed]
111. Gregor, P.; Feng, Y.; DeCarr, L.B.; Cornfield, L.J.; McCaleb, M.L. Molecular characterization of a second mouse pancreatic polypeptide receptor and its inactivated human homologue. *J. Biol. Chem.* **1996**, *271*, 27776–27781. [CrossRef] [PubMed]
112. Ishii, M.; Fei, H.; Friedman, J.M. Targeted disruption of GPR7, the endogenous receptor for neuropeptides B and W, leads to metabolic defects and adult-onset obesity. *Proc. Natl. Acad. Sci. USA* **2003**, *100*, 10540–10545. [CrossRef]
113. Sakurai, T. NPBWR1 and NPBWR2: Implications in Energy Homeostasis, Pain, and Emotion. *Front. Endocrinol.* **2013**, *4*, 23. [CrossRef] [PubMed]
114. Maletinska, L.; Ticha, A.; Nagelova, V.; Spolcova, A.; Blechova, M.; Elbert, T.; Zelezna, B. Neuropeptide FF analog RF9 is not an antagonist of NPFF receptor and decreases food intake in mice after its central and peripheral administration. *Brain Res.* **2013**, *1498*, 33–40. [CrossRef]
115. Hunt, S.C.; Hasstedt, S.J.; Xin, Y.; Dalley, B.K.; Milash, B.A.; Yakobson, E.; Gress, R.E.; Davidson, L.E.; Adams, T.D. Polymorphisms in the NPY2R gene show significant associations with BMI that are additive to FTO, MC4R, and NPFFR2 gene effects. *Obesity* **2011**, *19*, 2241–2247. [CrossRef]
116. Prud'homme, G.; Glinka, Y.; Wang, Q. GABA exerts anti-inflammatory and immunosuppressive effects (P5175). *J. Immunol.* **2013**, *190*, 68-15.
117. Bhat, R.; Axtell, R.; Mitra, A.; Miranda, M.; Lock, C.; Tsien, R.W.; Steinman, L. Inhibitory role for GABA in autoimmune inflammation. *Proc. Natl. Acad. Sci. USA* **2010**, *107*, 2580–2585. [CrossRef] [PubMed]
118. Kelley, J.M.; Hughes, L.B.; Bridges, S.L. Does gamma-aminobutyric acid (GABA) influence the development of chronic inflammation in rheumatoid arthritis? *J. Neuroinflamm.* **2008**, *5*, 1. [CrossRef]
119. Ikegami, R.; Shimizu, I.; Sato, T.; Yoshida, Y.; Hayashi, Y.; Suda, M.; Katsuumi, G.; Li, J.; Wakasugi, T.; Minokoshi, Y.; et al. Gamma-Aminobutyric Acid Signaling in Brown Adipose Tissue Promotes Systemic Metabolic Derangement in Obesity. *Cell Rep.* **2018**, *24*, 2827–2837.e5. [CrossRef] [PubMed]
120. Zhang, L.J.; Guerrero-Juarez, C.F.; Hata, T.; Bapat, S.P.; Ramos, R.; Plikus, M.V.; Gallo, R.L. Innate immunity. Dermal adipocytes protect against invasive Staphylococcus aureus skin infection. *Science* **2015**, *347*, 67–71. [CrossRef] [PubMed]
121. Ozata, D.M.; Gainetdinov, I.; Zoch, A.; O'Carroll, D.; Zamore, P.D. PIWI-interacting RNAs: Small RNAs with big functions. *Nat. Rev. Genet.* **2019**, *20*, 89–108. [CrossRef] [PubMed]
122. Grundy, C.B.; Schulman, S.; Tengborn, L.; Kakkar, V.V.; Cooper, D.N. Two different missense mutations at Arg 178 of the protein C (PROC) gene causing recurrent venous thrombosis. *Hum. Genet.* **1992**, *89*, 685–686. [CrossRef] [PubMed]

123. Romeo, G.; Hassan, H.J.; Staempfli, S.; Roncuzzi, L.; Cianetti, L.; Leonardi, A.; Vicente, V.; Mannucci, P.M.; Bertina, R.; Peschle, C.; et al. Hereditary thrombophilia: Identification of nonsense and missense mutations in the protein C gene. *Proc. Natl. Acad. Sci. USA* **1987**, *84*, 2829–2832. [CrossRef]
124. Blokhin, I.O.; Lentz, S.R. Mechanisms of thrombosis in obesity. *Curr. Opin. Hematol.* **2013**, *20*, 437–444. [CrossRef]
125. Margolis, J. Activation of Hageman Factor by Saturated Fatty Acids. *Aust. J. Exp. Biol. Med. Sci.* **1962**, *40*, 505–513. [CrossRef]
126. Didisheim, P.; Mibashan, R.S. Activation of Hageman Factor (Factor XII) by Long-Chain Saturated Fatty Acids. *Thromb. Diath. Haemorrh.* **1963**, *143*, 346–353. [CrossRef]
127. Levi, M.; van der Poll, T.; Schultz, M. Infection and Inflammation as Risk Factors for Thrombosis and Atherosclerosis. *Semin. Thromb. Hemost.* **2012**, *38*, 506–514. [CrossRef]
128. Wolfs, D.; Lynes, M.D.; Tseng, Y.H.; Pierce, S.; Bussberg, V.; Darkwah, A.; Tolstikov, V.; Narain, N.R.; Rudolph, M.C.; Kiebish, M.A.; et al. Brown fat-activating lipokine 12,13-diHOME in human milk is associated with infant adiposity. *J. Clin. Endocrinol. Metab.* **2020**, *106*, e943–e956. [CrossRef]

Research Square

Preprints are preliminary reports that have not undergone peer review.
They should not be considered conclusive, used to inform clinical practice,
or referenced by the media as validated information.

Immune privilege of adipocyte mitochondria protects from obesity

Anh Cuong Hoang
Ulm University
Haidong Yu
Ulm University
Ya-Tin Lin
Chang Gung University https://orcid.org/0000-0001-7910-1223
Jin-Chung Chen
Chang Gung University
Chia-Chun Chen
Chang Gung University
Victoria Diedrich
Ulm University
Annika Herwig
Ulm University
Kathrin Landgraf
University of Leipzig, Pediatric Research Centre, Department of Women's and Child Health
https://orcid.org/0000-0002-6878-6033
Antje Körner
Center for Pediatric Research Leipzig (CPL), University Hospital for Children & Adolescents, University of Leipzig, Leipzig https://orcid.org/0000-0001-6001-0356
Tamás Roszer (✉ **tamas.roeszer@uni-ulm.de**)
Ulm University

Article

Keywords: innate immunity, obesity, interferons, IFI16, vitamin D

Posted Date: November 4th, 2021

DOI: https://doi.org/10.21203/rs.3.rs-988599/v1

License: This work is licensed under a Creative Commons Attribution 4.0 International License.
Read Full License

Immune privilege of adipocyte mitochondria protects from obesity

Anh Cuong Hoang[1]; Haidong Yu[1], Ya-Tin Lin[2], Jin-Chung Chen[2], Chia-Chun Chen[3], Victoria Diedrich[1], Annika Herwig[1], Kathrin Landgraf[4], Antje Körner[4], Tamás Röszer[1*]

[1]Institute of Neurobiology, Ulm University, Ulm, Germany

[2]Department of Physiology and Pharmacology, Graduate Institute of Biomedical Sciences, School of Medicine; Healthy Aging Research Center, Chang Gung University, Taiwan

[3]Molecular Medicine Research Center, Chang Gung Memorial Hospital at Linkou, Taiwan

[4]Center for Pediatric Research, University Hospital for Children and Adolescents, University of Leipzig, Germany

*Correspondence to: tamas.roeszer@uni-ulm.de, Fax: +49 (0) 731-50-22629

Short title: Anti-mitochondrial immune response aggravates obesity

Key words: innate immunity – obesity – interferons – IFI16 – vitamin D

Abstract

Infant nutrition is rich in lipids, and the adipose tissue has been adapted to properly break down neutral lipids and oxidize fatty acids in infancy. Accordingly, infant adipose tissue contains so-called beige adipocytes, which burn off lipids to heat, and impede fat storage and obesity. We show here that infant adipocytes are immune privileged sites for mitochondria due to a blockade in interferon regulatory factor 7 (IRF7)-signaling, which allows mitochondrial RNA to trigger beige adipocyte differentiation through mitochondria-to-nucleus signaling. These mechanisms serve to maintain an extensive mitochondrial network in beige adipocytes and protect against obesity. By contrast, fat storing white adipocytes lack these mechanisms and respond to their mitochondrial content with inflammation. We show that obesity subverts the immune privilege for mitochondria in adipocytes, which reduces mitochondrial mass and abrogates beige adipocyte development. In turn, suppressing IRF7 signaling and restoring the RNA-mediated mitochondria-to-nucleus signaling in adipocytes effectively reduces obesity.

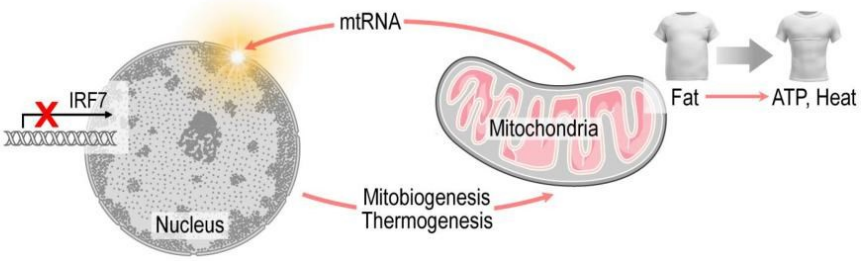

Graphical Abstract

Infant adipocytes have a suppressed IRF7 expression and a mitochondria-to-nucleus signaling through mitochondrial RNA (mtRNA), which stimulates the transcription of beige adipocyte genes, and is key for mitobiogenesis and burning off fat as heat.

Video summary

https://figshare.com/s/36e7ca6a4953471fba42

Childhood obesity is a serious public health crisis and is associated with an increased risk of obesity and diabetes in adulthood, which is projected to affect ~58% of the world's adult population by 2030 (1-3). Obesity is an excessive accumulation of white adipose tissue (WAT) mediated by a mismatch between energy supply and utilization. Infant nutrition is rich in lipids, and adipocytes in the infant WAT break down lipids to free fatty acids, and generate energy and heat from lipids in their extensive mitochondrial network (4-6). These fat oxidizing and thermogenic fat cells are termed as beige adipocytes (7, 8). In adults however, adipocytes of the subcutaneous fat depots are scarce in mitochondria and accumulate fat (9, 10). WAT is necessary for metabolic and endocrine health in adulthood, however its excess expansion accounts for metabolic diseases (1-3). Previous studies have suggested that the premature loss of fat oxidizing and thermogenic potential in infant WAT is accelerated in childhood obesity (2, 3, 10), and delaying or reverting the metabolic shift of WAT from fat catabolism to storage has therapeutic potential in the prevention of obesity (7, 8).

Cell metabolism of fat into ATP and heat requires an extensive mitochondrial network and mitochondrial uncoupling (8), which increases the abundance of "misplaced" mitochondria-associated danger signals in the cytoplasm, such as prokaryote-type mitochondrial DNA (mtDNA) and virus-like double stranded RNA (dsRNA). These signals trigger inflammasome activation and interferon (IFN) response (11), which abrogate the expansion of the mitochondrial network and the capacity of fat oxidation, and cause metabolic inflammation (12). Obesity is a hyper-inflammatory disorder, and IFNs trigger obesity-associated metabolic diseases (13, 14), especially in children with insufficient breastfeeding (15), who are prone for premature WAT expansion (7).

These observations prompted us to question whether infant adipocytes have a unique nucleic acid immunity that supports their mitochondrial network. We found that the infant

subcutaneous adipocytes were immune privileged towards mitochondria due to the suppression of cytosolic mtDNA recognition and interferon regulatory factor 7 (IRF7). Mitochondrial RNA (mtRNA) eventually activated a mitochondria-to-nucleus signaling which stimulated mitobiogenesis and beige adipocyte development without provoking an IFN-response against mitochondrial content. These mechanisms were lacking from the adult subcutaneous adipocytes, which responded with IFN-burst to mitochondrial content and were hostile for mitochondria. Obesity subverted mitochondrial immune privilege in adipocytes, and in turn, restoring mtRNA-mediated signaling effectively reduced obesity. Innate immune sensing of mitochondrial nucleic acids is hence a novel mechanism which controls early adipose tissue development and protects against obesity.

Results

Infant subcutaneous fat is immune privileged for mitochondria

After birth, subcutaneous adipose tissue is a relevant fat depot in mouse and human (6), hence we surveyed the transcriptional landscape of mouse inguinal adipose tissue (iAT) at postnatal day 6 (P6) and P56 by next-generation sequencing (NGS) (Fig. S1A, Fig. S2A,B). P6 iAT was rich in beige adipocytes and mtDNA, and expressed beige adipocyte-associated transcripts together with *Prdm16*, encoding PR domain containing 16, a key transcriptional regulator of thermogenic fat development (Fig. S1B-E) (10, 16). By contrast, P56 iAT lacked beige adipocytes, contained significantly lower amounts of mtDNA, and expressed transcripts associated with white adipocytes (Fig. S1B-E). Thus, infant but not adult mouse fat is rich in thermogenic, fat-oxidizing adipocytes (6). Beige adipocytes have been reported in the subcutaneous adipose tissue of human infants and children (7, 10), and we found that the level of *UCP1*, encoding uncoupling protein 10, in human

82 infant iAT correlated positively with the level of beige adipocyte genes and negatively with white
83 adipocyte markers (Fig. S1F).

84 IFN-stimulated genes (ISGs) were suppressed in adipocytes at P6 (Fig. 1A-C), and the
85 under-represented ISGs belonged to one network (Fig. S2B), and included the stimulator of
86 interferon genes (STING) and IFN-inducible protein absent in melanoma 2 (AIM2) pathways (Fig.
87 1B). These pathways trigger DNA-inflammasome assembly, inflammasome activation and IFN-
88 response to cytosolic DNA (17). Cytosolic B-DNA is recognized by DDX41 (DEAD-box helicase
89 41) and p204, also known as IFNγ-inducible protein 204 (IFI204) in BALB/C mice, IFI205 in
90 C57/BL6 mice, and IFI16 in human (17) (for details see Fig. S2C). Cytosolic Z-DNA, which is
91 prevalent in transcriptionally active cells (18), is recognized by ZBP1 (Z-DNA-binding protein 1,
92 also termed DAI (19)). Transcription of these cytosolic DNA sensors was low at P6, specifically
93 in adipocytes (Fig. 1B,C, Fig. S2D-H).

94 The STING and AIM2 pathways converge on interferon regulatory factor 3 and 7 (IRF3,
95 IRF7), and the adipocyte level of *Irf7* was significantly lower at P6 than at P56 (Fig. 1B,C).
96 Accordingly, P6 adipocytes were protected from inflammasome activation by cytosolic DNA (Fig.
97 1B, Fig. S3A-D, S4A-C) or endosomal DNA (Fig. S5A-F), and genetic ablation of IRF7 protected
98 adipocytes from IFN-response against mtDNA (Fig. S4E). IRF7 activation triggered the
99 expression of the STING/AIM2 pathway in P56 adipocytes (Fig. S4F), and consistently, the
100 STING/AIM2 pathway proteins were lacking in P6 adipocytes (Fig. 1D). In turn, AIM2, DDX41,
101 p204 and ZBP1 were present in the perinuclear region and in the cytoplasm of P56 adipocytes,
102 which distribution is consistent with their known tasks to monitor DNA fragments in specific
103 subcellular compartments (Fig. 1D) (19, 20).

104 We next examined the expression of the STING/AIM2 pathways and IRF7 in the inguinal
105 adipose tissue (iAT) of human infants and children (0.3–6.9 years of age, N=26). Overweight
106 (BMI-SDS>1.28) and obesity (BMI-SDS>1.88) strongly increased the expression of *IFI16*, *ZBP1*,
107 and *IRF7*, and moderately increased *TMEM173* level (Fig. 1E, S6A-C), which was coherent with
108 the loss of beige adipocytes in childhood obesity (3, 7, 21). IFI16 protein level positively correlated
109 with adipocyte size (Fig. 1E). IRF7 and IFI16 expression was triggered by *in vitro* white
110 adipogenesis (Fig. 1E, Fig. S6D), and *TMEM173* expression positively correlated with *IFI16* and
111 *IRF7* levels and was increased by premature loss of beige fat (Fig. 1E, Fig. S6D). We next extended
112 the age group of our analysis (7.0–11.0 years, N=73; 11.1–20.5 years, N=155) and found that in
113 lean subjects the STING/AIM2 pathways moderately increased with age, matching the time scale
114 of the physiological WAT expansion (Fig. S6E).
115 In summary, immune response to cytosolic mtDNA and mtRNA was lacking in P6
116 adipocytes and was dependent on IRF7 (Fig. 1F, Fig. S3D, Fig. S4C-E). Moreover, STING had
117 opposing functions in P6 and P56 adipocytes: activation of STING with its natural activator 2'3'-
118 cyclic-GMP-AMP (cGAMP), increased autophagosome number and mitophagy in P6 adipocytes
119 (Fig. 1G,H,I, Fig. S7A-C), while STING inhibition compromised mitophagy, reduced
120 mitochondrial mass and led to inflammation in P6 adipocytes (Fig S7D-G). On the contrary,
121 cGAMP triggered IFN-response in P56 adipocytes (Fig. 1F, Fig. S3D).
122 STING stimulates IFN-response against mtDNA (22), however it is known that the STING
123 signaling may also induce autophagy (23, 24). Mitophagy is a form of autophagy and protects the
124 cytosol from leaking mtDNA (25). Our data show that an autophagy-inducer effect of STING
125 protects from cytosolic mtDNA accumulation in infant adipocytes (Fig. S7D-G), and infant
126 adipocytes are also protected against the STING-induced IFN-response (Fig. 1I).

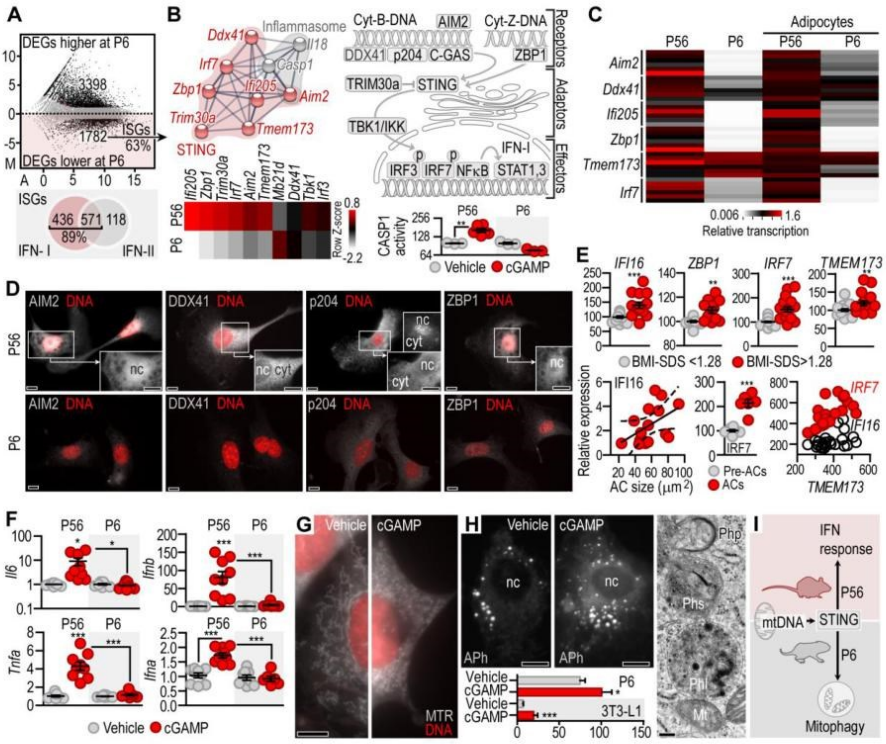

Fig 1. Infant adipocytes are immune privileged for mitochondria

(**A**) NGS analysis of mouse iAT, DEGs: differentially expressed genes, ISGs: interferon stimulated genes. (**B**) Excerpt of the interactome-, and heat map of genes underrepresented in P6 iAT. Scheme of STING signaling, and inflammasome-associated caspase 1 (CASP1) activity in P6 and P56 iAT in response to 18h cGAMP treatment. Cyt-B-DNA: cytosolic B-DNA; Cyt-Z-DNA: cytosolic Z-DNA. (**C**) Transcription of the STING/AIM2 pathways in mouse iAT at P6 and P56. (**D**) Expression of DNA sensors in adipocytes. (**E**) Transcription of the STING/AIM2 pathway in iAT of human infants and children. Correlation of IFI16 level and adipocyte (AC) size in human. IRF7 level in human preadipocytes (Pre-ACs) and white ACs. Correlation of *IFI16* and *IRF7* with *TMEM173* levels in human infant iAT. (**F**) Response of P6 and P56 adipocytes to 18h cGAMP treatment. (**G**) Mito-Tracker-Red (MTR) staining of P6 adipocytes after 2h cGAMP treatment. (**H**) *Top:* Labeling of autophagosomes (APh) in P6 adipocytes. nc: nucleus, *Bottom:* APh number in P6 adipocytes and in 3T3-L1 cells following vehicle or 2h cGAMP treatment. TEM image of a P6 adipocyte showing autophagosome formation. Php: phagophore, Phs: phagosome, Phl: phagolysosome, Mt: mitochondrion. Scale: 10 μm (D,G,H); 0.1 μm (TEM). **P*<0.05, ***P*<0.01, ****P*<0.001. Student's 2-tailed unpaired *t*-test or one-way ANOVA with Dunnett's post-hoc test. (**I**) Opposing effects of STING activation in P6 and P56 iAT.

127

Infant adipocytes employ mtRNA as a paracrine signal for beige fat development

We found that P6 adipocytes secreted mitochondrial contents in extracellular vesicles (EVs). Adipocyte EVs were generated in the endosomal pathway, by inverse budding of endosomes, leading to the formation of multivesicular bodies (MVBs) (Fig. 2A,B; S8A-G). In line with this, transcripts necessary for inverse budding of endosomes and the generation of MVBs were over-represented in iAT at P6 (Fig. 2B). Inverse budding allows cytosolic nucleic acids to be delivered to MVBs, and this process is a form of micro-autophagy (26). Endosomal content can be further targeted for degradation in the lysosomes; however lysosomal genes were underrepresented in P6 iAT and by contrast, transcripts required for exocytosis were over-represented in P6 iAT (Fig. 2B). P6 EVs were packed with mtDNA molecules and mitochondrial mRNA and rRNA species (Fig. 2C-E). Some of the EV cargo mRNAs, including *Nd5*, *Co1* and *Cytb*, are known to generate non-coding mtRNA species (27, 28). The adipose tissue mesenchymal stem cell EV-specific microRNA miR29a-5p was absent in P6 EVs (Fig. S8H). P6 EVs also contained minimal amounts of circular-RNA, piwi-RNAs and the adipocyte-specific microRNA miR34a, together with traces of *Ucp1* mRNA (Fig. S8I). P6 adipocytes released more EVs than their P56 counterparts (Fig. S8J), and inhibitors of EV generation suppressed both DNA and RNA release from adipocytes (Fig. S8K).

P6 EVs increased mitochondrial content, mitobiogenesis, uncoupling protein-1 (UCP1) expression and thermogenesis in recipient adipocytes, without inducing unfavorable mitochondrial swelling (Fig. 2F,G; Fig. S9A). P6 EVs also triggered the transcription of beige adipocyte genes (Fig. 2H). Adipocyte EVs carried dsRNA (Fig. 2E, S9B), which may activate Toll-like receptor 3 (TLR3), or the retinoic acid-inducible gene-I (RIG-I) and RIG-I-like melanoma differentiation-associated protein 5 (MDA5) signaling (29, 30). Cytosolic single stranded RNA, or stimulation of

TLR3 did not mirror the effects of EVs (Fig. S10A-C), unlike the activation of RIG-I/MDA5 which induced strong beige adipocyte gene transcription (Fig. 2I, S10D-H).

Beige-inducing effect of EVs was dependent on IL-6/STAT3 and RIG-I/MDA5 signaling (Fig. 2J, Fig. S11A-E), and the lack of RIG-I or MDA5 led to the loss of beige adipocytes and compromised mitobiogenesis, and compromised the expression of the nucleus-encoded mitochondrial succinate dehydrogenase complex (Fig. 11F,G).

Nucleic acids in EVs are protected from extracellular nucleases by the surrounding membrane and they may function as intercellular messengers (31). Accordingly, delivery of total mtRNA into the cytosol induced beige adipocyte gene expression, mitobiogenesis and mitochondrial thermogenesis (Fig. 2I, Fig. S10G,H) in a RIG-I/MDA5-dependent manner (Fig. 2J,K, Fig. S11H). Cytosolic mtDNA stimulated mitophagy in infant adipocytes (Fig. S12A,B). In summary, EVs of infant adipocytes conveyed mtRNA and mtDNA to recipient adipocytes and triggered beige adipocyte differentiation and mitophagy, respectively.

Breast milk is a known beige-inducing signal (7), and we found that human breast milk EVs were rich in mtRNA (Fig. S12C). Eventually, breast milk EVs – unlike formula milk EVs – induced beige adipocyte gene expression, mitobiogenesis and mitochondrial thermogenesis, and in turn reduced IRF7 abundance in human adipocytes (Fig. S12D,E).

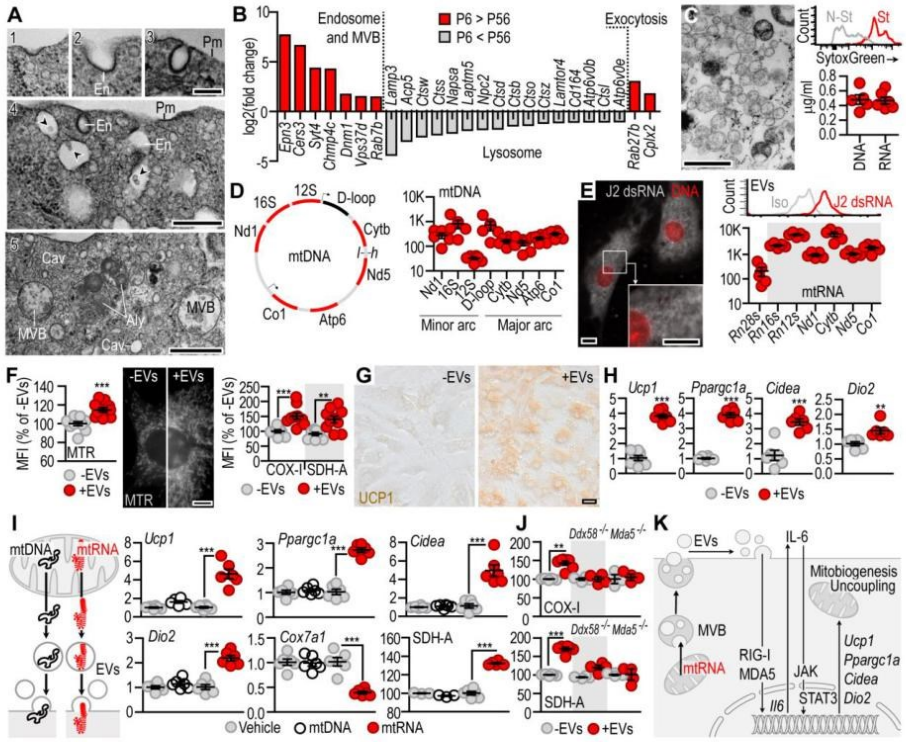

Fig. 2. Infant adipocytes cast away mtRNA to induce beige adipose tissue development
(**A**) Clathrin-coated pits, endosome budding [1–4] and multivesicular bodies (MVBs) [5] in P6 adipocyte. Pm: plasma membrane, En: endosome, Aly: autolysosome, Cav: caveolae, arrowhead: EVs in MVBs. Scale: 1 µm. (**B**) P6/P56 iAT comparison of transcripts associated with endosomes, MVBs, lysosomes and exocytosis. (**C**) TEM image of EVs released by P6 adipocytes. Scale: 0.1µm. FACS analysis of nucleic acids in EVs of P6 adipocytes. N-St: non-stained; St: stained with SytoxGreen. Amount of EV-bound nucleic acids in cell culture media of P6 adipocytes. (**D**) Level of mtDNA in EVs of P6 adipocytes. *l:* light chain; *h:* heavy chain. (**E**) Labeling of dsRNA with J2 antibody in P6 adipocytes; scale: 10 µm. Quantification of RNA species released by EVs of P6 adipocytes. Effect of P6 EVs on mitochondrial content, mitobiogenesis (**F**), UCP1 level (**G**) and beige gene expression (**H**) in P56 adipocytes. -EVs: cells cultured in EV-free media, +EVs: cells treated with EVs. Scale: 10 µm (MTR); 50 µm (UCP1), MFI: mean fluorescence intensity. (**I**) Cytosolic delivery of mtDNA and mtRNA into 3T3-L1 cells, and their effect on beige gene transcription and mitobiogenesis. (**J**) Effect of P6 EVs on mitobiogenesis of adipocytes. *Ddx58*$^{-/-}$: RIG-I (DDX58)-deficient adipocytes, *Mda5*$^{-/-}$: MDA5-deficient adipocytes. **P*<0.05, ***P*<0.01, ****P*<0.001. Student's 2-tailed unpaired *t*-test or one-way ANOVA with Dunnett's post-hoc test. (**K**) Scheme of mtRNA-activated signal transduction in infant adipocytes.

Suppressed IRF7 signaling permits beige adipogenesis by mtRNA

P56 adipocytes expressed IRF7, unlike P6 adipocytes. Activation of the STING/AIM2 and RIG-I/MDA5 pathway was strong in P56 adipocytes with synthetic ligands, with mtRNA or with mtDNA, leading to *Ifnb* expression (Fig. S13A). Ultimately, IFNβ damaged adipocyte mitochondria (Fig. S13B,C). In turn, IRF7-deificient adipocytes were immune privileged for mitochondria (Fig. 3A, S4E), and mice lacking IRF7 retained their beige adipocytes to adulthood (Fig. 3B). This is coherent with the protection of IRF7-deficient mice from obesity (32). Moreover, P6 EVs reduced *Irf7* mRNA and IRF7 protein levels in adipocytes (Fig. 3C) and did not induce IFN-response (Fig. S13D). On the contrary, P56 EVs induced IFN-response and triggered *Irf7* expression, and reduced mitochondrial content in adipocytes (Fig. S13D,E).

Vitamin D receptor (VDR)-controlled gene networks were highly expressed in P6 iAT (Fig. S2A). The known VDR-target *Camp*, encoding cathelicidin, an adipose tissue enriched antimicrobial peptide (33), was highly expressed at P6. In turn, the VDR-repressed gene *Coro1a* had a low transcript level at P6 (Fig. 3D). *Coro1a* encodes coronin A1, also known as tryptophan-aspartate containing coat protein (TACO), which inhibits autophagosome formation (34). Low levels of coronin A1 allow autophagy (34), which is in accordance with the prominent autophagy we found in P6 iAT (Fig. 1H). The transcription of vitamin D metabolizing enzymes favored the storage of vitamin D3 (Vit-D3) and the synthesis of the potent VDR-agonist calcitriol in P6 iAT (Fig. 3D). Moreover, miR434-3p, a VDR-controlled miRNA which had complementarity to *Irf7* mRNA (35) was also highly expressed in P6 iAT (Fig. 3E). IRF7 level and inflammasome activation was effectively reduced by miR434-3p in adipocytes (Fig. 3E). Moreover, P6 EVs were rich in Vit-D3, and cytosolic mtRNA increased the transcription of the calcitriol synthesis gene *Cyp27b1* in adipocytes (Fig. 3F). VDR protein expression was higher in P6 than in P56 iAT, and

191 Vit-D3 effectively suppressed *Irf7* transcription in a VDR-dependent manner in adipocytes (Fig.
192 3F). Diet-induced obesity diminished adipocyte *Vdr* expression, and concomitantly upregulated
193 *Irf7* in mice (Fig. 3G). Accordingly, inhibition of VDR signaling in young mice led to the loss of
194 beige adipocytes in iAT, along with increased IRF7 level in adipocytes (Fig. 3H). In turn,
195 suppression of IRF7 level with miR434-3p protected from inflammasome activation in adipocytes
196 of HFD-fed mice (Fig. 3I).

197 IRF7 is a hub for the transcription of AIM2/STING pathway (Fig. 13F,G), and thus
198 repression of IRF7 expression is a potential mechanism that protects infant adipocytes from an
199 IFN-response to cytosolic mtDNA/mtRNA (Fig. 13H). We found that VDR signaling suppressed
200 IRF7 expression and abolished immune response towards cytosolic mtDNA/mtRNA in mouse and
201 human adipocytes (Fig. 3J-L), but did not affect *Il6* transcription and IL-6 release (Fig. 3K,L).
202 VDR thus did not block the beige adipocyte-inducing IL-6 production, however suppressed IRF7-
203 dependent inflammatory signaling. This allowed cytosolic mtRNA to induce mitobiogenesis and
204 beige gene expression, and mtDNA to trigger mitophagy, without unfavorable induction of an
205 IFN-response (Fig. 3M).

206

207 **Obesity in early postnatal life compromises immune privilege of adipocyte mitochondria**

208 We found that childhood obesity compromised VDR-controlled gene networks and decreased the
209 expression of the calcitriol producing *CYP27A1* (Fig. 4A), and increased *IRF7* expression in the
210 iAT (Fig. 1E). Similarly, diet induced obesity compromised *Vdr* and increased *Irf7* expression in
211 mouse, and inhibition of VDR signaling in infant mice led to the loss of beige fat cells (Fig. 3G,H).
212 Next, we studied a mouse model of childhood obesity, using infant mice which were nursed by
213 dams fed with HFD (Fig. 4B) (36). In the offspring of HFD-fed dams adipocytes had a

compromised *Vdr*, and a robust *Irf7* expression (Fig. 4C), and beige adipocytes were lacking from the iAT (Fig. 4D). Eventually obesity developed and the adipocytes had a sustained inflammasome activation (Fig. 4E). Moreover, the mitochondrial network was compromised in adipocytes (Fig. 4F), and AIM2/STING pathway proteins were expressed in the cytosol and in the nuclei of adipocytes of mice nursed by HFD-fed dams (Fig. 4F). In turn, Vit-D3 reverted these adverse effects and protected the beige adipocyte content in infant mice (Fig. 4G), reduced obesity and adipocyte inflammation (Fig. 4H). In adult HFD-fed mice, cytosolic delivery of mtRNA into the iAT, combined with Vit-D3 treatment, reduced IRF7 level and increased beige adipocyte content in the iAT (Fig. 4I,J), reduced obesity and adipocyte inflammation, increased mitochondrial mass, thermogenesis and energy expenditure, inhibited inflammasome activation following STING activation, and induced adipocyte expression of calcitriol forming *Cyp27b1* (Fig. 4K-N, Fig. S14A-C).

Altogether, the immune privilege of mitochondrial content was dependent on the suppression of adipocyte IRF7 level by VDR. In human, childhood obesity compromised VDR signaling and increased *IRF7* expression in the adipose tissue. Adipocyte maturation increased IRF7 level, and in turn, Vit-D3 reduced IRF7 expression and immune response to cytosolic mtRNA and mtDNA in human adipocytes. Similarly, diet induced obesity compromised *Vdr* and triggered *Irf7* transcription in both adult and infant mice and triggered immune response against cytosolic mtDNA and mtRNA. These data show that beige adipocytes lack an immune response against mtDNA/mtRNA at least in part due to VDR signaling (Fig. 5A). When VDR sustains this immune privilege of mitochondria, cytosolic mtRNA stimulates the expression of nucleus-encoded mitochondrial genes and promotes beige adipocyte development (Fig. 5B). This mitochondria-to-nucleus signaling protects against obesity.

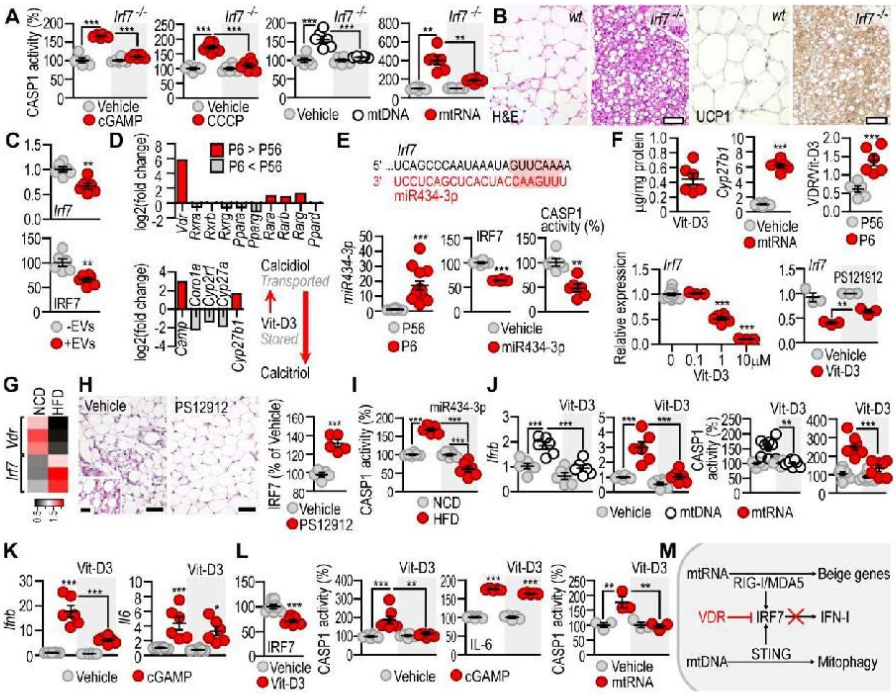

Fig. 3. VDR abrogates IRF7 expression in the infant adipocytes

(**A**) Response of P56 adipocytes to cGAMP, CCCP (carbonyl cyanide m-chlorophenyl hydrazone)-induced mitochondrial damage, cytosolic mtDNA and mtRNA. *Irf7*$^{-/-}$: IRF7-deficient adipocytes. (**B**) iAT of adult *wt* and *Irf7*$^{-/-}$ mice. Scale: 25 μm. H&E: hematoxylin-eosin (**C**) Effect or P6 EVs on *Irf7* and IRF7 level in mouse adipocytes (**D**) Structure of miR434-3p, its level in P6 and P56 iAT, and its effect on IRF7 level and inflammasome activity in mouse adipocytes. (**E**) P6/P56 transcript level of *Vdr,* VDR-controlled genes and vitamin D metabolism genes in iAT. (**F**) *Top:* Level of Vit-D3 in P6 EVs, effect of cytosolic mtRNA on the expression of calcitriol synthesizing *Cyp27b1*, and the ratio of VitD3/VDR in P6 iAT. *Bottom:* Effect of 48h Vit-D3 treatment on *Irf7* level in mouse adipocytes. PS121912: VDR inhibitor. (**G**) Level of *Vdr* and *Irf7* in iAT of HFD-fed mice. (**H**) *Left:* Histology of iAT at P10 of mice treated with vehicle or PS12912. Scale: 25 μm. *Right:* Adipocyte IRF7 protein level of the same mice. (**I**) Effect of overexpression of miR434-3p on HFD-induced inflammasome activation in adipocytes. (**J**,**K**) Response of 1 μM Vit-D3 pretreated mouse adipocytes to cytosolic mtDNA, mtRNA, or cGAMP. (**L**) IRF7 level and cGAMP response of human adipocytes treated with vehicle or Vit-D3. **P*<0.05, ***P*<0.01, ****P*<0.001. Student's 2-tailed unpaired *t*-test or one-way ANOVA with Dunnett's post-hoc test. (**M**) Scheme of VDR function in infant adipocytes.

237

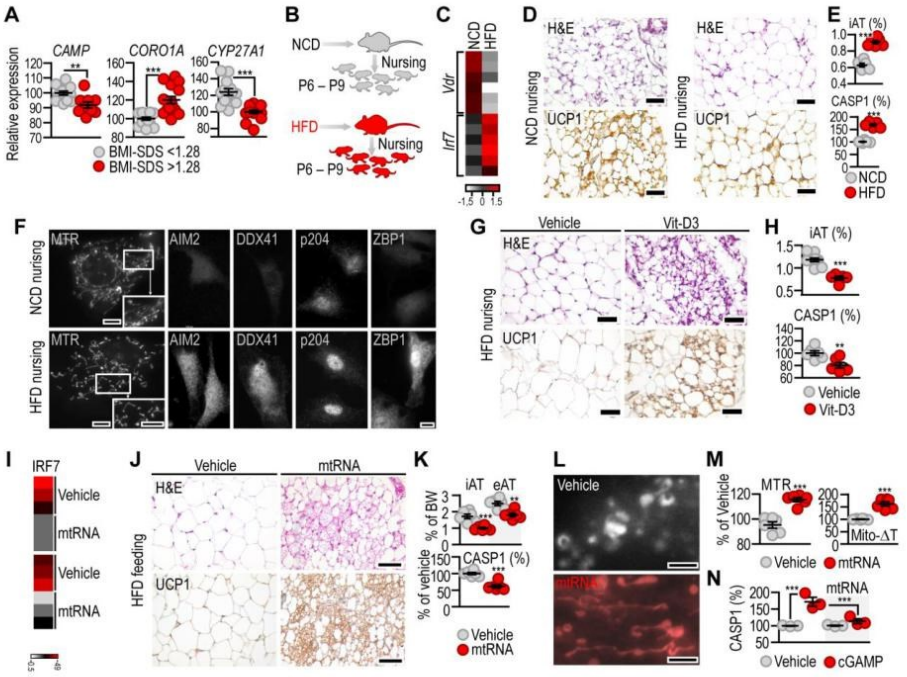

Fig. 4. Effect of cytosolic mtRNA combined vit Vit-D3 treatment in diet-induced obesity
(**A**) VDR-controlled gene expression in iAT of children. (**B**) Nursing mice received high-fat diet (HFD) or normal chow diet (NCD) between postnatal day 6 and 9 of the offspring. Mice nursed by NCD-fed or HFD-fed dams were analyzed on postnatal day 10 (P10). (**C**) *Vdr* and *Irf7* expression in iAT. (**D**) Histology of iAT. H&E: hematoxylin and eosin staining, UCP1: UCP1 immunostaining, Scale: 50 μm. Note the lack of multilocular adipocytes in mice nursed by HFD-fed dams. (**E**) Ratio of iAT and body weight, and inflammasome caspase 1 (CASP1) activity of the adipocytes. (**F**) Mitochondrial network and the expression of AIM2, DDX41, p204 and ZBP1 in adipocytes. MTR: MitoTracker Red. Scale 50 μm. (**G**) Mice were nursed by HFD-fed dams, and treated with vehicle or Vit-D3 from P6 to P9. Histology of iAT on P10. Scale: 100 μm (**H**) Ratio of iAT and body weight, and CASP1 activity of the adipocytes on P10. (**I**) In adult HFD-fed mice the iAT was transfected with vehicle or mtRNA, and IRF7 protein level was measured in adipocytes. (**J**) Histology of iAT of vehicle- or mtRNA-transfected mice. (**K**) Adipose tissue weight/body weight ratio, and CASP1 activity of adipocytes. eAT: epididymal adipose tissue (**L**) Mitochondrial network of adipocytes isolated from vehicle- or mtRNA-transfected mice. Scale: 10 μm. Note the expansion of the mitochondrial network after mtRNA treatment. (**M**) Mitochondrial mass (relative MTR fluorescent intensity) and mitochondrial temperature change (Mito-ΔT) in adipocytes isolated from vehicle- or mtRNA-transfected mice. (**L**) CASP1 activity of adipocytes isolated from vehicle- or mtRNA-transfected mice, and treated with vehicle of cGAMP for 4h. ***P*<0.01, ****P*<0.001. Student's 2-tailed unpaired *t*-test or one-way ANOVA with Dunnett's post-hoc test.

Discussion

Adipose tissue inflammation is considered deleterious for metabolism (37). However, various lines of evidence show that differentiation of thermogenic adipose tissue requires JAK/STAT3 signaling (7, 38, 39), and an autocrine IL-6/STAT3 signaling loop is sustained by breast milk-derived lipid signaling in the newborn adipose tissue (7). Some inflammatory signal mechanisms that cause obesity-associated metabolic impairment also sustain beige adipocytes (40, 41). Here we report the unexpected finding that beige adipocyte development is promoted by a potentially inflammation-evoking cytosolic RNA signal, released by the mitochondria of infant adipocytes.

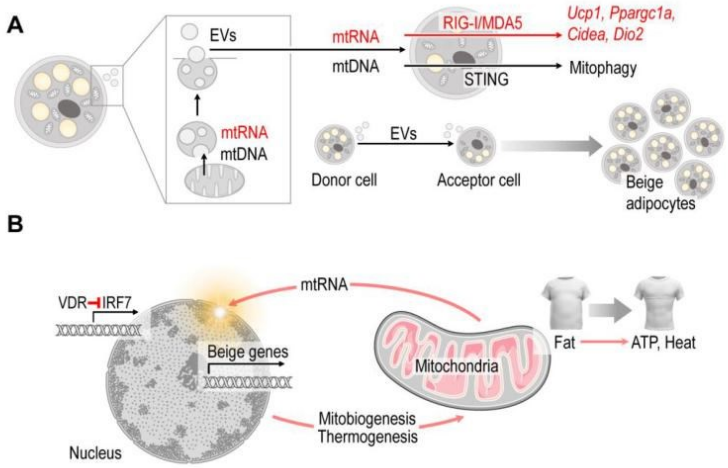

Fig. 5. Role of mtRNA signaling in beige adipocytes
(A) Under physiological conditions infant adipocytes release cytosolic mtRNA and mtDNA in extracellular vesicles (EVs). Eventually, mtRNA serves as endogenous signal for beige adipogenesis in neighboring cells through the RIG-I/MDA5/IL-6/STAT3 pathway. In turn, mtDNA content of the EVs triggers mitophagy through STING signaling. (**B**) Albeit cytosolic mtRNA and mtRNA are noxious signals, they can act as metabolically beneficial mitochondria-to-nucleus signals when IRF7 expression is suppressed. VDR is an effective suppressor of IRF7 and abrogates IFN-response to cytosolic mtRNA and mtDNA in infant adipocytes. Infant adipocytes are hence immune privileged sites for mitochondria, allowing a retrograde mitochondria-to-nucleus signaling through mtRNA, which is key for mitobiogenesis and beige fat development.

The endosymbiotic origin of mitochondria has led to a metabolic co-dependence of the mitochondria and the host cell (42). This is driven by a retrograde, mitochondria-to-nucleus signaling pathway, as the majority of genes required for the maintenance of mitochondria are encoded in the nuclear genome. We show that, analogous to a parasite-host interaction, mitochondrial nucleic acids are released by EVs, and are taken up by surrounding adipocytes to activate cytosolic RNA sensors that stimulate an autocrine IL-6/STAT3 signaling loop, ultimately triggering the nuclear expression of beige adipocyte genes (Fig. 2K, Fig. 5A). Non-coding RNA species of mitochondria are known to increase the transcription of mitochondrial genome-encoded genes (27). As an equivalent mechanism, we show that mtRNA species boost the transcription of nuclear genome-encoded genes for mitochondrial biogenesis and thermogenesis. This is key for mitobiogenesis since the majority of the mitochondrial genes are encoded in the nuclear genome (42). The release of EVs containing mitochondrial nucleic acids resembles the recently explored mechanism that allows nucleic acid delivery from bacteria to host cells in membrane microvesicles (43, 44).

The primary sensors of cytoplasmic mtRNA are RIG-I and MDA5. RIG-I detects dsRNAs with or without a 5′-triphosphate end; MDA5 binds uncapped RNA; and RIG-I and MDA5 selectively recognize short and long dsRNAs, respectively (29, 30). Given the prokaryote origin of mitochondria, various mtRNA species such as mitochondrial ribosomal RNAs, uncapped mitochondrial mRNA, and non-coding mtRNAs, can potentially stimulate the cytoplasmic RNA sensor system (45, 46). Beige adipocyte gene transcription was achievable by indirect RIG-I activation using cytosolic p(dA:dT), and also by MDA5 activation using cytosolic high molecular weight p(I:C), but not with cytosolic ssRNA. Coherently, lack of RIG-I and MDA5 signaling

compromised the mtRNA-mediated beige adipocyte development, and abrogated nucleus-encoded SDH-A expression and mitobiogenesis, and promoted the loss of beige adipocytes in mice.

Nevertheless, excessive release of mitochondrial content is a danger signal, and activates an IFN-response, which is detrimental for thermogenic fat development (16, 47, 48), triggers obesity, mitochondrial dysfunction and the mitochondrial pathway of adipocyte apoptosis (49, 50), and may aggravate obesity-associated metabolic diseases (51, 52). We show here that beige adipocytes lack cytosolic DNA sensors and show suppressed expression of IRF7. Consequently, cytosolic mtDNA and mtRNA do not stimulate an IFN-response in beige adipocytes. Instead, beige adipocytes respond by activating mitophagy to cytoplasmic mtDNA, allowing the removal of damaged mitochondria and curtailing inflammation. Moreover, cytosolic mtRNA stimulates mitobiogenesis. The key protective mechanism – i.e., compromised IRF7 signaling – is a trait of the infant adipocytes, and is lost in the course of adipocyte maturation. While the activation of STAT1 and NFκB signaling may account for the increasing IRF7 expression during adipocyte maturation (6), we show that VDR signaling contributes to the suppression of IRF7 level in infant adipocytes, and cytosolic mtRNA stimulates mitochondrial calcitriol synthesis – hence supplies a VDR ligand – in infant adipocytes. However, diet-induced obesity in mouse, and obesity in children were associated with robust expression of the cytosolic DNA sensor system and IRF7, leading to the loss of the immune privilege of mitochondria.

VDR signaling is involved in the innate immune response in the adipose tissue (33), and VDR may also skew IFN-response and IRF7 expression (53, 54). Vit-D3 supplementation is today routine in postnatal care, however, Vit-D3 deficiency is prevalent among obese children and adolescents and is a risk factor for metabolic diseases (55-57). Vit-D3/VDR is proposed to inhibit weight gain by activating UCP3 in the muscles (58), albeit VDR overexpression promotes weight

292 gain in mouse (59). Indeed, promotion of formula feeding originally served to increase Vit-D3
293 supply and induce weight gain (60). Formula milk lacks maternal lipid species that maintain beige
294 fat and has obesogenic effects (7). We also show here that formula milk lacks beige-inducing
295 mtRNA signals. Moreover, VDR signaling was impaired in the adipose tissue of obese children,
296 therefore despite its increased Vit-D3 level, formula milk is not sufficient to trigger beige
297 adipogenesis. However, when Vit-D3 supplementation is combined with stimulation of cytosolic
298 mtRNA signaling, beige adipocytes develop and obesity is reduced.
299 In summary, beige adipocyte development is dependent on a mtRNA-mediated signaling
300 and the suppression of IFN-response. Restoring the mtRNA-mediated mitochondria-to-nucleus
301 signaling may represent a novel and effective mechanism to increase beige fat and reduce obesity.

Methods

Animals and cells

We used *wt* male C57BL/6 (Charles River Laboratories, Wilmington, MA), *Irf7*$^{-/-}$ (RIKEN, Wako, Japan), *Ddx58*$^{-/-}$ and *Mda5*$^{-/-}$ (kindly provided by Gunther Hartmann, University of Bonn, Germany) mice. All mouse lines were housed under SPF conditions. Animal experiments were approved by the local ethics committees. Primary mouse adipocytes were isolated by collagenase digestion and separation of cell fractions and subsequently analyzed or cultured, as described (7).

Human samples

Subcutaneous adipose tissue from human infants, adolescents and young adults were collected in the Leipzig Childhood Adipose Tissue cohort during elective surgery (3). For all children included in the study written informed consent was obtained from the parents. The study protocol was approved by the local ethics committee of the Medical Faculty, University of Leipzig (#265-08-ff; NCT02208141). Adult adipocytes samples were collected in our previous study (7).

mRNA analysis and next-generation sequencing

Extraction of total RNA was performed as described (6). qPCR assays were carried out on the Quantabio platform (Beverly, MA), using *Bactin*, *Gapdh* and *Ppia* as references. Primer sequences are provided in Supplemental Table 1. NGS analysis was carried out on the BGISEQ-500 platform by BGI Genomics Inc. (Cambridge, MA), generating about 26.20M reads per sample (Fig. S15). EnrichR, Panther and Interferome-2.0 were used for annotation of transcripts; clustered image maps (CIMs, heat-maps) were rendered by CIM-Miner and Heatmapper. Gene expression in human samples was quantified by ILLUMINA HT12v4 Gene Expression BeadChip arrays and data were background corrected and quantile normalized (6).

Supplemental methods

Cytosolic delivery of RNA/DNA, viral infections, ELISA assays, overexpression studies, autophagosome/lysosome labeling, EV collection, FACS, histology, image analysis, and TEM analysis are provided in the Supplemental Information.

Data representation and statistics

Data are represented as mean±s.e.m, along with each individual data point. When data are represented as CIMs to visualize gene transcription differences between experimental conditions, we indicate fold changes or Z-scores of the relative abundance. Statistical significance is indicated as $*P<0.01$, $**P<0.01$; $***P<0.001$, Student's 2-tailed unpaired *t*-test, or 1-way ANOVA with Dunnett's post hoc test.

Data and materials availability

Materials and data are available for secondary use upon request. Flow Repository identifiers of FACS data are as follows: #FR-FCM-Z236, #FR-FCM-Z2R6, #FR-FCM-ZYPU, #FR-FCM-ZYUU. NGS data are deposited at GEO with the accession number #GSE185317. For secondary analysis, we used our previously published DNA Chip and NGS datasets, with accession numbers #GSE125405, #GSE90658, #GSE154925 and #GSE133500.

Acknowledgements

We thank Dr. Kenneth McCreath for editing the manuscript.

Funding

This study was supported by the German Research Fund (DFG, RO 4856-1, to TR; DFG, CRC1052 C05, to AK), the European Foundation for the Study of Diabetes on New Targets for Type 2 Diabetes, Supported by MSD (No. 96403, to TR), by the Federal Ministry of Education and Research (BMBF), Germany (FKZ: 01EO1501 IFB Adiposity Diseases, to AK.

348 **Author contribution**

349 ACH, HY, YTL, CCC, VD carried out experiments, AK, AH, JC designed experiments, TR
350 conceived the project, designed experiments and wrote the manuscript.

351

352 **References**

353 1. Chobot A, Górowska-Kowolik K, Sokołowska M, and Jarosz-Chobot P. Obesity and
354 diabetes—Not only a simple link between two epidemics. *Diabetes/Metabolism Research*
355 *and Reviews.* 2018:e3042.
356 2. Geserick M, Vogel M, Gausche R, Lipek T, Spielau U, Keller E, et al. Acceleration of
357 BMI in early childhood and risk of sustained obesity. *The New England journal of*
358 *medicine.* 2018;379(14):1303-12.
359 3. Landgraf K, Rockstroh D, Wagner IV, Weise S, Tauscher R, Schwartze JT, et al.
360 Evidence of early alterations in adipose tissue biology and function and its association
361 with obesity-related inflammation and insulin resistance in children. *Diabetes.*
362 2015;64(4):1249-61.
363 4. Herrera E, and Amusquivar E. Lipid metabolism in the fetus and the newborn. *Diabetes*
364 *Metab Res Rev.* 2000;16(3):202-10.
365 5. Stave U. *Perinatal physiology.* New York, London: Plenum Medical Company; 1970.
366 6. Hoang AC, Yu H, and Röszer T. Transcriptional Landscaping Identifies a Beige
367 Adipocyte Depot in the Newborn Mouse. *Cells.* 2021;10(9):2368.
368 7. Yu H, Dilbaz S, Coßmann J, Hoang AC, Diedrich V, Herwig A, et al. Breast milk
369 alkylglycerols sustain beige adipocytes through adipose tissue macrophages. *The Journal*
370 *of Clinical Investigation.* 2019;129(6):2485-99.
371 8. Ikeda K, Maretich P, and Kajimura S. The Common and Distinct Features of Brown and
372 Beige Adipocytes. *Trends in Endocrinology & Metabolism.* 2018;29(3):191-200.
373 9. Hahn P, and Novak M. Development of brown and white adipose tissue. *Journal of lipid*
374 *research.* 1975;16(2):79-91.

10. Rockstroh D, Landgraf K, Wagner IV, Gesing J, Tauscher R, Lakowa N, et al. Direct evidence of brown adipocytes in different fat depots in children. *PLOS ONE.* 2015;10(2):e0117841.
11. Zhong Z, Liang S, Sanchez-Lopez E, He F, Shalapour S, Lin XJ, et al. New mitochondrial DNA synthesis enables NLRP3 inflammasome activation. *Nature.* 2018;560(7717):198-203.
12. Beyerlein A, Donnachie E, Jergens S, and Ziegler A-G. Infections in Early Life and Development of Type 1 Diabetes. *JAMA.* 2016;315(17):1899-901.
13. Atkinson RL. Viruses as an etiology of obesity. *Mayo Clinic proceedings.* 2007;82(10):1192-8.
14. Shoelson SE, Lee J, and Goldfine AB. Inflammation and insulin resistance. *J Clin Invest.* 2006;116(7):1793-801.
15. Lempainen J, Tauriainen S, Vaarala O, Makela M, Honkanen H, Marttila J, et al. Interaction of enterovirus infection and cow's milk-based formula nutrition in type 1 diabetes-associated autoimmunity. *Diabetes Metab Res Rev.* 2012;28(2):177-85.
16. Kissig M, Ishibashi J, Harms MJ, Lim H-W, Stine RR, Won K-J, et al. PRDM16 represses the type I interferon response in adipocytes to promote mitochondrial and thermogenic programing. *The EMBO Journal.* 2017;36(11):1528-42.
17. Motwani M, Pesiridis S, and Fitzgerald KA. DNA sensing by the cGAS–STING pathway in health and disease. *Nature Reviews Genetics.* 2019;20(11):657-74.
18. Shin S-I, Ham S, Park J, Seo SH, Lim CH, Jeon H, et al. Z-DNA-forming sites identified by ChIP-Seq are associated with actively transcribed regions in the human genome. *DNA Res.* 2016;23(5):477-86.
19. Takaoka A, Wang Z, Choi M, Yanai H, Negishi H, Ban T, et al. DAI (DLM-1/ZBP1) is a cytosolic DNA sensor and an activator of innate immune response. *Nature.* 2007;448:501-5.
20. Lugrin J, and Martinon F. The AIM2 inflammasome: Sensor of pathogens and cellular perturbations. *Immunological Reviews.* 2018;281(1):99-114.
21. Geserick M, Vogel M, Gausche R, Lipek T, Spielau U, Keller E, et al. Acceleration of BMI in Early Childhood and Risk of Sustained Obesity. *The New England journal of medicine.* 2018;379(14):1303-12.

406 22. Bahat A, MacVicar T, and Langer T. Metabolism and Innate Immunity Meet at the
407 Mitochondria. *Frontiers in Cell and Developmental Biology.* 2021;9(2019).
408 23. Liu D, Wu H, Wang C, Li Y, Tian H, Siraj S, et al. STING directly activates autophagy
409 to tune the innate immune response. *Cell Death & Differentiation.* 2019;26(9):1735-49.
410 24. Devi TS, Yumnamcha T, Yao F, Somayajulu M, Kowluru RA, and Singh LP. TXNIP
411 mediates high glucose-induced mitophagic flux and lysosome enlargement in human
412 retinal pigment epithelial cells. *Biology open.* 2019;8(4):bio038521.
413 25. Nakahira K, Haspel JA, Rathinam VAK, Lee S-J, Dolinay T, Lam HC, et al. Autophagy
414 proteins regulate innate immune responses by inhibiting the release of mitochondrial
415 DNA mediated by the NALP3 inflammasome. *Nature immunology.* 2011;12(3):222-30.
416 26. Fujiwara Y, Wada K, and Kabuta T. Lysosomal degradation of intracellular nucleic
417 acids—multiple autophagic pathways. *The Journal of Biochemistry.* 2016;161(2):145-54.
418 27. Ro S, Ma H-Y, Park C, Ortogero N, Song R, Hennig GW, et al. The mitochondrial
419 genome encodes abundant small noncoding RNAs. *Cell Research.* 2013;23(6):759-74.
420 28. Rackham O, Shearwood A-MJ, Mercer TR, Davies SMK, Mattick JS, and Filipovska A.
421 Long noncoding RNAs are generated from the mitochondrial genome and regulated by
422 nuclear-encoded proteins. *RNA.* 2011;17(12):2085-93.
423 29. Dias Junior AG, Sampaio NG, and Rehwinkel J. A Balancing Act: MDA5 in Antiviral
424 Immunity and Autoinflammation. *Trends in Microbiology.* 2019;27(1):75-85.
425 30. Kato H, Takeuchi O, Mikamo-Satoh E, Hirai R, Kawai T, Matsushita K, et al. Length-
426 dependent recognition of double-stranded ribonucleic acids by retinoic acid-inducible
427 gene-I and melanoma differentiation-associated gene 5. *The Journal of experimental*
428 *medicine.* 2008;205(7):1601-10.
429 31. Abels ER, and Breakefield XO. Introduction to Extracellular Vesicles: Biogenesis, RNA
430 Cargo Selection, Content, Release, and Uptake. *Cell Mol Neurobiol.* 2016;36(3):301-12.
431 32. Wang XA, Zhang R, Zhang S, Deng S, Jiang D, Zhong J, et al. Interferon regulatory
432 factor 7 deficiency prevents diet-induced obesity and insulin resistance. *American journal*
433 *of physiology Endocrinology and metabolism.* 2013;305(4):E485-95.
434 33. Zhang LJ, Guerrero-Juarez CF, Hata T, Bapat SP, Ramos R, Plikus MV, et al. Innate
435 immunity. Dermal adipocytes protect against invasive Staphylococcus aureus skin
436 infection. *Science.* 2015;347(6217):67-71.

34. Seto S, Tsujimura K, and Koide Y. Coronin-1a inhibits autophagosome formation around Mycobacterium tuberculosis-containing phagosomes and assists mycobacterial survival in macrophages. *Cellular Microbiology.* 2012;14(5):710-27.
35. Yu P, Song H, Gao J, Li B, Liu Y, and Wang Y. Vitamin D (1,25-(OH)2D3) regulates the gene expression through competing endogenous RNAs networks in high glucose-treated endothelial progenitor cells. *The Journal of Steroid Biochemistry and Molecular Biology.* 2019;193:105425.
36. Masuyama H, and Hiramatsu Y. Additive Effects of Maternal High Fat Diet during Lactation on Mouse Offspring. *PLOS ONE.* 2014;9(3):e92805.
37. Christ A, and Latz E. The Western lifestyle has lasting effects on metaflammation. *Nature Reviews Immunology.* 2019;19(5):267-8.
38. Derecka M, Gornicka A, Koralov SB, Szczepanek K, Morgan M, Raje V, et al. Tyk2 and Stat3 regulate brown adipose tissue differentiation and obesity. *Cell metabolism.* 2012;16(6):814-24.
39. Babaei R, Schuster M, Meln I, Lerch S, Ghandour RA, Pisani DF, et al. Jak-TGFβ cross-talk links transient adipose tissue inflammation to beige adipogenesis. *Science Signaling.* 2018;11(527).
40. Alsaggar M, Mills M, and Liu D. Interferon beta overexpression attenuates adipose tissue inflammation and high-fat diet-induced obesity and maintains glucose homeostasis. *Gene Ther.* 2017;24(1):60-6.
41. Cao W, Daniel KW, Robidoux J, Puigserver P, Medvedev AV, Bai X, et al. p38 Mitogen-Activated Protein Kinase Is the Central Regulator of Cyclic AMP-Dependent Transcription of the Brown Fat Uncoupling Protein 1 Gene. *Molecular and Cellular Biology.* 2004;24(7):3057-67.
42. Youle RJ. Mitochondria—Striking a balance between host and endosymbiont. *Science.* 2019;365(6454):eaaw9855.
43. Toyofuku M, Nomura N, and Eberl L. Types and origins of bacterial membrane vesicles. *Nature Reviews Microbiology.* 2019;17(1):13-24.
44. Bitto NJ, Chapman R, Pidot S, Costin A, Lo C, Choi J, et al. Bacterial membrane vesicles transport their DNA cargo into host cells. *Scientific reports.* 2017;7(1):7072-.

45. Eberle F, Sirin M, Binder M, and Dalpke AH. Bacterial RNA is recognized by different sets of immunoreceptors. *European Journal of Immunology.* 2009;39(9):2537-47.
46. Eigenbrod T, and Dalpke AH. Bacterial RNA: An Underestimated Stimulus for Innate Immune Responses. *The Journal of Immunology.* 2015;195(2):411-8.
47. Kumari M, Wang X, Lantier L, Lyubetskaya A, Eguchi J, Kang S, et al. IRF3 promotes adipose inflammation and insulin resistance and represses browning. *J Clin Invest.* 2016;126(8):2839-54.
48. Bai J, Cervantes C, He S, He J, Plasko GR, Wen J, et al. Mitochondrial stress-activated cGAS-STING pathway inhibits thermogenic program and contributes to overnutrition-induced obesity in mice. *Communications Biology.* 2020;3(1):257.
49. Bai J, and Liu F. The cGAS-cGAMP-STING Pathway: A Molecular Link Between Immunity and Metabolism. *Diabetes.* 2019;68(6):1099-108.
50. Gkirtzimanaki K, Kabrani E, Nikoleri D, Polyzos A, Blanas A, Sidiropoulos P, et al. IFNα Impairs Autophagic Degradation of mtDNA Promoting Autoreactivity of SLE Monocytes in a STING-Dependent Fashion. *Cell reports.* 2018;25(4):921-33.e5.
51. Tian Y, Jennings J, Gong Y, and Sang Y. Viral Infections and Interferons in the Development of Obesity. *Biomolecules.* 2019;9(11).
52. Birk RZ, and Rubinstein M. IFN-alpha induces apoptosis of adipose tissue cells. *Biochem Biophys Res Commun.* 2006;345(2):669-74.
53. Cippitelli M, and Santoni A. Vitamin D3: a transcriptional modulator of the interferon-γ gene. *European Journal of Immunology.* 1998;28(10):3017-30.
54. Stoppelenburg AJ, von Hegedus JH, Huis in't Veld R, Bont L, and Boes M. Defective control of vitamin D receptor-mediated epithelial STAT1 signalling predisposes to severe respiratory syncytial virus bronchiolitis. *The Journal of Pathology.* 2014;232(1):57-64.
55. Roth CL, Elfers C, Kratz M, and Hoofnagle AN. Vitamin d deficiency in obese children and its relationship to insulin resistance and adipokines. *J Obes.* 2011;2011:495101-.
56. de Oliveira LF, de Azevedo LG, da Mota Santana J, de Sales LPC, and Pereira-Santos M. Obesity and overweight decreases the effect of vitamin D supplementation in adults: systematic review and meta-analysis of randomized controlled trials. 2020;21(1):67-76.
57. Pramono A, Jocken JWE, and Blaak EE. Vitamin D deficiency in the aetiology of obesity-related insulin resistance. 2019;35(5):e3146.

58. Fan Y, Futawaka K, Koyama R, Fukuda Y, Hayashi M, Imamoto M, et al. Vitamin D3/VDR resists diet-induced obesity by modulating UCP3 expression in muscles. *J Biomed Sci.* 2016;23(1):56-.
59. Xu Y, Lou Y, and Kong J. VDR regulates energy metabolism by modulating remodeling in adipose tissue. *European journal of pharmacology.* 2019;865:172761.
60. Biggs K, Hurrell K, Matthews E, Khaleva E, Munblit D, and Boyle R. Formula Milk Supplementation on the Postnatal Ward: A Cross-Sectional Analytical Study. *Nutrients.* 2018;10(5):608.

8.2. List of figures

Figure 1: Anatomy and histology of iAT in young and adult mice. 26
Figure 2: Assays to compare DEGs in different adipose tissues of both age groups 28
Figure 3: BAT and beige adipocyte defined marker genes in P6 and P56 fat depots 31
Figure 4: Gene ontology analysis of young and adult BAT 32
Figure 5: Signaling networks overrepresented in P56 BAT and in P6 iAT 33
Figure 6: Difference in NFκB signaling-related gene expression in P6 iAT and P56 BAT. 35
Figure 7: Genes involved in the immune response of iAT and BAT 37
Figure 8: Underrepresented genes related to immune response in P6 iAT 40
Figure 9: P6 adipocytes are protected from mtDNA-mtRNA-triggered IFN response 42
Figure 10: P6 and breast milk EVs induce beige adipocyte development 44
Figure 11: Beige adipocyte development through paracrine mtRNA signal 46
Figure 12: Absent of IRF7 supports beige adipocyte development 48
Figure 13: Vitamin D3-mediated Irf7 suppression impairs triggered IFN response 50
Figure 14: Treating diet-induced obese mice with cytosolic mtRNA and Vit-D3 52
Figure 15: Role of mtRNA and Vit-D3 in the mitochondria-to-nucleus signaling 65

8.3. List of tables

Table 1: Antibodies used in the thesis for protein detection 17
Table 2: Mouse primer pairs for RT-qPCR 18
Table 3: Mouse primers for the detection of mitochondrial DNA 19
Table 4: Mouse primers for the detection of mitochondrial RNA 19

9. Statutory declaration

I, Anh Cuong Hoang, hereby confirm that the monography “Exploring mechanisms of gene expression regulation in the developing murine adipose tissue” was an independent work. I acknowledge all the literature, materials, and methods I showed in this thesis. I declare that my dissertation was performed under the principles of good scientific practice which is in line with the “*Satzung der Universität Ulm zur Sicherung guter wissenschaftlicher Praxis*”. This work has not been published for a doctoral degree at any universities or institutions before. The underline signature will confirm that the submitted, printed work will be handled as equal as the electronic one.

Date _____ Signature _____